INFORMATION TO USERS

This manuscript has been reproduced from the microfilm master. UMI films the text directly from the original or copy submitted. Thus, some thesis and dissertation copies are in typewriter face, while others may be from any type of computer printer.

The quality of this reproduction is dependent upon the quality of the copy submitted. Broken or indistinct print, colored or poor quality illustrations and photographs, print bleedthrough, substandard margins, and improper alignment can adversely affect reproduction.

In the unlikely event that the author did not send UMI a complete manuscript and there are missing pages, these will be noted. Also, if unauthorized copyright material had to be removed, a note will indicate the deletion.

Oversize materials (e.g., maps, drawings, charts) are reproduced by sectioning the original, beginning at the upper left-hand corner and continuing from left to right in equal sections with small overlaps. Each original is also photographed in one exposure and is included in reduced form at the back of the book.

Photographs included in the original manuscript have been reproduced xerographically in this copy. Higher quality 6" x 9" black and white photographic prints are available for any photographs or illustrations appearing in this copy for an additional charge. Contact UMI directly to order.

UMI

A Bell & Howell Information Company
300 North Zeeb Road, Ann Arbor MI 48106-1346 USA
313/761-4700 800/521-0600

SEISMIC DETECTION OF TRANSIENT CHANGES BENEATH BLACK RAPIDS GLACIER, ALASKA

A

THESIS

Presented to the Faculty

of the University of Alaska Fairbanks

in Partial Fulfillment of the Requirements

for the Degree of

DOCTOR OF PHILOSOPHY

By

Matthew Allen Nolan, B.S., M.S.

Fairbanks, Alaska
May 1998

SEISMIC DETECTION OF TRANSIENT CHANGES

BENEATH BLACK RAPIDS GLACIER, ALASKA

By

Matthew Allen Nolan

RECOMMENDED:

Advisory Committee Chair

Department Head

APPROVED:

Dean of College of Science, Engineering and Mathematics

Dean of the Graduate School

12-3-97

Date

ABSTRACT

To gain new insight into the mechanisms of basal motion, I have demonstrated the feasibility of an active seismic technique to measure temporal changes in basal conditions on sub-hourly time-scales. Using changes observed in the summer of 1993 on Black Rapids Glacier, I have determined part of the basal morphology and the mechanisms of seismic change there.

One region of the glacier's bed was monitored daily using seismic reflections, for a period of 45 days. The majority of these reflections were nearly identical. However, the englacial drainage of two ice-marginal lakes and one supra-glacial pothole upglacier of the study site each caused significant anomalies in the daily reflections, as well as dramatic increases in basal motion. Two of these seismic anomalies were nearly identical despite the fact that their drainage events occurred at different locations. Further, these two seismic anomalies were followed by records identical to the non-anomalous state, showing that the changes were seismically reversible. In one of these events, two records taken 36 minutes apart revealed that the transition between the anomalous and normal states occurred completely within this short interval.

Reflection arrival times during the anomalies require that a basal layer at least 5 m thick was either created or changed *in situ*. Reflection amplitudes indicate that such a layer could be either water or a basal till, but water layers of such thickness are not physically reasonable. Published values of wave speeds and densities of till are then compared to those constrained by the observed reflection coefficients. Only a *decrease* in till saturation can produce the observed changes in reflection amplitudes in the time required. Because the transition from anomalous to normal states can occur in as little as 36 minutes, any mechanisms involving the diffusion of water through a thick till layer are ruled out, such as a change in porosity or pore-water (or effective) pressure. We therefore interpret the cause of the seismic anomalies as due to a temporary decrease in saturation, and propose that such a change may occur quickly and reversibly following a lake drainage by a redistribution of the overburden pressure.

TABLE OF CONTENTS

LIST OF FIGURES

LIST OF TABLES

PREFACE

This thesis is a combination of two papers written for the Journal of Glaciology, presented as Chapters One and Two. They were submitted with the same main title as this thesis, followed by "Part I: Observations" and "Part II: Basal Morphology and Processes" respectively. I am responsible for their content and clarity as first author, but gratefully acknowledge the many useful discussions I had with my Committee Chairman and second author, Keith Echelmeyer.

Several changes were made to turn these papers into this thesis. The abstracts have been combined, reworded, put in the first person, and placed at the beginning of the manuscript. The references have also been combined, and placed at the end of the manuscript. The figure numbers for Chapter Two have been renumbered beginning with Figure 11 for continuity with Chapter One. Figures 1 - 10 are found at the end of Chapter One, and Figures 11 - 19 are found at the end of Chapter Two.

The text was not altered. This leads to some duplication of material as the Introduction to Chapter Two is essentially a recapitulation of the main findings of Chapter One. Also, references to "Nolan and Echelmeyer (submitted)" refer to Chapter One or Two depending on whether the reference is found in Chapter Two or One, respectively.

The decision was made to submit a substantial amount of material as appendices to these two papers rather than a third paper/chapter. These appendices primarily focus on the uncertainties in seismic wave speeds in ice and till and how this uncertainty affects the data analysis and interpretations. Including the material as appendices keeps it close enough at hand so that journal readers can evaluate it along with the main body of work if they choose, but separate enough not to slow down the pace for non-seismologists. I wrote an additional paper (Nolan and others, 1996), as part of my graduate studies, about seismic work done on Taku Glacier near Juneau. It was not included in this thesis because it distracted from its theme of temporal changes on Black Rapids Glacier.

ACKNOWLEDGMENTS

I am especially indebted to Dr. Keith Echelmeyer, who found me wandering about the Juneau Icefield and gave me a focus when I needed it. The many discussions I have had with him regarding both the ideas presented in this thesis and those that did not make the cut were always something I looked forward to. Likewise for discussions with my other Committee members: Will Harrison, Craig Lingle, and Doug Christensen.

I also gratefully acknowledge field assistance from Chris Larsen, who spent many, many hours exactly 1350 m away from me, when most of these data were collected. I also received much needed assistance in the field from Tony Gades, Howard Conway, Charlie Raymond, Karen Gaborik and Jon Roman. Thanks also to the National Science Foundation (Grant OPP-9122783) and the Geophysical Institute of the University of Alaska Fairbanks for supporting this research.

Lastly, I thank my parents. I aspire to match the patience and restraint they have shown in letting me choose my own path in life. I hope one day they will understand the choices I have made. And then explain them to me.

CHAPTER ONE: OBSERVATIONS

INTRODUCTION

An understanding of basal motion is essential to many studies of glacier dynamics, including those of ice stream flow, glacier surges, and seasonal and short-term velocity fluctuations. However, the difficulties of directly observing the basal interface have left the mechanisms of such motion obscure, and our understanding of the processes occuring at the bed is still far from complete. Boreholes, caves and tunnels provide a means to observe the bed on a local scale, but they are often logistically unfeasible, and can affect the dynamics. For instance, a single borehole is not a reliable indicator of the spatial extent of subglacial changes, and it may disturb the existing subglacial drainage system by introducing a new source for basal water. Aside from these localized measurements, the bed of a glacier can be investigated only after the ice leaves, or it may be imaged by geophysical methods such as electromagnetic or seismic sounding.

Seismic techniques have been used as a non-invasive method to investigate basal motion over large areas on a variety of glaciers. For example, passive seismic techniques have been used to measure the extent and nature of subglacial and englacial seismic events related to glacier motion on Ice Streams B and C (Anandakrishnan and Alley, submitted) and Variegated Glacier, Alaska (Raymond and Malone, 1986), as well as to monitor events related to iceberg calving (e.g., Wolf and Davies, 1986; Power and Echelmeyer, 1986). Active seismic measurements of ice thickness, using explosive sources, have been used to estimate the deformational component of glacier speed, and thus infer the component of motion at the bed, on Taku Glacier, Alaska (Nolan and others, 1995) and Jakobshavns Isbrae, Greenland (Clarke and Echelmeyer, 1996). Active seismic methods have also been used to investigate basal and englacial layer properties over extensive regions of Antarctica (e.g. Bentley, 1971). Similar

methods have been employed to determine the thickness, porosity, and effective pressure of subglacial tills* beneath Ice Stream B (Blankenship and others, 1987), as well as their spatial variation (Rooney and others, 1987; Atre and Bentley, 1993). Such measurements have also been made on Rutford Ice Stream, Antarctica (Smith, 1997). In a study similar to ours, seismic reflection methods have been used to observe changes that occurred between pre-surge and surge conditions at the bed of Variegated Glacier (Richards, 1988).

In 1993 we applied seismic reflection techniques to investigate changes at the bed of Black Rapids Glacier (Fig. 1) during its annual spring speed-up, and during subsequent short-term velocity fluctuations. This glacier was selected for study because it has a well documented history of large seasonal changes in basal motion (Heinrichs and others, 1996; W. Harrison, pers. comm.). These seasonal changes appeared to occur on a reliable schedule, and our intent was to study the nature and extent of concomitant changes at the bed by comparing the properties of reflected seismic waves before, during, and after this speed-up. The repeated measurements were made at a high temporal resolution to pinpoint the timing and location of basal changes, and thus to increase our understanding of the mechanisms of motion at the glacier bed.

Our study was part of a larger project in which researchers from the University of Washington (T. Gades and C. Raymond) conducted analogous radio echo sounding (RES) investigations, and the outlet stream of the glacier was monitored for hydrological parameters (Cochran, 1995). From mid-May to mid-July, coincident with the geophysical research, we surveyed ice-motion twice daily (including 3-D position and horizontal strain over 5 km); measured vertical strain and passive seismicity hourly near the survey site; monitored the outlet stream for stage, conductivity, and turbidity

* Following Paterson (1995), we use the term 'till' to refer to any unlithified basal debris, whether glacially-derived or overridden material, such as incompetent fault gouge beneath glaciers situated along major faults or marine sediments beneath tidewater glaciers.

using automated equipment; and occupied a stream-camp continuously for related studies. These data provide the background against which comparisons of the geophysical data will be made. In this paper we present only the seismic observations, focussing on their spatial and temporal changes. In Nolan and Echelmeyer (submitted; denoted as "N&E" (in journal form) and Chapter 2 (in this thesis)) we give an interpretation of these seismic observations in terms of subglacial morphology and the mechanisms of seismic change. The hydrologic data have been analyzed by Cochran (1995), and the radio echo sounding results are forthcoming (T. Gades, pers. comm., 1997).

BLACK RAPIDS GLACIER: MOTION HISTORY AND DRAINAGE EVENTS

Black Rapids Glacier is a surge-type glacier in the central Alaska Range. Much of it lies in an east-west valley along the Denali Fault, a major tectonic fault extending for several hundred kilometers through the Alaska Range. Motion along this predominantly strike-slip fault has placed granitic rocks adjacent to metasediments across the fault (Nokleberg and others, 1992) and has caused a loss of competancy of the rocks directly on the fault. It is interesting that three other large surge-type glaciers (Susitna, West Fork and Yanert) lie along this fault just to the west (Harrison and others, 1994); these glaciers appear to surge every 50 to 70 years (Clarke, 1991).

The glacier is about 43 km long, with an area of 246 km^2. It flows from an elevation of about 2500 m to a terminus at about 1000 m, with an average surface slope of about 2.3° (Heinrichs and others, 1996). Centerline ice thickness is about 630 m near our field site (Fig. 1a). The glacier is temperate (Harrison and others, 1975), and it is situated in the cold, dry continental climatic regime characteristic of interior Alaska.

Black Rapids Glacier last surged in 1936-37 (Hance, 1937), and relic moraines indicate that previous surges have crossed the current location of the Trans-Alaska

Pipeline and a major highway (Reger and others, 1993), closing off the valley and damming the Delta River (Fig. 1a). Since its last surge the glacier has thinned by up to 220 m near the terminus, while thickening by about 50 m on the upper glacier (K. Echelmeyer and W. Harrison, unpub. data, 1996).

Average centerline surface speeds in the neighborhood of our field site are about 55 to 65 m a^{-1} . Based on a 20-year record of surveying (Heinrichs and others, 1996) and 15 years of time-lapse photography (W. Harrison, pers. comm.), we know that the average annual velocity in the region between 14 and 20 km (Fig. 1) varies by about 50% (30 m a^{-1}), possibly periodically. The seasonal fluctuations in speed mentioned above are superimposed on these longer term variations, with speeds in spring and early summer being about 100 to 300% faster than those in winter, as averaged over a few weeks. The spring transition in speed occurs abruptly within about a day, and the velocity generally remains high for two to four weeks. Afterwards there is a slow decay to a minimum in late summer, followed by a gradual increase through the winter. This spring speed-up usually occurs between 1 to 10 June. All of these variations in speed are due primarily to changes in basal motion (Heinrichs and others, 1996).

Unfortunately, in 1993 the spring speed-up occurred about two and a half weeks earlier than expected (May 22), on the day that our seismic monitoring began. During the subsequent measurement period, however, we observed three jökulhlaups* upglacier of our monitoring site. Associated with each jökulhlaup was a period of increased glacier speed, with up to a fourfold increase in speed during each event, as well as up to 15 cm increases in surface elevation (Fig. 2). The high speeds lasted about a day each, while the elevation changes varied in duration (Fig. 2). Such events appear to be annual phenomena (Sturm and Cosgrove, 1990; Raymond and others, 1996;

* Here we follow Paterson's (1995, p. 127) definition of 'jökulhlaup': 'the sudden and rapid draining of a glacier-dammed lake or of water impounded within a glacier', and use 'drainage event' to include all survey, seismic, and hydrologic anomalies apparently caused by a jökulhlaup.

Truffer and others, 1996). For a period of about 45 days encompassing these events, we made nearly daily seismic reflection surveys of one section of the bed that was affected by these transient water inputs. This paper describes the seismically detected changes at the bed that occured during these events.

The three jökulhlaups varied in size, location, drainage method, and glacier-dynamic effects. We observed the first and third jökulhlaups, located at ice-marginal lakes on the north side of the valley (labelled I and III in Figure 1), and afterwards completed maps of their empty basins. About 10^6 m^3 of highly turbid water drained from each. The second jökulhlaup, located at a supra-glacial pothole (II, Fig. 1), was neither directly observed nor was its basin surveyed afterwards. No more than about 10^5 m^3 of clean meltwater drained from this pothole, but other nearby potholes may also have drained at the same time. Details of these events will be provided in a later paper; we introduce only as much of these data as is necessary herein.

SEISMIC BACKGROUND AND METHODS

Wave types and speeds

Seismic waves are characterized by the type of particle motion they induce through a medium (Fig. 3). The direction of particle motion for compressional (P) waves is the same as wave propagation, whereas for shear (S) waves it is perpendicular. S-wave particle motion can be decomposed into vertical (SV) and horizonal (SH) polarizations. Rayleigh waves (or 'ground roll') only travel along the ice surface and are are considered to be coherent noise in this study.

Upon reflection of a P-wave at non-normal incidence, some of the incident energy is converted to SV motion (Fig. 3), and vice versa. SH motion does not undergo such conversion. Unlike P-waves, S-waves are often difficult to generate with explosives, and thus converted P-to-SV (P-SV) reflections may be the only means to study S-wave response. This was true in our study: no useful S-waves were

generated by our sources. In addition to these reflected and converted waves, direct P- and multiple P-wave reflections are often observed in seismic studies on glaciers.

The speeds of P- and S-waves, V_p and V_s, respectively, in temperate ice are not well constrained. They are sensitive to the amount of liquid water at the grain boundaries (Roethlisberger, 1972). The speeds in colder ice, where little water is present, are much better determined. The wave speeds for temperate ice that we use in this paper were derived from data obtained during our project, as described in Appendix A. The results are presented in Table 1. In particular, we found an average P-wave speed of $V_p = 3704$ m s^{-1}, which is at the upper end of the range recommended by Roethlisberger (1972, p. 20) of 3600 to 3700 m s^{-1}.

Table 1. Wave speeds, densities and wavelengths for various media. Wavelengths are calculated assuming 80 Hz, the dominant frequency of our reflections. Ice values are discussed in Appendix A. Rock values are those given by Richards (1988). Till values (except wavelength) were measured by Blankenship and others (1987) on Ice Stream B. The maximum and minimum values refer to the effect on the reflection coefficients.

Media	V_p m s^{-1}	V_s m s^{-1}	Density kg m^{-3}	Wavelength m
Ice	3704	1850	910	46
Rock	4200	2600	2700	53
Water	1412	0	1000	18
UpB till, max	1700	130	2000	21
UpB till, min	1400	160	2000	18

Experimental design

In his study of the 1982 surge of Variegated Glacier, Richards (1988) showed that P-SV reflections would change polarity in response to the development of water layers as

thin as 0.1 m, whereas P-P-waves would remain virtually unaffected. Such thin water layers are hypothesized to occur in a system of linked cavities over a wide area during surges (Kamb and others, 1985) and may exist beneath part of Black Rapids Glacier during non-surging flow (Raymond and others, 1996). Since we expected the changes causing the spring speed-up to be related to increased water at the bed, our experimental set-up followed Richards' emphasis on recording P-SV reflections. However, instead of seismic recordings made almost a year apart (pre-surge and surge conditions), we made daily measurements, allowing us to observe changes over the short time intervals inherent in spring speed-ups.

Recording P-SV reflections requires large shot-receiver offsets because the conversion is weak at near-normal incidence. To accommodate such large offsets, we placed the shot-reciever axis in the direction of glacier flow, near the valley centerline (Fig. 1). Our shot-receiver offset was chosen so that we would clearly record P-SV reflections, as well as direct, reflected and multiple P-waves, without significant interference from the ground roll. The smallest offset which met these criteria was 1350 m, giving nominal incidence angles (θ in Fig. 3) of 45 to 55° for the reflections, as discussed below (Fig. 1b). The actual shot locations varied within a 5 m radius of 1350 m to avoid excessively fracturing the ice at a single location and thereby potentially changing the source characteristics among the approximately 100 shots taken there.

The seismic data were recorded using a 12 channel Bison 7012 seismograph, with a 0.25 or 0.5 ms sample rate, and a record length of 0.5 or 1 s, respectively. High frequency geophones, with a linear response from about 14 to 400 Hz, were used throughout the study. Shots were typically 0.7 kg of nitro-glycerine based explosive (tradenames: Gelmax or Unimax), and were placed about 1.5 m below the ice surface. As a potential alternative to dynamite, we experimented with a sled-mounted 'Thumper' unit, which used an enormous rubber band and hydraulic pistons to slam a weight onto a metal plate on the ice. This system did not release enough energy into the ice to create usable results even with multiple stacking of the records. Radio triggers

provided the timing between shot detonation and seismograph recording; these were the cause of variable and intermittent timing delays, as described below and in Appendix B.

Both vertical and horizontal geophones were deployed. The vertical geophones are optimal for recording P-waves, and the horizontal geophones, oriented parallel to the shot-receiver axis (a 'radial' orientation), are optimal for SV waves (Fig. 3). Two parallel cables of 12 geophones each (one of vertical and one of horizontal geophones) were deployed such that one geophone from each cable was placed in each of 12 snow pits, directly on ice. The pits (initially 2.5 m deep) were about 27 m apart, yielding a total spread length of 300 m. Other than occasional resetting due to snow and ice melt, and occasional reorientation of the horizontal geophones to record SH waves, the geophones remained undisturbed for the duration of the study. The geophones farthest from the shot (1650 m offset) are labelled as geophones 1V and 1H, for the vertical and horizontal cables, respectively; those closest to the shot (1350 m offset) are 12V and 12H.

There were primarily two types of seismic data collected for this study; we refer to them as the daily and longitudinal data sets. The daily set consists of 38 and 44 records from the vertical and horizontal geophone cables, respectively, all with a nominal offset of 1350 m from geophone 12. We attempted to make one record per day on each cable; bad weather, misfires, and timing errors account for the different number of measurements. As our emphasis was on recording P-SV waves, we made the horizontal measurements first. If the timing was bad, we sometimes opted to make a second measurement with those geophones. Such was the case on Day 175, and this resulted in a very fortuitous experimental result, as described below. The longitudinal data set consists of a total of four longitudinal sections for each of the two geophone orientations, collected at different times throughout the summer. These longitudinal measurements were made by leaving the geophones in place at their "daily" locations, and moving the shot down-glacier in 300 m increments (one geophone-spread length)

for a maximum offset of 4500 m from geophone 12; the sections varied in number of shots and longitudinal coverage. The objective of the longitudinal data was to better identify the type of waves, the wave speeds and the location of the reflectors, as well to constrain the longitudinal extent of any subglacial changes.

Two types of timing errors affect our results. Our data collection suffered from a variable and intermittent delay that caused the seismograph to turn on 0 to 150 ms after shot detonation. This error affected both daily and longitudinal data sets. The accuracy of any analyses that compare records from two or more shots is, therefore, limited by our attempt to shift each record to the common-zero time of shot detonation. We used a combination of techniques for this shifting, as described in Appendix B, and we estimate their combined accuracy to be ±1 ms. As a simple means to provide timing synchronization between the daily horizontal and vertical shots, albeit in a limited way, we traded one horizontal geophone for a vertical one at location 12. Thus each cable had 11 geophones of one orientation and one of the other. This allowed us to correct for any timing shifts due to the shape of the recorded waves.

Once the seismograph was triggered, the timing accuracy was limited only by our ability to distinguish the signal (e.g., arrival times and amplitudes) from the noise. We did this digitally, and believe such measurements are accurate to ±1 ms. The seismic data were filtered with a 32 to 1000 Hz bandpass filter prior to recording in an effort to minmize the effects of the low frequency ground roll.

WAVE IDENTIFICATION AND REFLECTOR MIGRATION

We were able to identify the type of waves present by comparing the arrival times of the observed waves along the geophone spread (the so-called 'moveout') to theoretical time-distance curves (also known as traveltime curves). Preliminary identification was made in the field using a normalized time-distance chart (Roethlisberger, 1972). The seismograms in Figure 4 are examples of our longitudinal data. The superimposed

time-distance curves were calculated using a simple geometry with ice of a uniform thickness over bedrock. We used these curves to identify the most coherent P-P, P-SV, and multiple P-P (P-P P-P) waves in the seismograms, as well as the direct P-wave and ground roll. (Here P-P denotes an incident P-wave reflected as a P-wave.) As can be seen in these figures, there are several waves of each type in the longitudinal sections. They come from different parts of the valley bottom and walls, as identified below. This multitude of different waves is a feature of seismic reflection studies on valley glaciers, due to the bed's curved shape, and is not commonly found on ice sheets.

We interpret the converted reflections as P-SV rather SV-P (both would have the same moveout for a parallel ice surface and bed) because they have a larger amplitude on the horizontal geophones (Fig. 4a). Additionally, no direct or reflected S-waves were recorded, and it is probable that no S-waves (or only very weak ones) were generated by our source.

Several coherent P-P and P-SV waves in show up on only limited sections of the records, and some are unaccounted for by time-distance curves (Figure 4). In addition, the correspondence between the labelled waves and their respective time-distance curves is not exact because the subglacial valley, which comprises the envelope of the reflectors, is characterized by ridges and troughs, not the smooth, flat surface we assume for calculations.

Knowing the locations of the reflectors, especially those seen in the daily records, is essential for a complete glaciological interpretation of any observed changes in them. For example, are the different P-P reflectors located beneath each other, or are they spread across the width of the valley? Our simple traveltime model yields only a reflector's distance measured perpendicular to the shot-receiver axis. The location itself is unconstrained in the transverse direction because even though the shot, the geophone array, and the reflector all must lie within a single plane, that plane may not be vertical. This again is a significant difference between seismic investigations on valley glaciers and those on ice sheets. We need further information from outside this

plane to determine the three-dimensional locations of the reflectors (so-called 'migration') within the glacier valley.

One method we used to obtain this three-dimensional information was to make seismic shots with a portion of the geophone array aligned transverse to glacier flow, giving the array an 'L' shape. (These were made before the geophones were fixed in their permanent "daily" positions.) Because the P-P-waves overlapped, we could not pick arrival times that were accurate enough to invert for location (P-SV waves cannot be uniquely inverted). However, the effects of varying the shot location while recording on the 'L' arrays indicated that at least three of the P-P-waves (labelled N, C, and S in Figure 4) are the result of focussing - that is, the concavity of valley walls concentrates reflections from widely separated reflectors located on the valley bottom and walls toward the geophones.

We next applied foward modelling techniques as a means of migration. Ray tracing provided information on the longitudinal position of the reflectors. The tranverse position of the reflectors was determined by comparing the radial distance of a reflector measured on the time-distance curves (Fig. 4) to a transverse cross section of the study area, measured by seismic reflections and radio echo sounding (RES). These techniques are not fully three dimensional (we only have a linear array), but they do give an estimate of the three-dimensional location of the reflectors which utilizes the partially known geometry of the glacier valley. The limited accuracy of these techniques makes it difficult to positively identify any reflections arising from the lower interface of a subglacial till layer (if present), as could be done by Blankenship and others (1987) using the seismic records from Ice Stream B.

Applying geometric ray tracing methods within a longitudinal section of the glacier (i.e., imposing Snell's Law at the reflector) leads to the results shown in Figure 5. In this vertically exaggerated figure the approximate longitudinal locations of the daily P-P, multiple P-P, and P-SV reflectors are shown, as obtained by tracing the first arrivals of each type of wave to each geophone. The bed was specified by RES and the

glacier surface by surveying (T. Gades, pers. comm., 1994); RES data works well for this purpose because of its high spatial resolution. This migration is only strictly valid for reflectors located along this centerline profile. It indicates that the reflectors are distributed over a 1300 m length of the bed, and that the irregular bottom, combined with the large shot-receiver offset, results in reflectors for the different wave types that do not overlap. Therefore, comparisons of changes in P-P and multiple P-P reflections, for example, require caution because they represent different parts of the bed and the reflectors may be affected differently as subglacial conditions change. The P-P reflections come from a section of the bed about 650 m downstream of geophone 12. The P-SV and multiple P-P reflectors, unlike the P-P, are unevenly spaced compared to surface spacing of the geophones, and they may lie on both the lee and stoss sides of bumps in the bed, as shown in Fig. 5. Again, since such reflectors might be affected differently, two geophones 27 m apart on the surface may be recording changes within two independent subglacial regimes. As we will later show, the measurements of both P-SV and multiple P-P-waves reveal that some of the reflectors were in fact topographically discontinuous and each region was affected differently.

The transverse positions of the different reflections were determined using a cross-section of the valley measured at the approximate location of the P-P reflectors shown in Figure 5, 650 m downglacier from geophone 12. This transverse cross-section (Fig. 6) was determined from a combination of RES measurements from 1993 (T. Gades, pers. comm., 1994), seismic measurements made in 1993 and 1996 (migrated using techniques of Clarke and Echelmeyer, 1996), and hot-water boreholes drilled in 1996. The radius of each of the three semi-circles in this figure is equal to the distance from the shot-receiver axis to the three P-P reflectors N, C, and S labelled in Figure 4; they are the loci of all possible locations for each of the reflectors (assuming travel through ice only). Note that the annotated distances are not depths, instead they are distances from the shot-reciever axis at the ice surface. Barring any unlikely englacial reflectors, reflection N (corresponding to a distance of 540 m) is

unambiguously located about 350 m north, and 100 m above, the deepest part of the bed (Fig. 6), at a depth of about 500 m.

The locations of the two other P-P reflectors, C and S, are more ambiguous because their loci have two intersections with the bed. From Snell's law, we know that the tangent to each circle must be parallel to the transverse slope of the bed for a reflection to be recorded. Figure 6 shows the intersections that best meet this condition for reflectors C and S. This figure shows the significance of labelling these reflections N, C, and S - North, Center and South (or, PP_N, PP_C, and PP_S). Reflection PP_C comes from the center of the valley at a depth of about 600 m, and reflection PP_S probably comes from a point about 350 m to the south of the centerline at a depth of 550 m. There is the possibility that one or both of these waves could have traveled through a subglacial layer that has a slower wave speed (e.g., till, Table 1) for part of its path. In that case, the radius of its reflection locus would be decreased somewhat. On the other hand, if these reflections came from the top of a subglacial layer, other reflectors could be beneath; such reflections are impossible to identify confidently, yet they would contribute to the complex suite of P-P reflections shown in Figure 4.

The angles of incidence of these P-P reflections at the subglacial interface are important for later interpretion (N&E). Because of the large shot-reciever offsets and the measured ice thickness, we expect these angles to be about 45 to 50°, which cannot be taken as "near normal" (i.e., zero) incidence in any analysis. To obtain a more accurate value for the angle of incidence for reflection PP_N, we utilize the moveout of its unobscured arrival times to calculate the slope of the basal interface relative to the surface following the migration procedures developed by Clarke and Echelmeyer (1996). This method shows that reflector PP_N was inclined upward about 2°. This implies an angle of incidence of about 49 to 54° for the rays reaching geophones 12 to 1, respectively. The incidence angles for reflection PP_C were estimated from ray tracing (Fig. 5), and were in the range 47 to 53° across the geophone line. For PP_S, they were estimated to be 44 to 49° .

The traveltime of the brightest P-SV reflection (labelled in Fig. 4) corresponds to a distance of about 620 m from the shot-receiver axis, implying that this reflector is probably located near the deepest point of the cross-section, similar to reflector PP_C. An earlier, unlabelled P-SV reflection, with a 550 m distance, is probably located along the northern valley wall at a location similar to PP_N in the cross-section. Again we note that these P-SV waves need not come from the same reflector as the corresponding P-P returns, as shown in Figure 5a.

There are two multiple P-P-waves with similar arrival times (620 m and 630 m from the shot-receiver axis), distinguishable only because sometimes one changes and the other does not (shown most clearly in Figure 7 and on the daily seismograms, Fig. 9, described below). There are at least two geometric possibilities for each wave: its two reflectors are located near deepest part of the valley (e.g., Fig. 5), or the two are located on opposite walls of the valley near PP_N and PP_S (Fig. 6). Of the two possibilities, the former is the only one that we can geometrically verify with ray tracing; the latter is speculative. The difference in arrival time between the two different multiples could also result from the later one travelling through a slower subglacial layer. The uncertainty in both the wave speeds and subglacial topography prevent us from distinguishing these possibilities.

We also observed a refracted wave in the longitudinal section with the farthest shot offset (4500 m). This indicates that the ice is underlain by a medium with a faster P-wave speed, such as any of the metamorphic and granitic rocks found in the area. This wave travels along the interface at the wave speed of the lower medium. Due to poor signal to noise ratio, curvature of the valley, and the possibility of low velocity till layers, we can only constrain V_p of this lower medium to be 4500 ± 500 m s^{-1}, which is about what we expect for the local rock types.

To summarize, our analysis shows that there are three prominent P-P reflections: the one labelled PP_N comes from the north side of the valley about 100 m above the deepest part of the channel (500 m depth), the one labelled PP_C comes from

the near deepest part of the channel (about 610 m) near its centerline, and the one labelled PP_S from the south side at a depth of about 550 m. There are also relatively strong P-SV and multiple P-P reflections that probably come from the deepest part of the channel and, in the case of one of the P-SV waves, from the north side. It is the temporal changes in these reflections, particularly PP_N, that form the basis of our analysis of the basal morphology of Black Rapids Glacier in N&E (Chapter 2).

TEMPORAL CHANGES IN SEISMIC DATA

We observed reflections from the same locations on the bed (e.g., PP_N, PP_C, and PP_S) on a daily basis for about six weeks from 20 May (Day 140) to 5 July (Day 186). The daily records were examined to determine what changes, if any, occurred in the various reflections from the basal interface(s) throughout the study period. Because of the large number of individual traces and the fact that some of the observed changes were relatively small, we had to develop analysis methods that would clearly illuminate the trace-to-trace differences. These methods are discussed next, after which the results are presented.

Analysis methods

All of the daily traces from a particular geophone were initially 'gathered' as in Figure 7 and visually inspected for differences. Clearly erroneous or noisy traces were eliminated. Since neither the absolute timing (due to faulty triggers) nor the absolute amplitudes (due to variable source coupling) could be compared directly between traces, both of these values were then normalized using another wave in the same trace. However, it should be noted that source coupling was remarkably uniform throughout the study period, as can be seen in Figure 7, and this normalization was minimal. Quantitative comparisons of the changes in arrival time (e.g., Fig. 8a) and amplitude were then made. This was done with most combinations of the direct, reflected (P-P

and P-SV), and multiple waves, realizing that normalizations using reflected waves are of questionable validity because their reflectors are at different locations.

Cross-correlating daily records was another effective way to quantitatively characterize their similarity. The set of daily traces at a given geophone was analyzed by comparing: 1) every trace with every other trace, 2) every trace with a single 'typical' trace, 3) every trace with the average of all the traces at that geophone, or 4) each trace to the preceding trace. Different effects were illuminated by each method. Figures 8b and c are examples of the fourth cross-correlation method -- comparing each geophone's recording to that of the preceding day. The mean correlation over all twelve geophones for each daily record is shown.

Digitally overlaying two records often proved to be the most useful technique for determining the nature and extent of the differences between them, particularly on days when large-scale changes occurred at the bed. On such days, comparisons of the amplitude of a particular wave had little value because it was often not clear if the same reflections were still being compared. Examples of such a comparison are shown in Figure 9.

In undertaking these analyses, we found that there were two major categories of daily records, which we label as 'normal' and 'anomalous'. Although there was some variation between the records within each category, the two categories are well distinguished. For most of the summer, the records were nearly identical, with only minor variations. The similarity in waveforms throughout the summer can be seen in Figure 7, which shows all of the daily traces for geophone 10H. Most of these traces show very few changes in amplitude or timing throughout the summer; these are the 'normal' records. Only those associated with the drainage and motion events are 'anomalous'; they occurred on Days 165-167, 169-171 and 175. At first glance, the differences between these two record-types are not large, but they are significant. We first describe the features of the normal records as these will be useful for illuminating the anomalous features of the second category.

Features of the normal records

There were no trends in arrival times for the various waves in the normal records. Figure 8a shows the difference in arrival time between the direct P-wave and PP_N for all horizontal geophones, along with their mean for each seismogram (heavy circles). This pattern is typical of both vertical and horizontal geophones. The standard deviation of these means (not including the outliers) is about 2 ms, which is about the combined accuracy of our picking ability. The prominent outliers in this figure are associated with anomalous records. The apparent scatter of individual traces about the mean for a particular day is real – the moveouts of the direct and reflected P-waves are not the same, so each geophone records a slightly different time difference.

In general, there were few trends in the amplitudes of the various waves in the normal records. Those trends that we did identify were only apparent on the horizontal geophones; the vertical geophones showed almost no coherent changes. These include: 1) the P-P to P-SV amplitude ratio gradually decreased throughout the summer; 2) the ratio of P-P to multiple P-P increased after the second jökulhlaup (Day 169), primarily due to a change in the multiple P-P; 3) the P-SV to multiple P-P amplitude ratio increased after Day 169; and 4) in general, most of the amplitude ratios show more scatter after Day 169. Here P-P refers to reflection N, P-SV to the 620 m P to SV reflection, and multiple P-P to the most prominent (630 m) P-P-wave multiple. We might expect to find some variations as the geophones were displaced relative to the bed by glacier motion throughout the study period (a total of about 12 m), yet such changes are impossible to predict. However, using the cross-correlation techniques above, we can distinguish the effects of such daily motion from those related to changes in basal conditions.

Applying the second cross-correlation approach above, namely selecting one particular day as a standard for comparison, reveals that the greater the time interval between two records, the more dissimilar they were (that is, their correlation coefficient was reduced). This trend was linear with the number of days between the records, and

thus was not related to temporal variations in basal conditions. It is probably caused by the changing location of the geophones relative to the bed, as well as to the gradual increase in ground-roll wave speed as the snow melted, which would cause a decrease in correlation between records spaced further apart in time. The third technique, comparing each trace to the average trace, accounted for this bias, although this suffered from using a somewhat artificial standard for comparison.

The fourth technique of cross-correlation, that of comparing each trace to the previous one, highlights the difference between successive records, and is not affected by the daily motion. Results of this correlation over the study period for the vertical and horizontal geophones are shown in Figures 8b and 8c, respectively. Most of the records have a cross-correlation coefficient with the previous record of 0.75 or higher; these 'nearly identical' records are the normal ones. There is somewhat more variation in the horizontal geophone records.

There are several 'normal' records that have a cross-correlation coefficient less than 0.75, but they each have extenuating circumstances. For example, records from Days 144 and 146 have a poor ice-shot coupling and all waves -- including the direct P-wave and ground roll – are of a lower amplitude, as can be seen in Figure 7. This lower amplitude causes slight differences in waveforms, and thus a weaker correlation. Measurements made on Days 180 and 184 have low coefficients because several of the geophones on each geophone cable were temporarily switched or reoriented to study local effects, causing some traces to be inverted (Fig. 7). Inspection of these records using overlays reveals that they too are 'normal' once these experimental discrepancies are accounted for.

Overlays of two such normal records highlight their similarity (Fig. 9a). The cross-correlation between the two records overlayed in this figure was about 0.9; no amplitude scaling was applied. This shows that the source/ice coupling was nearly equal for the two records, as was typical throughout the summer.

Features of the anomalous records

There were only three periods throughout the summer when significant changes in the seismic reflections were observed. We refer to these as anomalies I, II, and III; each corresponds to one of the three lake drainage events. Unfortunately, no longitudinal cross-sections were made during these events and therefore none could be used to constrain their longitudinal extent.

Anomaly I: There were several changes associated with the first jökulhlaup, on Days 165-167. In Figure 9b, which compares Day 166 (anomalous) to Day 159 (normal), reflection PP_N was unaffected (Figs. 7 and 9b), but there were minor changes to PP_C and larger changes to PP_S, particularly on the horizontal geophones. The latter appears to have changed polarity, but this finding is somewhat ambiguous.

The early multiple (corresponding to a distance of 620 m from the shot-receiver axis, immediately preceding the time-distance curve labelled 'P-P P-P: 630 m' on Figure 9b) also appears to have changed polarity following the first drainage event. The later multiple appears only slightly shifted, with perhaps a minor increase in amplitude. The changes in these multiples were smaller on the horizontal geophones, partly due, perhaps, to the fact that these P-waves were much clearer on the vertical geophones. Minor changes were observed on the horizontal geophones for the 620 m P-SV wave.

Anomalies II and III: Seismic anomalies were observed following the second and third jökulhlaups as well. The changes from the normal records were more prominent than those observed during anomaly I. It appears that each of the three P-P reflectors were affected, as well as the multiple P-P and P-SV waves; these reflectors span the entire 700 by 1300 m study area (Figs. 5 and 6). These anomalies, on Days 169, 170, and 171 and then on Day 175, were nearly identical to each other despite being separated by normal records on Days 173 and 174 (Figs. 9c, d, and e), so we discuss their

changes together. Two measurements were made using the horizontal geophones during the early part of third lake draining event: the first was anomalous and the second, 36 minutes later, was completely back to normal (labelled Day 175.688 and Day 175.713, respectively, on Fig. 7). There are several interesting features of these anomalous records, and it is these anomalous features that give us the most definitive constraints on the changing morphology of the basal interface.

The first P-P arrival on these anomalous records was about 10 ms later than normal (Figs. 7, 8a, and 9c; no data points exist for days 170 and 175.688 on Fig. 8a because no direct P-wave was recorded due to timing errors). *This first P-P arrival no longer originates from reflector N.* If it did, the 10 ms increase would then require that either the ice thickened by over 17 m in one day, or that the bulk-ice wave speed temporarily dropped by almost 150 m s^{-1}, while the near-surface wave speed remained constant. Neither scenario is plausible, especially given the 36 minute time constraint. This new first arrival may be from a new reflector or simply a second arrival in the normal records; alternatively it may be from the bottom of a basal layer beneath reflector N (implying that reflector N is at the top of a basal layer).

Most of the subsequent reflections during anomalies II and III are also uncharacteristic of the normal records. Several of the P-P-waves seem to be phase-reversed from those on the normal records, and they have changed in about the same manner on both the vertical and horizontal geophones. Of all the P-P-waves, reflection PP_C, from near the deepest part of the valley, appears to have changed the least.

The change in the P-SV waves is different on the two orientations of geophones. On both, the first peak of the earlier P-SV wave (corresponding to about 550 m distance from the shot-receiver axis) decreases to near zero amplitude and the next peak may be phase reversed. The second P-SV wave (620 m distance) remains essentially unchanged in amplitude or phase on the horizontal geophones, while it is somewhat phase shifted on the vertical geophones. These two waves display complex structure. For example, the shape of the anomalous 620 m P-SV wave (Fig. 9c)

sometimes has two peaks without an intervening trough. This effect can only be caused through superposition of more than one wave; interpretation of such changes will be ambiguous. The changes to both P-SV waves is more pronounced on the geophones closest to the shot, suggesting that the reflectors for different geophone arrivals are located in different subglacial regimes along the bed. This possibility is also suggested by Figure 5.

Significant changes were also observed in the P-P multiple waves. On both the horizontal and vertical geophones, the later-arriving, more prominent multiple appears to have changed polarity and possibly increased in amplitude. The earlier multiple does not seem to have change significantly on the vertical geophones. Changes in polarity and amplitude are apparent on the horizontal geophones with offsets between 1450 and 1650 m, but not on the closer ones. Similar to the P-SV waves, this suggests that this multiple results from discontinuous reflectors that are affected independently.

There are only minor differences between the anomalous records from Days 169, 170, 171 (event II) and Day 175.688, as is shown by example in Figure 9e and the cross correlations in Figures 8b and 8c. The anomalous record from Day 175 in Figure 9e is missing the direct P-wave arrival because of timing errors, but it has been shifted properly and is nearly identical to the anomalous records from the previous event. Each of the reflections returned to normal after events II and III, except for the 620 m P-SV wave, which continued to have a slight phase shift during the interval between the two events. That these two anomalous records are separated in time by three normal daily records and yet are nearly identical indicates that the basal conditions existing after the second and third jökulhlaups, which came from different lakes, were similar over much of the bed and that the changes are the result of similar processes.

It is significant that the seismic records during event I were only slightly changed from normal ones, while those during events II and III were markedly different, especially given the magnitude and timing of the associated glacier motion events, as is discussed in the following section.

CORRELATION OF DRAINAGE, SURVEY AND SEISMIC MEASUMENTS

The sequence of drainage events, seismic anomalies, increased motion, and surface elevation change is shown in Figure 10. This figure allows us to constrain the duration of the seismic anomalies, assuming that no changes occurred between our measurements. As we will discuss, this assumption should be regarded with caution. We use the initiation of the jökulhlaups as a minimum estimate for the initial time of a seismic anomaly.

The initiation of each jökulhlaup can be estimated fairly accurately. In the early afternoon of Day 164 we observed water from the first lake draining through a channel cut into its bank. This muddy water travelled downglacier along the ice surface, filling several small lakes bordering the moraine of a tributary glacier, before entering a moulin. We estimate that the water first reached the bed by Day 164.6 ± 0.1 days, at the earliest. The second jökulhlaup was not observed, but we did find a freshly-drained supra-glacial pothole a day later; automated camera data indicates that several such potholes may have drained simultaneously (W. Harrison, pers. comm.). Our survey data shows that increased motion associated with this jökulhlaup began as early as Day 168.5 and certainly by Day 169.3. We closely observed the third jökulhlaup, which emptied water directly into a tunnel at the lake bottom, and estimate drainage onset at Day 175.1 ± 0.2 days. These estimates are shown in Figure 10 as vertical lines.

All of the seismic records measured during the three days of the first drainage event showed some variation from normal (shown with an 'x' in Figure 10). Although the next lake drainage event occurred before the records returned to normal, we assume that this first anomaly was reversible because records following anomalies II and III were back to normal. Thus, we estimate the minimum duration of anomaly I as the time between the first anomalous record and the last record before the second jökulhlaup (2.1 days), and the maximum duration as the time between the initiation of the first and second jökulhlaups (3.9 days) (Fig. 10). The last anomlous record during

event I was obtained at least one day *after* the period of increased basal motion had ended (Fig. 10).

Several seismic records obtained after the second jökulhlaup began were anomalous ('*' in Fig. 10); they were followed by normal records until the initiation of the third event. We estimate the minimum duration of this second anomaly as the interval between anomalous measurements (1.9 days), and the maximum duration from the initiation of draining to the next normal record (4.4 days). Our first anomalous seismic measurement during this event occurred after the increase in motion began, but we continued to record anomalous measurements for another full day *after* the glacier speed returned to the pre-drainage magnitude (Fig. 10).

The third seismic anomaly was recorded during the early stages of the third jökulhlaup, but ended *before* the increase in basal motion began (Fig. 10). We have only one seismic record during this anomaly ('*' in Fig. 10 on Day 175.688), and we therefore estimate its maximum duration as beginning at drainage initiation and extending to the next normal record (0.6 days). If we assume this anomaly began immediately prior to its measurement and ended immediately prior to the next (normal) measurement, the actual duration could be as little as 36 minutes. However, as the record following the anomalous one was completely back to the normal state with no hysteresis, it seems possible that the transitions between states could take even less than 36 minutes.

That we have unequivocal measurements of transitions occurring over about one square kilometer of the bed in less than 36 minutes is an unexpected result. It indicates that our daily seismic sampling interval was too coarse to measure all the potential changes that may have occurred and that, at least following jökulhlaups, this interval could justifiably be decreased to fifteen minutes during jokulhaups.

The number of processes that can affect such a large area so quickly and reversibly is limited, and these timing constraints are important for interpretation in terms of basal morphology (N&E; Chapter 2). A further constraint to be considered is

that, while the lake drainages appear to have caused both the seismic anomalies and the increased motion, the two effects may result from different processes as they often do not strictly overlap, as shown in Figure 10.

CONCLUSIONS

We recorded seismic reflections from the bed of Black Rapids Glacier for a period of 45 days in spring 1993. During that period there were three lake drainage events from separate lakes upglacier of our measurement site, and during each event the glacier speed increased dramatically. After these jokulhaups, each of which lasted about a day, the glacier speed dropped back to the springtime level. The seismic records from before, during and after these events show the following:

1) Most of the measurements were nearly identical. The only measurements which showed significant variation were immediately following jökulhlaups that also caused increased glacier motion. Thus, seismic reflection methods can be used to investigate changing subglacial conditions that relate to variations in glacier speed. The spatial scale of these reflectors is much larger than that sampled by individual boreholes. It should also be noted that changing surface conditions, such as the amount of meltwater present or small amounts of normal glacier motion, do not affect the seismic reflection data.

2) Two of the seismic anomalies, resulting from jökulhlaups from different locations on the glacier, were identical. In both cases, the anomalous measurements returned to nearly identical pre-anomalous forms within two days or less.

3) The transition from the anomalous state to the normal state can be rapid, lasting less than 45 minutes, but the anomaly itself can persist for several days. The transition from normal to anomalous can only be constrained to within about a day.

4) Each of the three jökulhlaups caused both a seismic anomaly and rapid glacier motion, but the seismic anomalies were detected before, during, and after the periods of increased motion. The pattern of overlap for the three events was not the same, however. The seismic anomalies generally persisted longer than the corresponding surface drainage events, but our temporal resolution is insufficient to illustrate the details.

The most important specific changes in the seismic records were:

i) The first P-P reflection disappeared during two of the events, then returned to normal. This reflection comes from a location which is about 100 m above the deepest part and on the north side of the glacier valley (PP_N in Fig. 6).

ii) The P-P reflection that comes from the deepest part of the valley cross-section (PP_C in Fig. 6) showed the least change of any reflection.

iii) The P-SV reflection coming from a location near P-P reflector PP_N decreased in amplitude to near zero during the second two anomalies. The P-SV reflection from the deepest part of the valley (near PP_C in Fig. 6) did not show strong changes on the horizontal geophones, but it did on the vertical ones.

iv) During the second two anomalies the 630 m P-P-wave multiple (most likely from the deepest part of the valley cross-section) showed clear phase reversals.

The seismic results impose stringent constraints on the changing properties of the bed: the bed must be able to change rapidly and reversibly over a fairly large region. These changes are related to the abrupt and substantial increases in basal motion because both result from the jökulhlaups, but the relationship between motion and basal conditions is unclear. In a second paper in this issue (N&E; Chapter 2) we investigate what changes in basal morphology can lead to the observed seismic changes.

Figure 1a. Location map for Black Rapids Glacier, Alaska. The glacier is shown with its centerline coordinates, beginning with '0 km' at the head. Lake locations are numbered in the order that they drained in the summer of 1993.

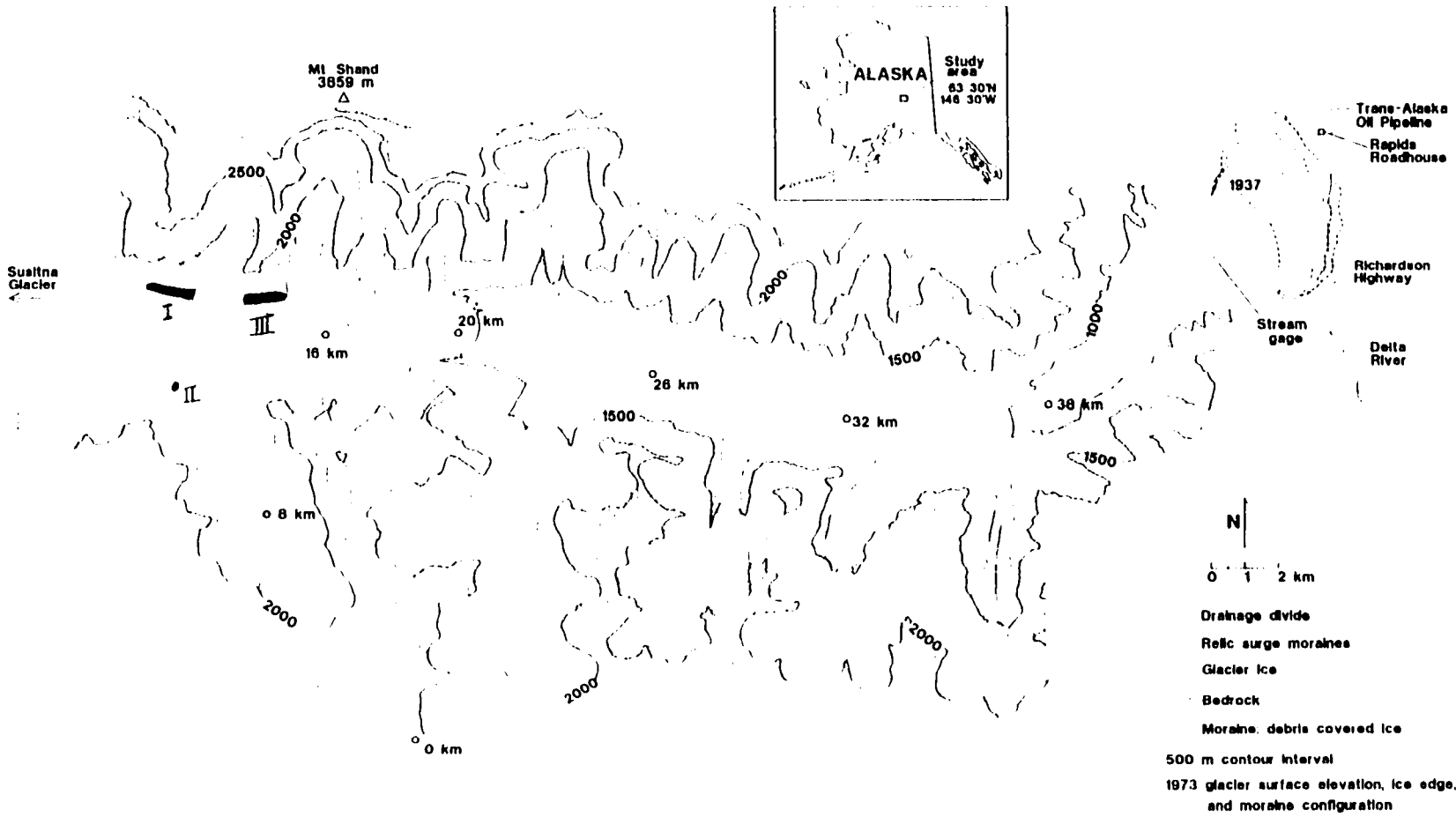

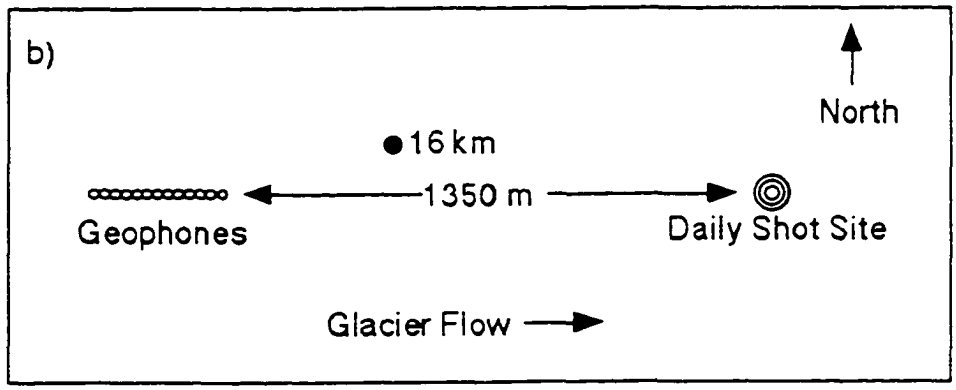

Figure 1b. A close-up view of the study area.

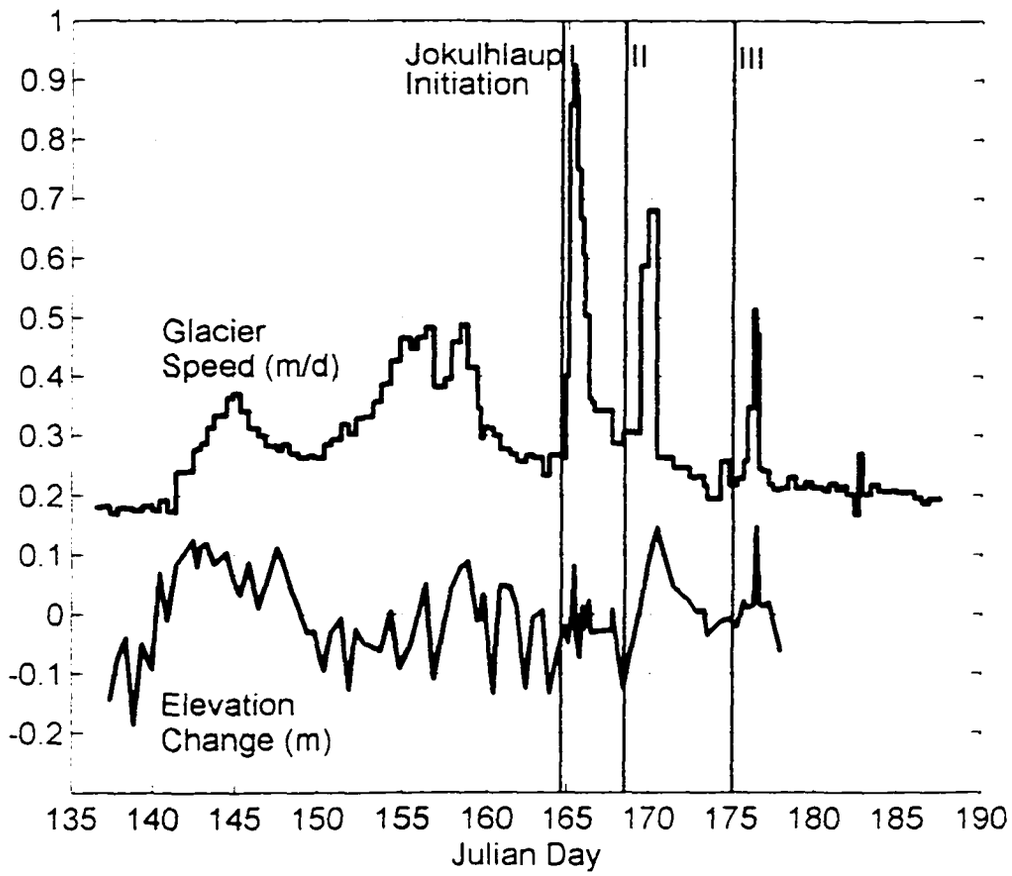

Figure 2. Surveyed speed of Black Rapids Glacier near 16 km in 1993. The initial spring speed-up occured about Day 142 (22 May), following a storm. The three peaks in speed labelled with Roman numerals correspond to drainage of the lakes identified in Figure 1. Elevation change is calculated from the vertical coordinate minus the mean decrease throughout the summer due to surface slope.

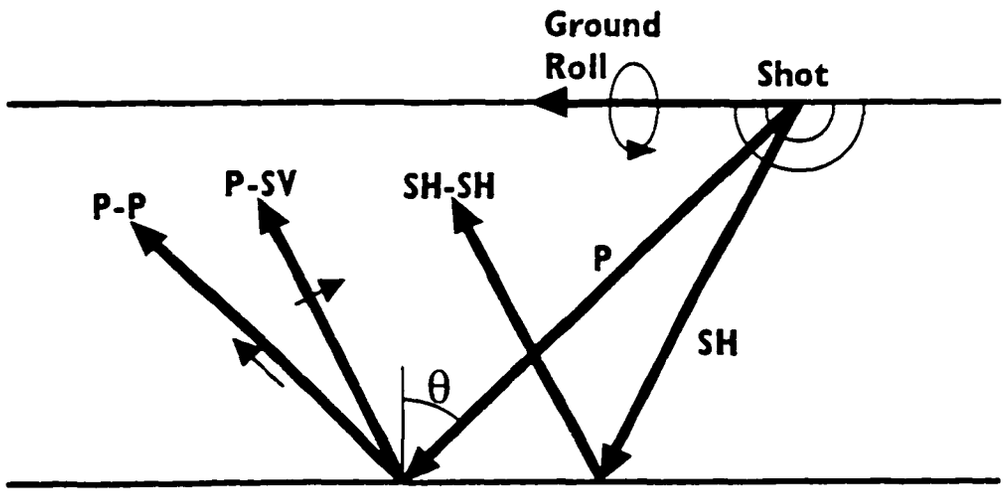

Figure 3. Schematic of seismic waves. Heavy arrows show the direction of wave propagations while light arrows show the direction of particle motion. SH particle motion is into and out of the page.

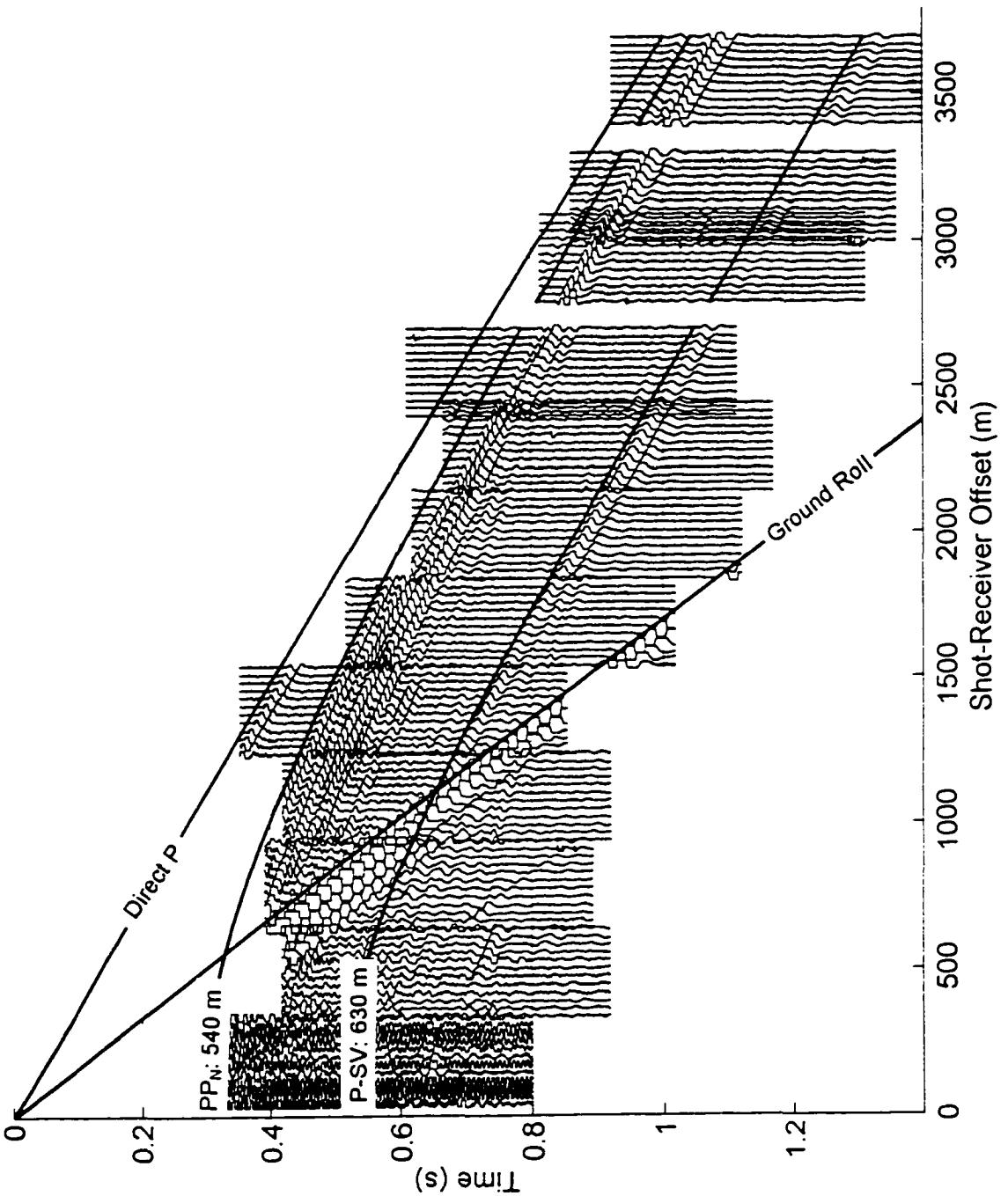

Figure 4a. Longitudinal cross-section using horizontal geophones. Superimposed lines represent the theoretical time-distance curves for various waves, as annotated.

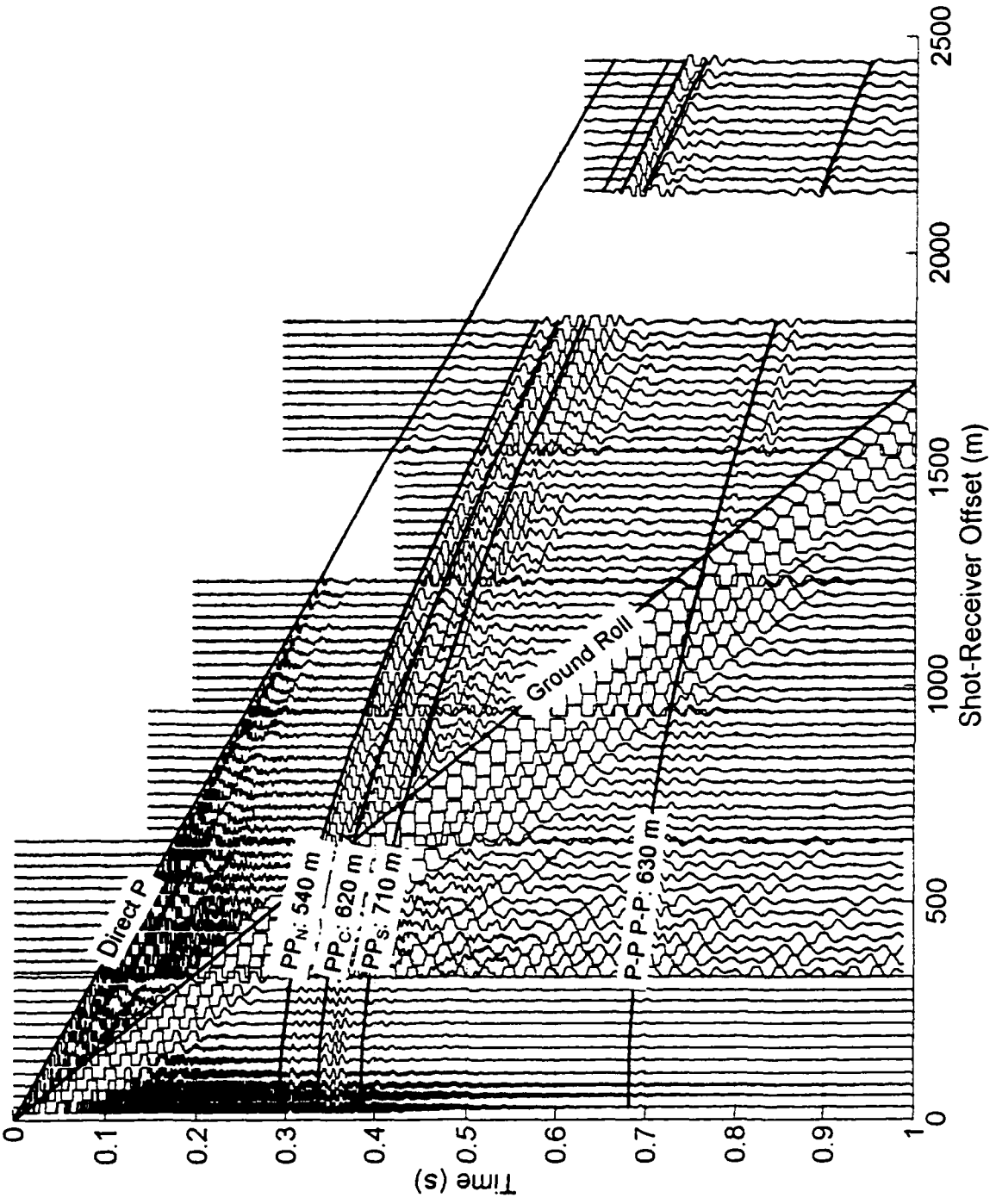

Figure 4b. Longitudinal cross-section using vertical geophones. Note that this figure has different axes limits than Figure 4a.

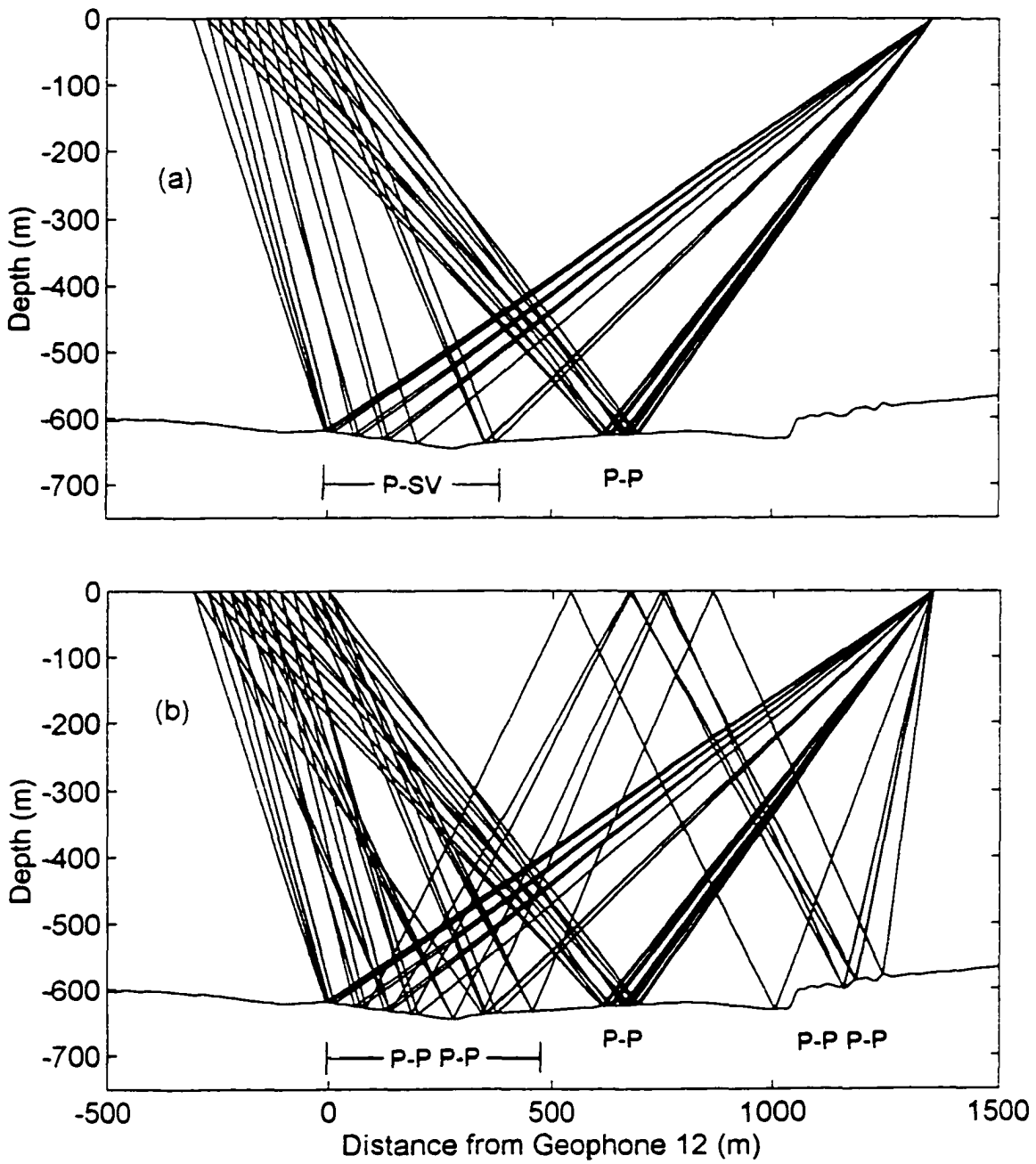

Figure 5. First-arrival ray-tracing for daily-shot geometry. In (a), P-P and P-SV rays are shown, and in (b), the same P-P rays are shown with multiple P-P waves. The P-P reflector does not overlap with the others, suggesting that changes in P-P measurements may occur independently of P-SV or multiple P-P measurements.

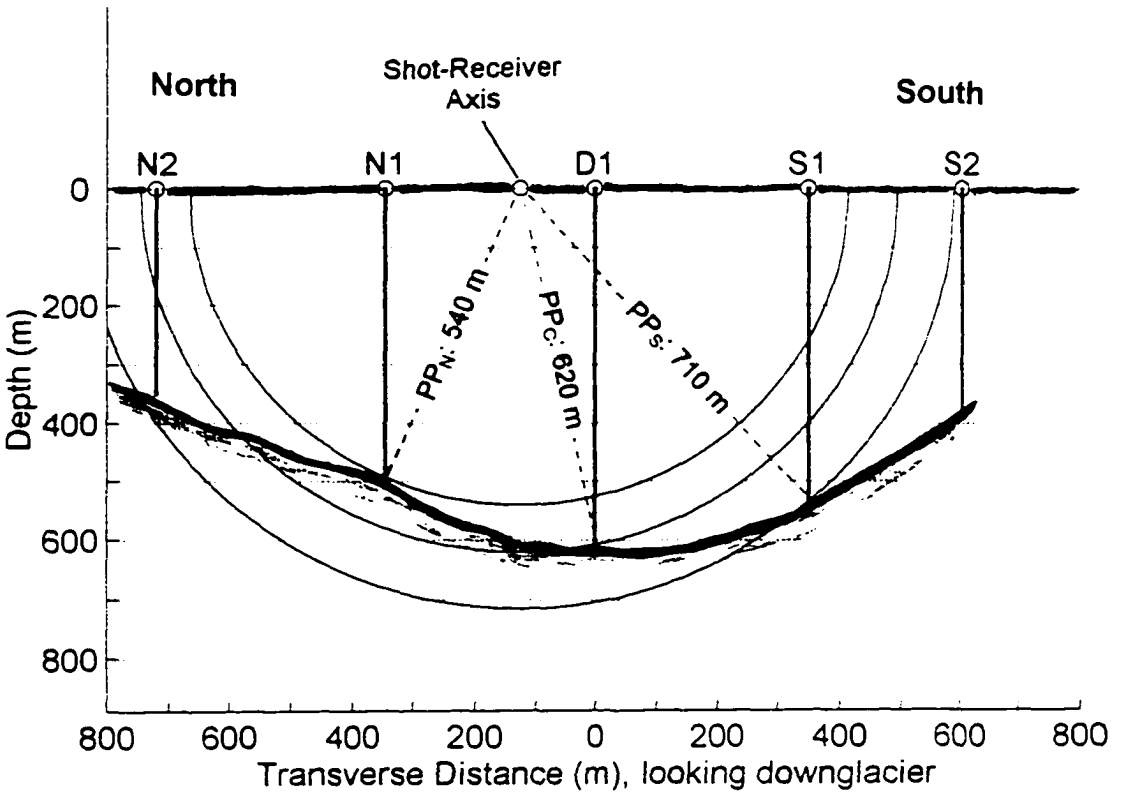

Figure 6. Transverse cross-section of Black Rapids Glacier near 16 km. The bed is a composite sketch derived from seismic measurements made in 1993 and 1996, RES measurements made in 1993 (T. Gades, pers. comm.), and hot-water boreholes made in 1996. The vertical lines represent the borehole locations, purposefully selected to match seismic reflector locations used in this study. The semi-circles represent the loci of the reflector locations for the P-P waves annotated in Figure 4. The dashed lines represent the most likely reflector locations for these waves.

Figure 7. Gather of traces from horizontal geophone #10 throughout summer. These are raw data with no amplitude modifications or filtering. For most of the summer, the measurements are nearly identical. Significant changes are apparent on Days 169-171 and Day 175.688. Also apparent, at the lower right of the figure, is the increase in ground roll speed due to the decreasing snow thickness. Measurements on Days 180 and 184 are different because the geophone was temporarily reoriented to measure SH waves.

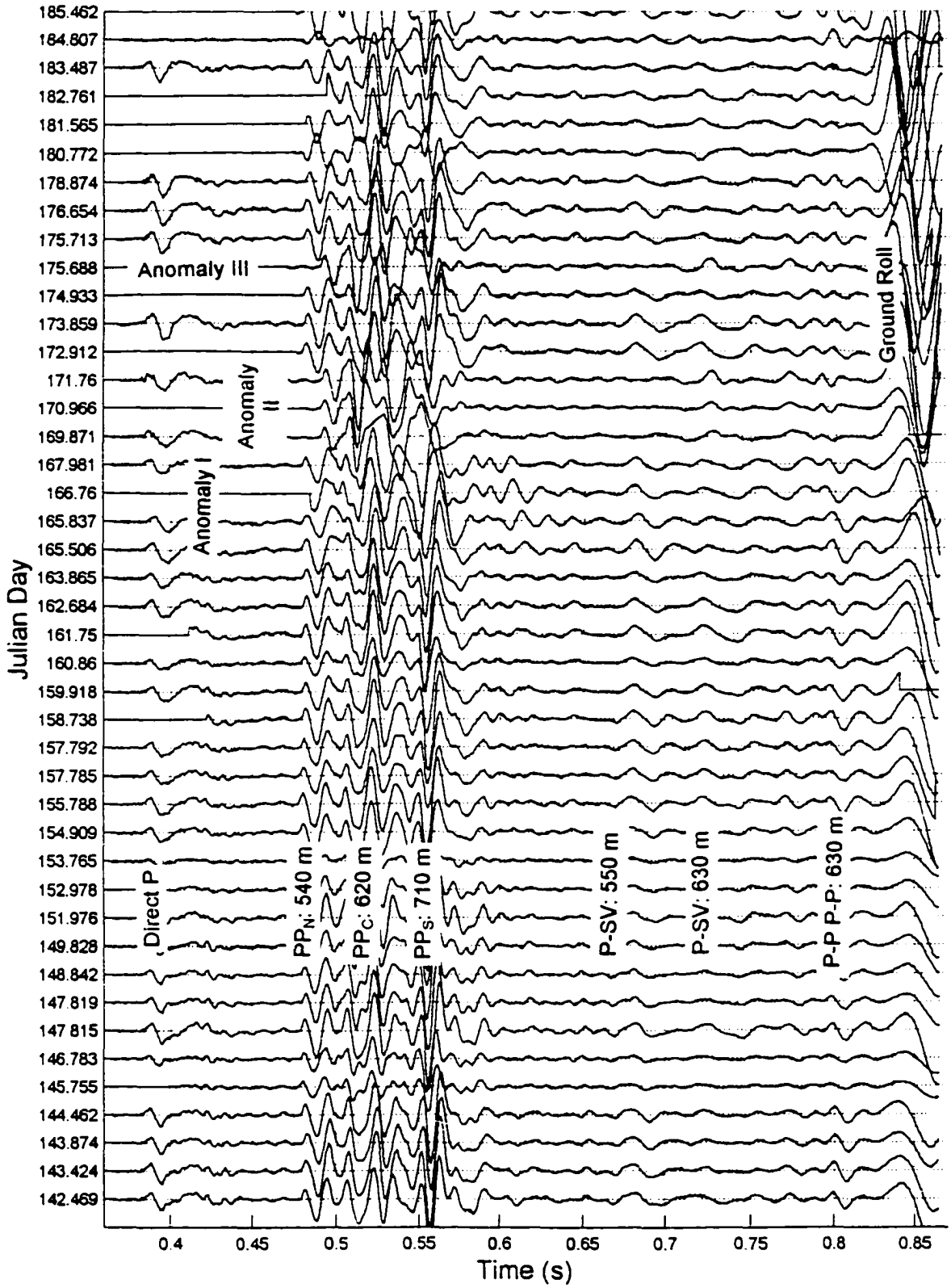

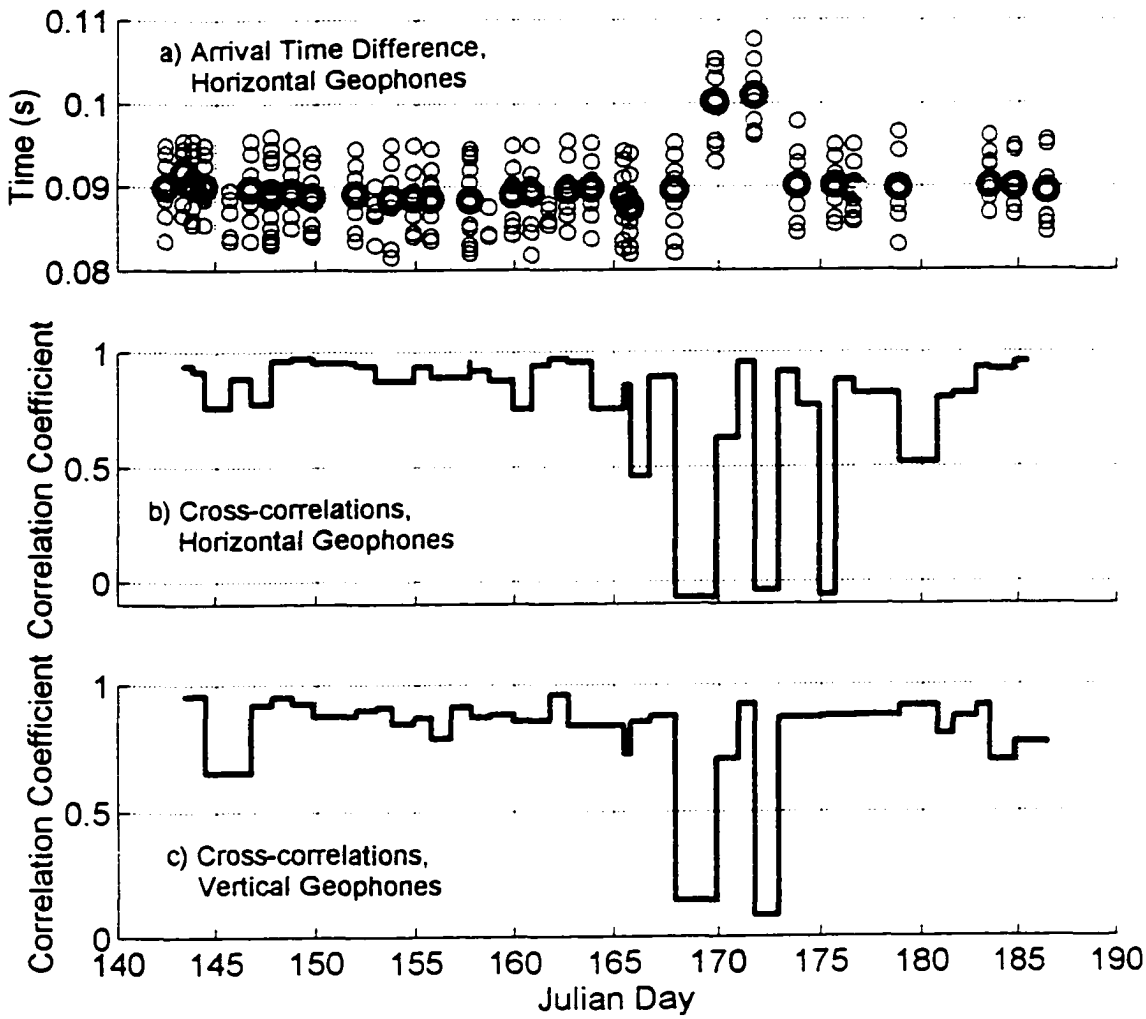

Figure 8. Examples of timing and cross-correlation analyses. In (a), the difference in arrival times of the direct P-wave and the first P-P arrival is plotted: the light circles are from individual traces and the dark circle is the mean of all the traces. Several records are missing because the direct P-wave was not recorded. In (b) and (c), cross-correlations were made of each trace to the previously measured trace (e.g., trace #10 on Day 158 to trace #10 on Day 157) and the mean of these cross-correlations for all 12 traces for each seismogram are shown for the horizontal and vertical geophones, respectively. Although not resolved in (b), there are two data points on Day 175, each with a correlation coefficient of about -0.05; no measurements were made using the vertical geophones on Day 175.

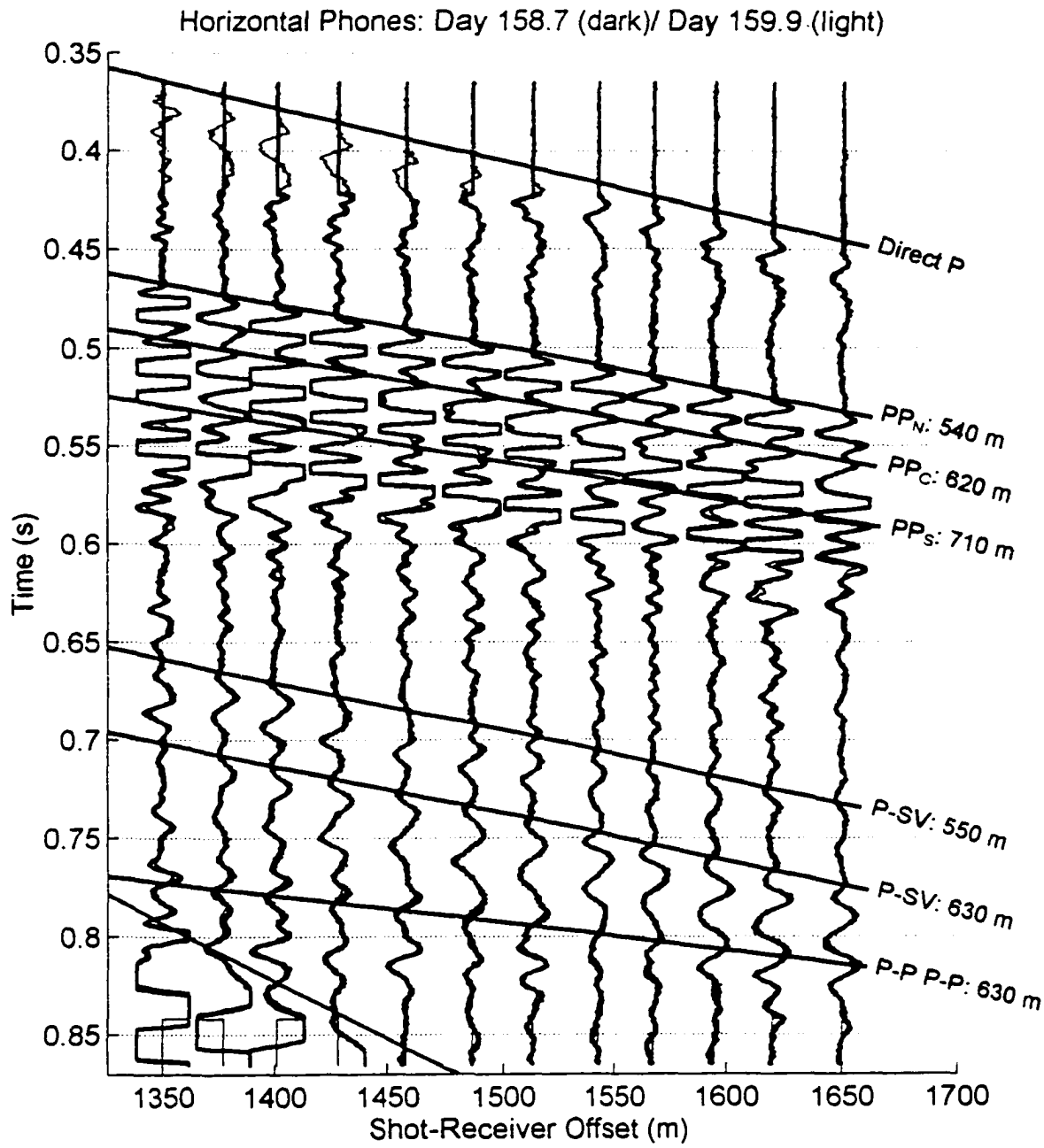

Figure 9a. Overlay comparison of two normal seismograms. Two normal seismograms, Days 158 (heavy) and Day 159, are shown which have a cross-correlation coefficient greater than 0.9. These seismograms are typical of most of the measurements throughout the summer. Superimposed on all of the overlays are traveltime curves of various waves along with their one-way distance from the shot-receiver axis to the reflector, as annotated.

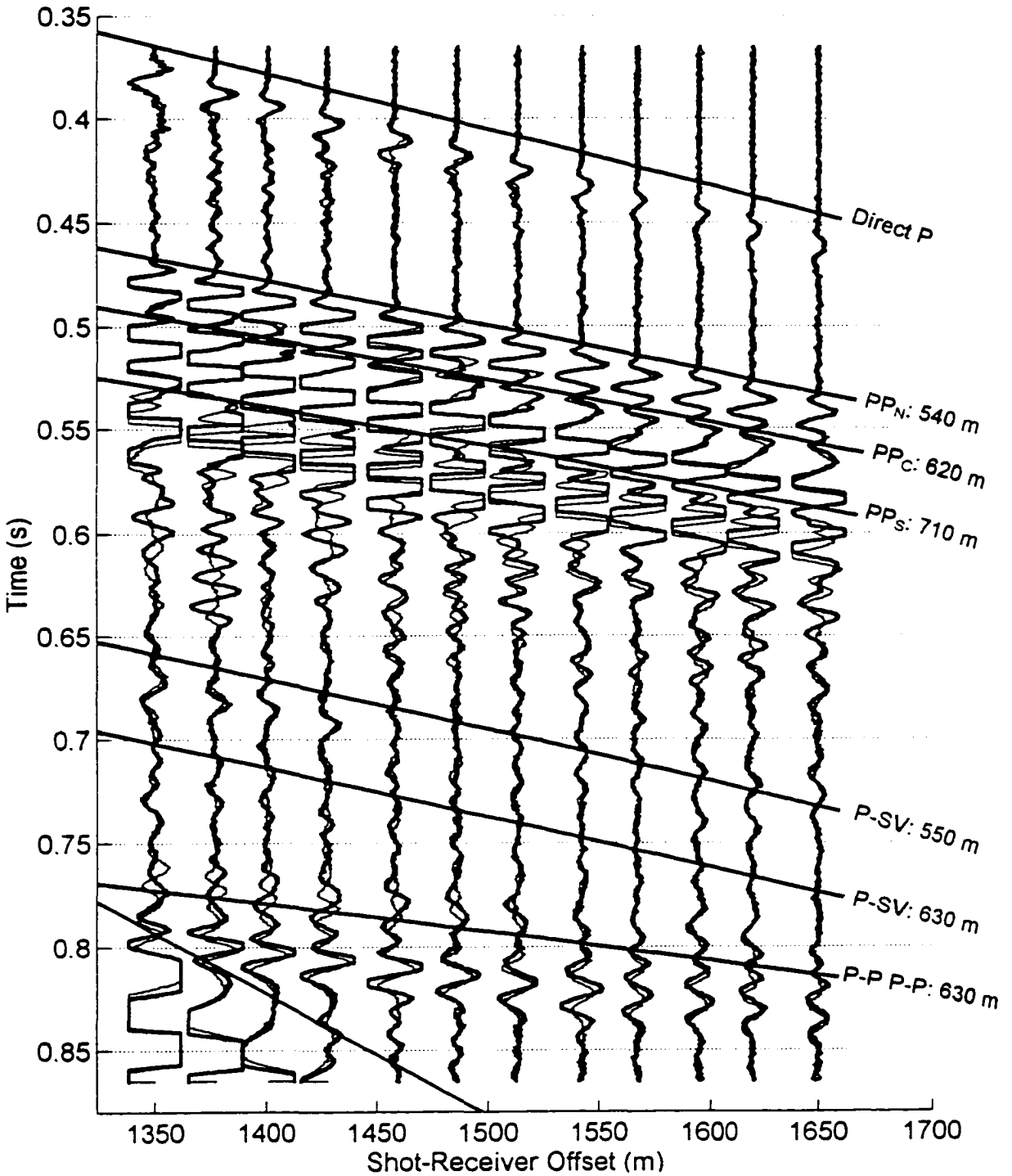

Figure 9b. Overlay comparison of anomaly I to a normal day. A seismogram from anomaly I, Day 166 (dark), is compared to one of the same normal records in Figure 9a (Day 159). Several changes are apparent in the later arriving P-P waves and in the P-P multiple arrival immediately preceding 630 m multiple.

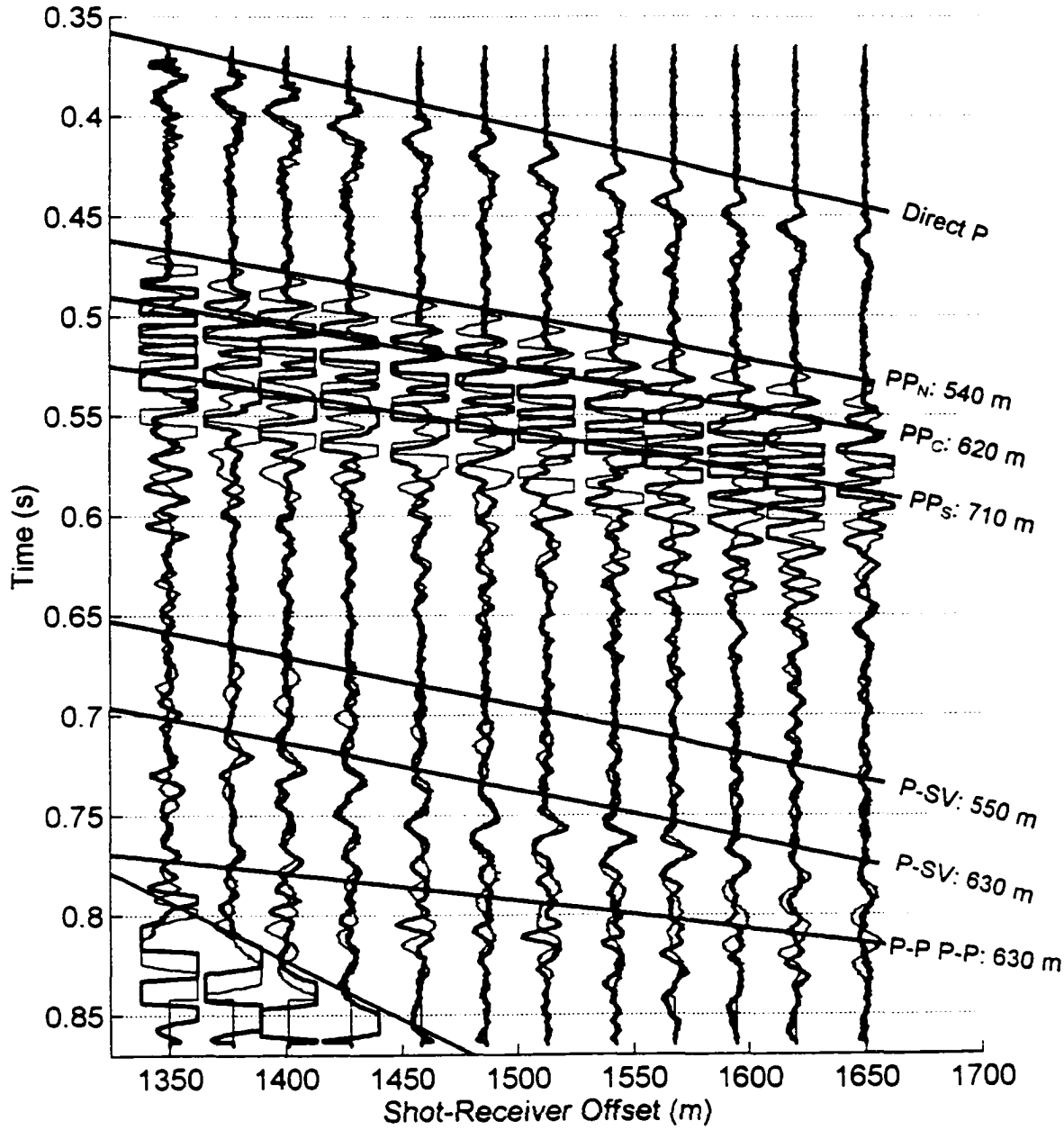

Figure 9c. Overlay comparison of anomaly II to a normal day, using horizontal geophones. A seismogram from anomaly II, Day 171 (dark) is compared to Day 159. Major changes are apparent in almost all of the waves. The horizontal and vertical (Fig. 9d) geophones did not change identically during this anomaly. For example, slight changes are apparent on the 620 m P-S wave on the horizontal geophones, but much larger changes are observed on some of the vertical geophones.

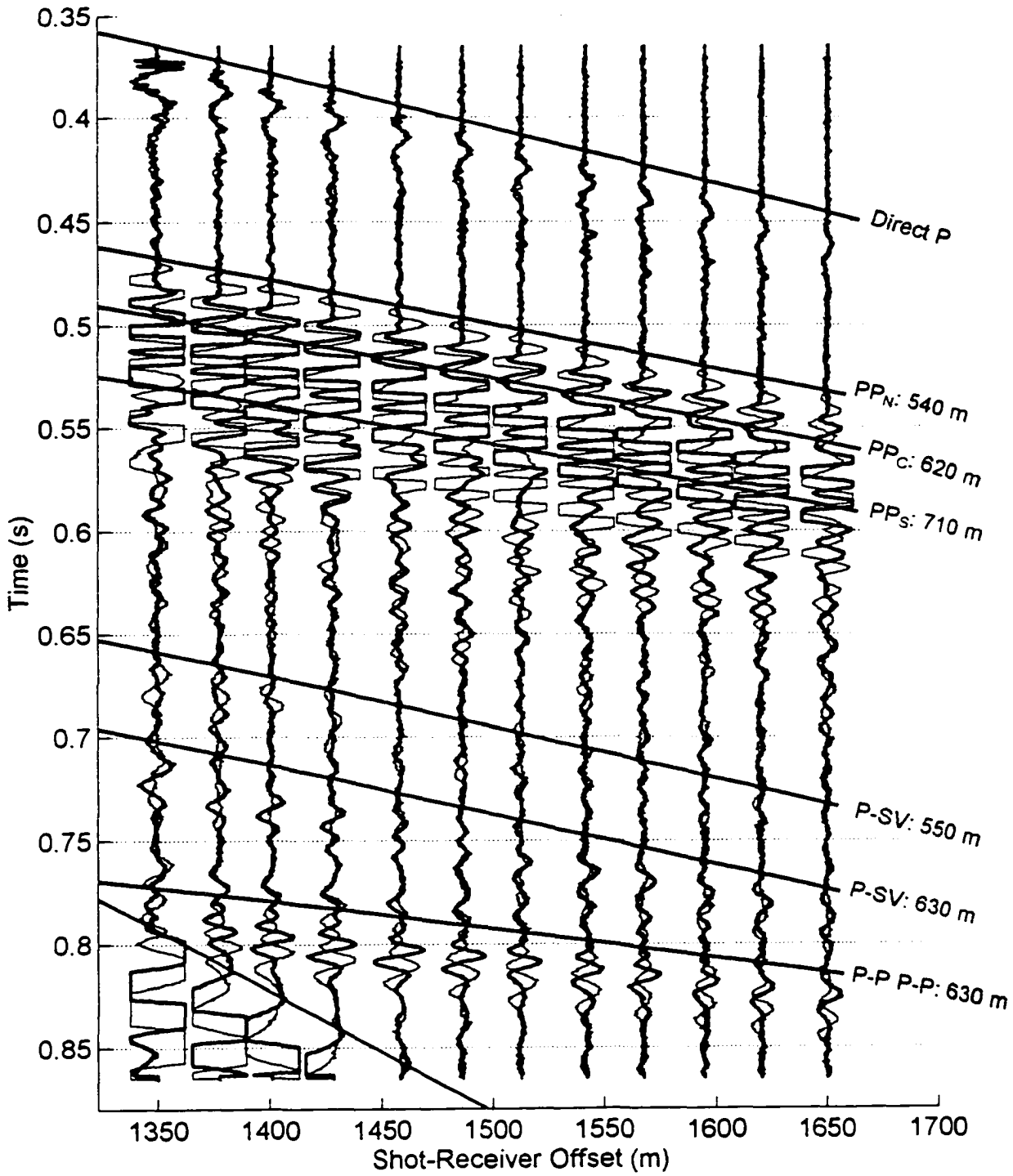

Figure 9d. Overlay comparison of anomaly II to a normal day, using vertical geophones. Seismograms from the same days as 9c are used (Day 171, dark).

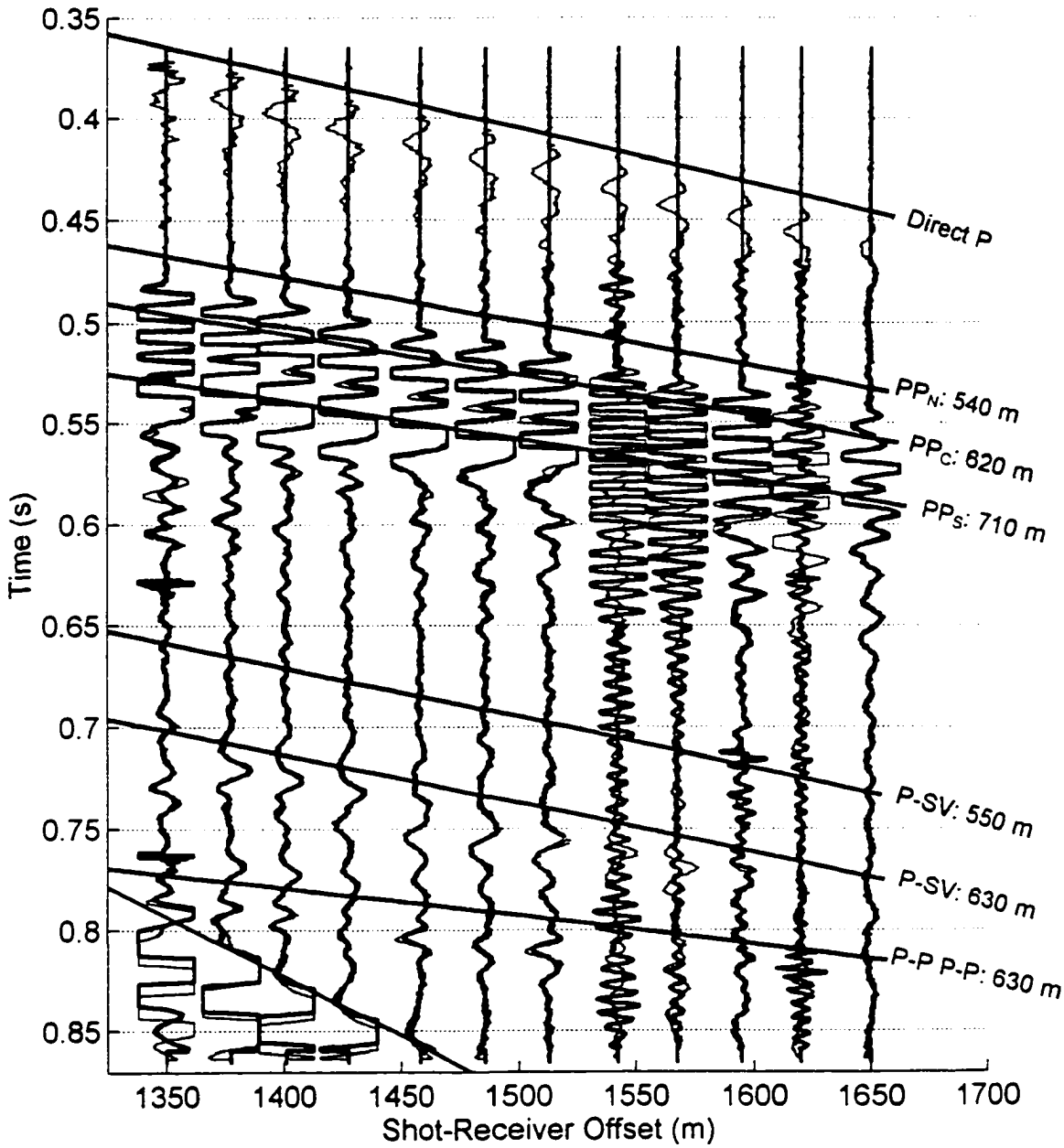

Figure 9e. Overlay comparison of anomaly III to anomaly II. The only seismogram from anomaly III, recorded by the horizontal geophones on Day 175.688 (dark), is compared to the same anomaly II seismogram (Day 171) shown in Figure 9c. Although the direct P-waves were truncated due to timing errors and several traces were noisy due to melted out geophones, it is clear that the remaining measurements on Day 175.688 are nearly identical to those of Day 171.

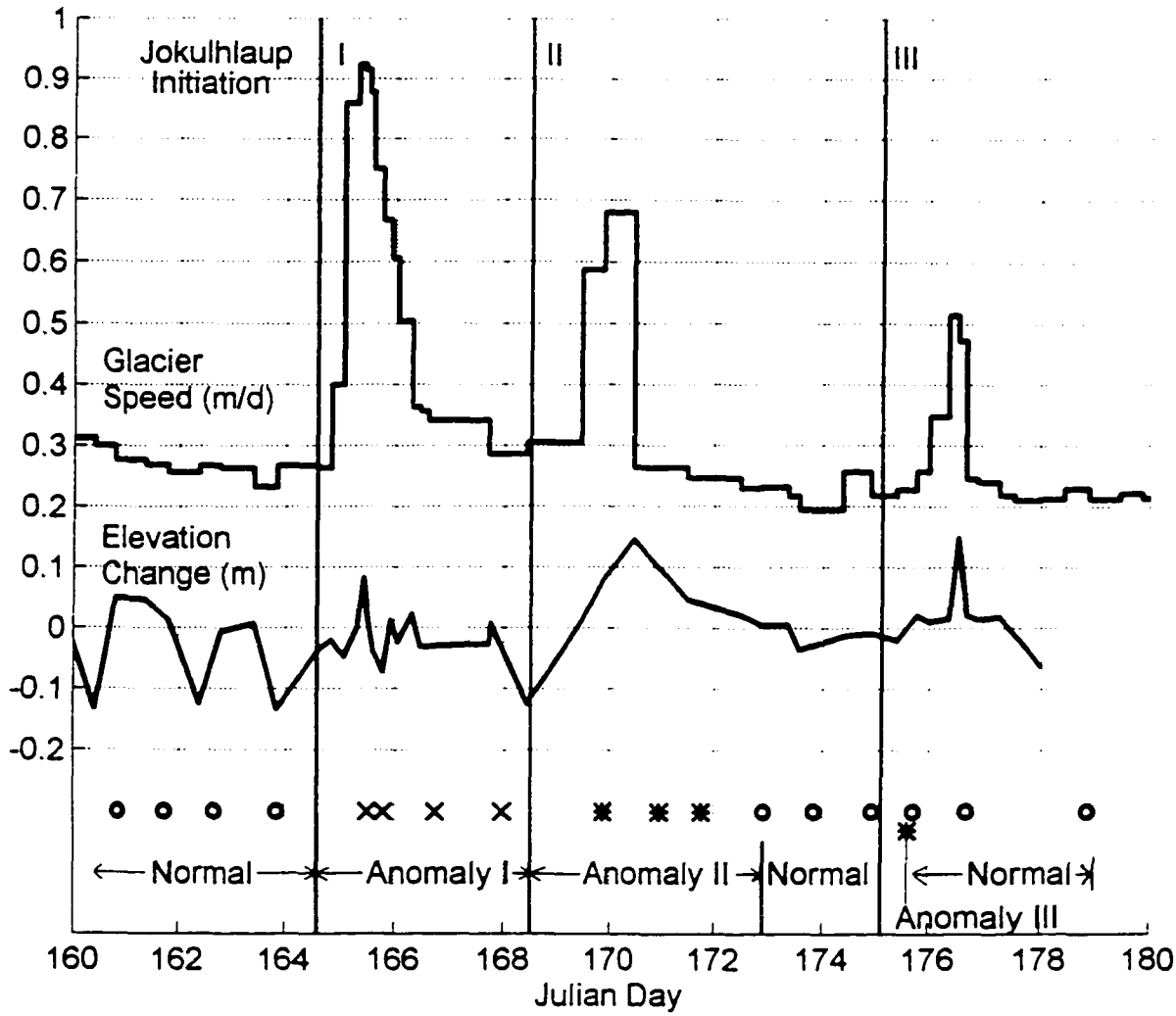

Figure 10. Correlation of jokulhlaups, increases in ice motion, surface elevation change and seismic anomalies. Estimated initiation of jokulhlaups are represented by thin vertical lines with Roman numerals corresponding to those in Figures 1 and 2. Survey data is a portion (9 June to 29 June) of that shown in Figure 2. Circles at bottom represent 'normal' seismic measurements. The remaining symbols, 'x' and '*', represent the two types of anomalous seismic measurements.

CHAPTER TWO: BASAL MORPHOLOGY AND PROCESSES

INTRODUCTION

An understanding of the processes of basal motion is key to answering questions of glacier surges, ice stream motion and seasonal variations in glacier speed. Most glaciologists suggest that a decrease in effective pressure, the difference between ice overburden and subglacial water pressure, plays an important role in basal motion, but the specific mechanisms remain unclear (e.g., Paterson, 1995; Willis, 1995). Models of this motion fall into two general categories, based on the nature of the bed. In hard bed models, the bed is hypothesized to be consolidated rock or undeformable sediment, and sliding is the dominant mechanism. In soft bed models, the bed is composed of a till that can deform. The soft bed models are complicated by the fact that two water pressures are involved: that of the water within conduits or hydraulically-linked cavities and that within the pore-space of the till. The bed of each glacier is unique and probably consists of regions of both hard and soft beds, and it is likely that effective pressure affects each glacier somewhat differently.

While we do not directly address the mechanisms of basal motion in this paper, our observations and interpretations provide information on the role of till parameters, such as effective pressure and saturation, in basal processes occurring coincident with abrupt changes in basal motion. In Nolan and Echelmeyer (submitted; here denoted "N&E" (in journal form) and Chapter 1 (in this thesis)), we described the use of seismic reflection techniques to directly measure temporal changes of about 1 km^2 of the bed of Black Rapids Glacier, Alaska (N&E/Chapter 1, Fig. 1). These subglacial changes followed the sudden drainage of supraglacial lakes ('jökulhlaups') upglacier of our study site, and they were accompanied by large, temporary increases in basal motion.

We refer the reader to N&E (Chapter 1) for detailed descriptions of Black Rapids Glacier, the experimental methods, basic seismic theory, the observations, and sample seismograms. In the present paper we use these observed seismic changes to determine the subglacial morphology and the processes responsible for the changes. We begin with a summary of the observational findings from that paper which form the basis of these seismic interpretations.

In the spring of 1993, we measured seismic reflections nearly every day in the same spot for over six weeks. Occasionally more than one measurement was made within a single day. Longitudinal arrays of both horizontal and vertical geophones were used, with explosive sources placed 1350 m downglacier of the nearest geophone in the arrays. Coincident with the seismic research, we surveyed horizontal and vertical glacier motion and horizontal strain, as well as passive seismicity and vertical strain using automatic logging equipment. During the study period, englacial drainage of two ice-marginal lakes and at least one pothole, all located upglacier of the study area, caused the surface speed to temporarily increase by as much as 400%. Figure 11a shows the part of this survey record that includes these events, along with a summary of the seismic measurements described below. The subglacial locations of some of the seismic reflectors discussed in this paper are shown in Figure 11b.

Most of these daily records were nearly identical and showed no significant changes. We refer to these records as 'normal'. After each of the three jökulhlaups, however, the seismic record showed anomalies lasting up to two days. Important observations for the interpretations presented here are:

1) The second and third anomalies were nearly identical and both were followed by normal records (Fig. 12). The third anomaly was observed to revert to normal in less than 36 minutes. We refer to this reversion-to-normal as 'reversibility'. This observation is very robust as it does not rely on any interpretation. Each anomaly was characterized by a different

pattern of surface elevation change, although temporary increases were observed in each case (Fig. 11a).

2) The amplitude of the first reflected P-wave changed from positive to zero during the second and third anomalies (Fig. 12). The reflector for this wave, PP_N (Fig. 11b), was located along the northern valley wall, about 350 m north and 100 m above the deepest part of the bed in that transverse section. Most of the interpretations presented in this paper deal with this reflector. It is the first reflection arrival, and thus it is not obscured by preceding waves and is less ambiguous than subsequent returns (Fig. 12).

3) Each jökulhlaup caused both a seismic anomaly and an increase in basal motion, although the timing between these two phenomena varied in each case: the seismic anomalies were observed to occur before, during and/or after the increased basal motion on the time scale of several hours to a day (Fig. 11a).

The changes observed during the first anomaly were obscured in the seismic record because they did not involve the first arrival (PP_N), but we do know that these changes were relatively minor compared to the later anomalies (Fig. 12). Similarly, many of the remaining P-to-P (P-P), P-to-SV reflections (P-SV), and multiple P-P reflections also changed amplitude and/or phase during the second and third anomalies, but the actual changes were obscured by interference from other waves. The reflections sampled an area on the bed with length 1300 m and transverse width 700 m, although the coverage within this area was not complete, and they indicate that the responsible mechanism must act over a large area of the bed.

When we began this work in 1993, we had no *a priori* information about the basal morphology of Black Rapids Glacier. However, during the final preparation of

this manuscript in the spring of 1997, basal cores were retrieved at reflectors PP_N and PP_C (Fig. 11b) as part of the University of Alaska's ongoing research program on Black Rapids Glacier (W. Harrison, M. Truffer, K. Echelmeyer, R. Motyka, M. Nolan, unpub. data). These cores provide conclusive evidence that this glacier is underlain by a meters-thick till layer at these sites. These cores also provide a "ground truth" for our seismic interpretations of basal morphology, and substantiate our seismic methods for remote sensing of the bed.

In the first section of the paper, we discuss the seismic analysis methods we employed for comparing various possible morphologies with the constraints imposed by the observations. In the next section, we use these methods to test two morphological models: the transient formation or thickening of a water layer between ice and rock (a hard bed model) and the transient change in one or more properties of a subglacial till layer (a soft bed model). The hard bed model is shown to be insufficient to explain the seismic anomalies adequately. In the final section, we concentrate on the properties of till and how they can change in time. We show that a temporary decrease in saturation of the till or an increase in effective pressure are the only properties among the possibilities that we have identified that can satisfy the observed reflection coefficient constraints. However, we have found no mechanism by which effective pressure can increase within the measured time constraints. A glaciological mechanism by which till saturation can temporarily decrease is proposed.

SEISMIC THEORY

Ice, water, rock, and tills each have a fairly unique range of three seismic parameters: P-wave speed (V_P), S-wave speed (V_S), and density (ρ). We use the observed seismic waves to constrain these parameters, and thus constrain the possible basal morphology.

Blankenship and others (1987) and Rooney and others (1987) were able to generate and record both P-P and S-S reflections, and then use these waves to

determine the basal morphology of Ice Stream B (UpB). Since the ice stream has no steep valley walls, the reflecting interfaces were safely assumed to be vertically beneath the shot-receiver axis. Thus the two basal reflections they measured were interpreted as coming from the top and bottom of a basal layer, and since S-waves cannot travel through water, the slow basal layer had to be till. Layer thickness and wave speeds were determined from traveltimes using common depth point (CDP) methods. Knowledge of V_P was used to constrain the till's porosity, and V_S constrained the effective pressure in what they assumed was a saturated till.

Our traveltime information alone is inadequate for a similar analysis, and we do not have incident S-waves to work with. While the first P-P arrival (from reflector PP_N, Fig. 11b) may be reflecting from the top of a till layer, we know that at least two of the subsequent P-P-waves (from PP_C and PP_S) are reflecting from other parts of the valley, and not from the bottom of the layer beneath PP_N. We cannot single out any two reflections as defining the top and bottom of the same till layer. Even with the 1997 drilling data, we do not have enough information to confidently distinguish any particular reflection as coming from the bottom of a till layer.

Direct measurements of V_P and V_S, such as Blankenship and others' (1987), are the preferred method for constraining morphology. Unfortunately, their method for reliably generating S-waves remains a mystery, as later experiments conducted with nominally the same set-up failed to generate them (C. Bentley, pers. comm., 1996). The inability to generate S-waves reliably is endemic to exploration seismology, and alternative methods have been developed to help constrain V_S using only incident P-waves.

One such method involves the use of reflection coefficients, the theoretical ratio of the amplitude of the reflected (P-P) or converted (P-SV) wave to the amplitude of the incident wave, which is calculated by assigning the three seismic parameters (V_P, V_S, and ρ) to each of the two media at an interface. Continuity of displacements and

tractions then leads to a set of nonlinear equations giving the reflection coefficients as a function of the incidence angle. The seismic parameters, and thus morphology, can be determined by inverting these equations using the observed reflection coefficients. This approach is similar to that used to determine lithology and pore content by studying reflection amplitude variation with increasing source-receiver offset (so-called 'AVO' techniques). The majority of AVO literature concerns the detection of spatial anomalies, but some studies have successfully detected temporal changes, such as those associated with steam injection into oil wells (Tsingas and Kanasewich, 1991; Ito and others, 1979).

AVO analysis is often used for seismic exploration of gas or liquid-bearing rocks and sediments. Rocks generally have similar densities and V_P V_S ratios, but the presence of only a few percent gas or oil in the rock matrix can decrease V_P by 50% while hardly affecting V_S (Murphy, 1982). These variations lead to changes in the reflection coefficient and are often called 'bright spots'. Without knowing V_S, however, these bright spots cannot be confidently distinguished from unrelated phenomena that produce the same result. S-wave data is, unfortunately, usually lacking (as in our case), and the V_P V_S ratio cannot be determined directly. However, this ratio strongly influences shear wave conversion at non-normal incidence, and this in turn affects how reflection coefficients vary with incidence angle (Castagna, 1993; Spratt and others, 1993).

There are several limitations to this approach. In practice, the amplitudes of reflected waves are often difficult to determine because of interference from other waves, variable source coupling and material inhomogeniety. On a valley glacier, these problems are further compounded because the U-shaped valley tends to focus energy from widely separated points back toward the geophones that are located along the glacier centerline (Roethlisberger, 1972).

Reflection coefficients and AVO

A seismic reflection is caused by a discontinuity in particle displacement arising from a contrast of sufficient magnitude in either elastic (wave speeds and density) or anelastic (e.g., attenuation, permeability; Bourbie and others, 1987) properties. The amplitude and polarity of the reflected wave are dependent on the magnitude of these various contrasts and on the wave's incidence angle. This dependence is expressed in the amplitude reflection coefficient, $\Re$, defined as the ratio of the amplitudes of the reflected and incident waves. $\Re$ can have an elastic, $\Re_{el}$, and an anelastic, $\Re_Q$, component. At normal incidence, the approximation $\Re = \Re_{el}+\Re_Q$ is valid (Bourbie and others, 1987; Nolan, 1997, Appendix C).

Bourbie and Nur (1984) found that, under all conditions, $\Re_Q$ was negligible for incidence angles greater than about 30 degrees and typically only important at smaller angles when $|\Re_{el}|$ was less than about 0.1. Although attenuation contrasts can be quite large in glaciological situations, our conclusions are similar to theirs in that for the incidence angles of interest in this study (>45 degrees), the reflection coefficient due to a contrast in attenuation is much smaller than the corresponding elastic reflection coefficient. Therefore, we consider only elastic contrasts (i.e., $\Re=\Re_{el}$) in the following analysis. A more detailed discussion of attenuation contrasts can be found in Nolan (1997) as they are likely to be important in glaciological seismic studies at near-normal incidence.

For reflections from the welded interface of two half-spaces at normal incidence, the reflection coefficient for a P-P reflection can be expressed simply as

$$\Re_{PP} = \frac{\rho_2 V_{P2} - \rho_1 V_{P1}}{\rho_2 V_{P2} - \rho_1 V_{P1}} \qquad (1)$$

where the subscripts 1 and 2 specify the upper (incident wave) and lower medium, respectively, and ρV_P is the acoustic impedance of the medium. Note that when the acoustic impedance of the lower medium is less than that of the upper, a change in polarity is expected between the reflected and incident waves. We use 'polarity' to

describe real phase changes (i.e., 0° and 180°); imaginary phase changes require velocity dispersion due to attenuation, which we consider negligible for this part of our study. A reflection is considered positive when the direction of first motion matches that of the direct wave. The equations for reflection coefficients at non-normal incidence are considerably more complicated because of P-to-SV conversion; these are the so-called Zoeppritz equations (e.g., Aki and Richards, 1980).

For our daily records, the incidence angles for the P-P, P-SV, and multiple P-P-waves were about 45° to 55°, 55° to 65° , and 15° to 25°, respectively. These large incidence angles preclude the use of Equation (1), for reasons made clear in Figure 13. This figure shows examples of reflection coefficients derived from the Zoeppritz equations for ice over half-space beds of rock, till, and water as a function of incidence angle. Representative densities and wave speeds for the media are given in Table 1; we have chosen specific values within the tabulated ranges for calculating the results shown in these figures. As can be seen, both the polarity and amplitude of P-P and P-SV reflections can vary significantly with incidence angle.

We included Figure 13, in part, because the only previous plot of such data published in the *Journal of Glaciology* (Richards, 1988) is in error. It appears that a minus sign was dropped in coding (in the 2nd equation on p. 150 in Aki and Richards, 1980), causing all of his P-to-SV curves to be of the wrong polarity. Such a difference has significant implications to the seismic interpretation of changes at the basal interface of Variegated Glacier during its 1982-83 surge.

Before continuing our discussion of modeling basal morphology, we take a closer look at the work of Blankenship and others (1987) to emphasize the necessity of considering amplitude and polarity variation with offset. When determining arrival times, Blankenship and others (1987) stated that they picked the first trough and the first peak for reflections from the top and bottom of the till layer, respectively, "because a phase reversal should occur between these arrivals, since the acoustic impedance in the till is less than in the ice and presumably less also than in the substrate". While the

latter assumption is true at all incidence angles, a P-P reflection from an ice/till interface will only be negative at near-normal incidence (< 25°, Fig. 13a) for the wave speeds and densities that they determine in their analysis. However, the incidence angles of Blankenship and others ranged from near-normal to 60°. As Figure 13a shows, the majority of their reflections should *not* have had their assumed phase reversal. This means that the traveltimes used by these authors are probably off by a 1/4 period (either delayed or advance, we cannot tell which). Such an error in traveltime would cause substantial errors in either their calculated values of V_P, till thickness (h_{till}), or both. Using their frequency of about 300 Hz, we estimate that the maximum effect on one or the other parameter is about ± 25%. If both parameters are in equally in error, then they would both be off by about ± 20% (i.e., V_P = 1550 ± 300 m s^{-1}, h_{till} = 7.6 ± 1.5 m), which nearly doubles their range of uncertainty.

Thin layers and resolution

The Zoeppritz equations are defined for a welded interface between two half-spaces. While 600 m of ice can be regarded as a half-space, basal layers of till or water might not be. Here we apply these equations to layers thinner than a seismic wavelength. We assume that a reflection from a layer is observable at the seismometer if the source energy, the size of the impedance contrast, and the signal-to-noise ratio are all of sufficient magnitude, regardless of the thickness of the layer.

Ricker (1953), Widess (1973), and Kallweit and Wood (1982) provide useful criteria for determining how thick of a layer can be detected and resolved to determine thickness. The basic idea is that reflections from the top and bottom of a layer can be distinguished accurately in practice only when the layer is at least 1/4 wavelength (λ) thick, due to destructive interference. In what follows, we use the terms 'thick' and 'thin' to distinguish between layers where we can potentially resolve the top and bottom of the layer according to this criteria, from those where we cannot, respectively. For example, a water layer less than 5 m thick is considered thin (λ = 18 m, Table 1). We

model thick layers as half-spaces (Figs. 13a & b) and thin layers as a part of a three layer system (Figs. 13c & d).

However, as Widess (1973) and Koefoed and deVoogd (1980) have shown, a layer may be detectable far below the 1/4 wavelength limit, even though the top and bottom reflections are no longer distinguishable. In such cases, the amplitude of a wave reflected from a thin layer is related to its thickness by constructive superposition of the reflected waves from the top and bottom of the layer. Therefore, temporal changes in the seismic properties of such thin layers should result in changes in amplitude of the reflections.

In our three layer models, reflections from the top and bottom of the thin middle layer add constructively. For very thin layers, multiple reflections within the layer may also be included if they, too, arrive within one half-cycle. The additional energy of these multiples is small, however, and, for the case of a thin till layer, we simply trace the incident wave down through the middle layer, with a transmission coefficient, reflecting off the substrate (a till-rock reflection coefficient) and back up into the ice (transmission). We modeled the ice-water-rock sandwich by analytically summing the infinite series of multiples (similar to Richards, 1988).

Figures 13c and 13d show the theoretical response of thin layers of water and UpB till between ice and rock. As can be seen, the reflection from the bottom of the layer, at the rock, dominates $\Re_{PP}$. In neither case does the reflection from the lower interface destructively interfere with that from the upper interface to yield $\Re_{PP}=0$. These curves for thin layers are typical for the probable range of their seismic parameters. The significance of this will be clarified further in the next section, when we enforce $\Re_{PP} = 0$ as an observational constraint

Horizontal resolution, like vertical resolution, is typically described in terms of the constructive interference that would occur if two reflections from nearby reflectors arrive at a geophone within one half-cycle of each other. For normal incidence, assuming a planar interface, all reflections of a spherical wavefront from within a circle

of radius $(\lambda H/2)^{1/2}$ should constructively interfere, where H is ice thickness. This circle defines the horizontal resolution (Sheriff and Geldart, 1995). In our case, λ in ice is about 45 m and H is about 450 to 600 m, yielding a radius of about 100 to 120 m. Thus, any subglacial layers that we observe seismically should be fairly continuous over an area of about 40,000 m^2 for each geophone. The sampled area for adjacent geophones will often have some overlap, but we might expect that a reflected wave arriving at each of the geophones along the 300 m-long array would illuminate a region on the order of 200 m wide by 350 m long. This estimate is important for discussing the spatial extent of seismically-observed changes at the bed.

Inversion of reflection coefficients

Our seismic measurements give us an estimate of the temporal changes in P-P and P-SV reflection coefficients. The Zoeppritz equations express these reflection coefficients as nonlinear functions of the seismic parameters (V_P, V_S, ρ) for the two media and the angle of incidence. We have reasonable knowledge of these parameters for ice, and wish to solve for those within the underlying material. However, these equations cannot be analytically inverted without linearization (e.g., Demirbag and others, 1993; Carazzone and Srnka, 1993). Such linearization tends to break down for offsets greater than about 30°, which is less than the minimum value for P-P-waves in our investigation. Therefore, we have used a simple iterative approach by which we fix two of the three seismic parameters (V_P, V_S, and ρ) and iterate on the third until the calculated reflection coefficient is sufficiently close to that observed. This can be done for each parameter, yielding the locus of points in (V_P, V_S, ρ)-space that leads to a given reflection coefficient at a specified angle of incidence. In some cases, one or more of the parameters for the reflecting layer can be estimated *a priori*, such as for water or bedrock, in which case the inversion is better constrained. We use this approach herein.

BASAL MORPHOLOGY

Our goal in this section is to determine the basal morphology using our seismic measurements. We do this by inverting the observed reflection coefficients on normal and anomalous days for the seismic parameters V_P, V_S, and ρ of the bed, and comparing these values to the physically permissible ranges for the hard and soft bed models. Use of this method assumes that we can quantify $\Re_{PP}$, and that we can specify the permissible ranges for V_P, V_S, and ρ of ice, water, rock and till. Each of these assumptions requires caution. Of the seismic parameters, the only well-established values are for water. The range of seismic parameters for the bedrock beneath Black Rapids Glacier (granodiorite, diorite and metasedimentary rocks) can also be estimated well enough for our purposes (we use values from Richards (1988), in Table 1, for consistency with Figure 13). For temperate ice, ρ is well constrained, V_P is fairly well-constrained (± 40 m s^{-1}), and V_S is less constrained (± 75 m s^{-1}) (N&E). The values for till are much less constrained, and described in detail below.

Reflection coefficient on normal days

Quantification of reflection coefficients in seismic studies is often difficult. For Black Rapids Glacier under what we term normal conditions, we can estimate $\Re_{PP}$ by comparing P-P and multiple P-P reflection amplitudes (Roethlisberger, 1972; Smith, 1997). These techniques are only valid if both waves are reflecting from the same location with the same incidence angle, which we know is not true for our daily reflection data (Figs. 5 & 7 in N&E). These conditions are probably met, however, for our longitudinal seismic section near zero offset (Fig. 4b in N&E). Using this method, the reflection coefficient for the 'normal' reflection is about 0.3.

Since this value of $\Re_{PP}$ is measured at near normal incidence along the glacier centerline, we can invert Equation (1) for the acoustic impedance of the (half-space) bed:

$$\rho_{bed} V_{bed} = \frac{1 + \Re_{PP}}{1 - \Re_{PP}} \rho_{ice} V_{ice} \qquad (2)$$

Using densities given in Table 1 for water, rock, and UpB till, we obtain a value for V_P of the lower half-space equal to 6191 m s^{-1}, 2319 m s^{-1}, and 2751 m s^{-1} respectively. Under any reasonable conditions, V_P for water and till are much lower than these values. Therefore $\Re_{PP} \cong 0.3$ indicates that the reflector at this location is either consolidated bedrock or highly compacted, dense till, or that a thin layer of water or till exists over rock (Fig. 13).

There are several uncertainties inherent with this approach. First, we are assuming that the primary and multiple reflectors overlap and are at normal incidence. Second, the attenuation of temperate ice, used in this calculation, is not well known. Third, at normal incidence, the reflection coefficient for many reasonable tills is close to zero, and thus the top of such a layer could be seismically transparent at zero offset. In this last case, the measured $\Re_{PP}$ would be that of the lower interface of a till layer (i.e., the till/rock interface). Because of these uncertainties, and the ambiguities of the resulting wave speeds, we cannot use this value of $\Re_{PP}$ alone to distinguish between hard and soft bed models. Instead, we determine an $\Re_{PP}$ during the second and third anomalies and use it to further constrain the bed morphologies.

Reflection coefficient during anomalies

As already stated, the seismic observation that places the tightest constraints on bed morphology is the change in PP_N during the second and third anomalies. During these anomalies, the amplitude of this reflection decreased from a positive value (perhaps as high as 0.3) to zero on all geophones (Fig. 12). In N&E we discuss why we believe this wave disappeared and was not simply delayed. The average incidence angle across the geophones for PP_N was 50°. We use the shorthand $\Re_{PP}(50°)=0$ to refer to this

constraint of a zero reflection coefficient for PP_S under anomalous conditions. We have more confidence in this reflection coefficient than the 'normal' value at 0° ($\Re_{PP}(0°) \cong 0.3$) because of the latter's inherent uncertainties, as described above.

There is, however, still some uncertainty in the anomalous $\Re_{PP}$. Theoretically, any non-zero $\Re_{PP}$ should produce a reflection. Practically, attenuation and our finite signal-to-noise ratio creates a range $|\Re_{PP}|$ that can be considered 'effectively zero'. This range is somewhat arbitrary, but we can limit it based on the observations of other researchers. Blankenship and others (1987) state a range of V_P and ρ values for their basal till layer that yields $-0.03 \leq \Re_{PP} \leq 0.01$ at normal incidence from Figure 13a, and their reflections were clearly above the noise. Atre and Bentley (1993), examining the same records, reported that $\Re_{PP}$ was positive at near-normal incidence. Anelastic effects should play a role at these incidence angles and might add as much as +0.1 to the value of $\Re_{PP}$ shown in Figure 13a (Bourbie and others, 1987). If so, Blankenship and others' range of wave speeds and densities would always yield a positive value of $\Re_{PP}$ as determined from seismograms. Reflection coefficients of around 0.05 to 0.1 are often reported in the literature (e.g. Bentley, 1971; Smith, 1997). Based on these and other seismic exploration studies, we adopt $|\Re_{PP}| < 0.01$ as 'effectively zero'. Thus, the constraints we use in our study are $\Re_{PP}(50°) > 0.01$ (and, more likely, >0.05 and possibly as high as 0.3) for the normal PP_S reflections and $\Re_{PP}(50°) \cong 0$ (i.e., $|\Re_{PP}(50°)| < 0.01$) during the second and third anomalies.

The hard bed model

In our hard bed model, we hypothesize that basal motion is the result of ice sliding over bedrock, and that, during the jökulhlaups, increased water and water pressure at the bed led to increased basal motion and somewhat synchronous changes in the seismic reflections. Using the change in $\Re_{PP}$ from normal to anomalous states, we can test whether the anomalous state is caused by either a change in thickness or areal extent of an existing subglacial water layer, or by the formation of a new water layer. During

normal conditions, we assume that only thin layers, O(1 cm), are present at the bed (Weertman, 1964). We then invert the half-space and thin-layer models for the anomalous conditions.

For water, V_S is zero, and ρ is nearly constant ($\approx$1000 kg m^{-3}) over the pressure (P) and temperature (T) range we consider likely at the bed. V_P varies somewhat under these conditions; Wilson's (1959) study of V_P(P,T) for water limit the range to 1403 to 1425 m s^{-1} near 0°C and P$\in$[0, 6 MPa]. Here we assume that the salinity of the subglacial water is low.

Under the condition that $\Re_{PP}(50°)\cong 0$, we find that a water layer beneath the glacier can indeed produce a zero reflection coefficient (Fig. 14) within the reasonable range for V_S of temperate ice given in Table 1. In this figure we plot V_S for ice against V_P for water (shaded region), subject to the constraint of a zero reflection coefficient at 50° (the solid curve). For water at 0°C and 5.4 MPa (600 m of ice), V_P=1411 m s^{-1} (Wilson, 1959). This corresponds to V_S=1911 m s^{-1} for ice, which is both within our range of uncertainty and is less than the value of 1944 m s^{-1} determined by Blankenship and others (1987) at Ice Stream B, as expected for our warmer ice.

The possibility exists, therefore, that water at the bed is seismically transparent ($\Re_{PP} = 0$) at an incidence angle of 50°. This means that we cannot detect the presence of a water film in the normal state or the formation of a new water layer at a hard bed interface, except by the increase in traveltime it would cause. From Figure 12, the increase in first reflection arrival traveltime is about 10 ms. If the sole cause of this increase in two-way traveltime was the formation of a water layer, such a layer would have to be at least 7 m thick, determined using $V_{P,water}$ = 1414 $\pm$ 11 m s^{-1}. Destructive interference at 50° within a thin (i.e., <5 m) water layer is not a tenable conclusion, because the strong reflection from the lower (water/rock) interface gives rise to a high layer reflection coefficient with such a thin layer, as can be seen in Figure 13c.

The hypothesis of a hard bed and the observed change in reflected waves from the northern side of the valley thus leads to the conclusion that a water layer of

thickness greater than 7 m temporarily formed, and then quickly disappeared, between the ice and bedrock at the PP_S reflector. Based on our discussion of horizontal resolution, this layer must extend nearly continuously over an area with dimensions of at least 200 by 350 m. Such a layer is neither glaciologically reasonable nor was the required surface uplift observed by surveying (Fig. 11a). This conclusion does not change even if the water layer were underlain by a soft bed instead of bedrock.

Thus it seems unlikely that transient water layers of any thickness can produce the observed seismic effects -- thin ones based on seismic reflection theory and thick ones based on glaciological considerations. We cannot seismically rule out the possibility that thin water layers formed, but we can state that they were not the sole cause of the observed changes.

The soft bed model

In the soft bed model, we hypothesize that a till layer at PP_S becomes seismically transparent (i.e., $\Re_{PP}=0$) during the anomalies II and III, causing the 10 ms delay in first reflection arrival (Fig. 12). As there is then no reflection from the top of the layer, the anomalous first reflected arrival is then either from the base of the till layer or from a different part of the bed (e.g., nearer to PP_C in Figure 11). We can constrain the minimum "seismic" thickness of this layer to be 5 m by assuming that the entire 10 ms (two-way traveltime) was caused by a change in acoustic properties within it, using a (conservative) minimum V_P of 1000 m s^{-1} (i.e., 10 ms x 1000 m s^{-1} / 2). We refer to this as the seismic thickness of the layer; it is comparable to the till-layer thickness of 6 m ± 1 m determined from drilling in 1997 (M. Truffer, pers. comm.).

Any changes in the seismic parameters (V_P, V_S, ρ) must occur over the entire seismic thickness to account for the observed changes in the reflection coefficient. Presumably these changes are the result of a change in one or more properties of a subglacial till layer (i.e., porosity, effective pressure, saturation). As yet, we have no direct measurements of these properties or of the seismic parameters and, unlike the

hard bed model, none of these variables are well constrained by a literature review. This is due to the fact that there are few *in situ* measurements and that tills underlying glaciers originate from a variety of rock types by a variety of processes (such as water deposition or fault action). In this section we compare the permissible range of V_P, V_S and ρ (estimated from the literature) to the results of an inversion for these parameters within the till beneath Black Rapids Glacier.

The seismic properties of tills are dependent on a number of factors (see Appendix D for a detailed discussion). The grain size distribution, as well as the shape of the grains and their pore space, significantly affect both the wave speeds -- by *hundreds* of meters per second -- and the way in which these speeds depend on effective pressure. Porosity (ϕ), defined as the percentage of the total volume that is pore space, and saturation (S), the percentage of this pore-space that is water-filled, both strongly affect the wave speeds. Further, given any one combination of these physical variables, changes in the *in situ* effective pressure also have a large effect on wave speeds. Based on the discussion in Appendix D, we consider the permissible range of seismic parameters for subglacial tills to be $V_p \in [1000, 2100]$ m s^{-1}, $V_s \in [150, 550]$ m s^{-1}, and $\rho \in [2000, 2330]$ kg m^{-3}. The porosity of a fully saturated till, which is a glaciologically more interesting parameter than density, is related to the density by

$$\rho_{till} = \phi\rho_w + (1-\phi)\rho_s \qquad (3)$$

where ρ_w is the density of water filling the pore space, ρ_s that of the solid matrix, and porosity is expressed as a fraction. Our range of density is calculated from Equation (3), using $\rho_s = 2700$ kg m^{-3} and a range of porosity of 20 to 40%.

A zero reflection coefficient for a *thin* till layer with such properties is not likely (Fig. 13c). Inversion of a model with a thin till layer over bedrock and $\Re_{PP}(50°)=0$ yields a maximum P-wave velocity of about 600 m s^{-1} given a reasonable range of V_S

and ρ. This speed leads to a violation of the assumptions behind the thin layer model: if the wave speed were 600 m s^{-1}, the layer thickness would need to be at least 3 m (i.e., 600 m s^{-1} x 10 ms / 2). This exceeds the λ/4 (=1.9 m) limit that defines the thin layer model, and a zero reflection coefficient for the thin layer could not be obtained. Thus, any solutions involving till must be found using the thick layer (half-space) model.

The seismic parameters that lead to a zero reflection coefficient at an ice/till interface in a *thick* layer model are shown in Figure 15. Each of the solid curves in this figure represents those values of V_P and ρ (or, equivalently, porosity) for which $\Re_{PP}(50°) = 0$ at a fixed value of V_S. Parameters yielding $\Re_{PP}(50°)>0$, the constraint for the normal state, are to the upper right of the appropriate V_S curve. For example, the symbol labeled 'UpB' marks the reflection coefficient obtained using the best estimate of V_P (1700 m s^{-1}), V_S (145 m s^{-1}) and ϕ (0.35) for Ice Stream B till as given by Blankenship and others (1987); this yields $\Re_{PP}(50°) = 0.185$, which is to the right of the $\Re_{PP} = 0$ curve for this value of V_S. This figure also shows that, for a given S-wave speed, there are continuous ranges of V_P and ρ that lead to $\Re_{PP}(50°) \cong 0$. Also shown in Figure 15 are regression curves from various researchers (discussed in Appendix D) that loosely constrain a corridor of physically acceptable V_P as a function of fully saturated porosity.

If a temporary increase in fully saturated porosity (i.e., with no change in saturation) were solely responsible for the seismic anomalies, Figure 15 indicates that the porosity throughout a 5 m thickness of till would have to change from below about 30% in the normal state to above 50% in the anomalous state. The reverse process would have to take place in less than 36 minutes. Not only is a porosity of 50% unlikely, but several studies have shown that such a large change is not possible for a till with typical permeability.

Clarke (1987) modeled changes in porosity within a till layer due to increased water pressure at the ice/till interface. Deformational dilatation of the till near the

interface led to a 12% increase in porosity there, but ϕ was unchanged below about 0.5 m, even after 50 hours. Further, these changes were not completely reversible. Similarly, Boulton and Hindmarsh (1987) indicate that timescales of thousands of years are required to change porosity by 15% at depths of several meters.

The remaining analysis relies on knowing whether we can consider till 'drained' or 'undrained' on the time-scale of hours. Here we use 'drained' to mean that the pore-water is free to leave the pore-space in response to changes in pore-water pressure caused by increased normal stress (as well as the reverse process). We use 'undrained' to mean that the amount of the pore-water is not free to change on the time-scale of interest. A change in the amount of pore-water is driven by a gradient in pore-water pressure, P_{pw}. Till will respond to changes in pore-water pressure in an *undrained* manner on the time-scale of hours because changes in the amount of pore-water at 5 m depth require a high pressure source to exist for hundreds of hours. This is because such changes are normally governed by a diffusional process, with a diffusivity k that depends on the porosity, compressibility and permeability of the till, as well as the properties of the pore-water itself (de Marsily, 1986); k ranges from about $4\text{x}10^{-4}$ to $6\text{x}10^{-7}$ m^2 s^{-1} (Paterson, 1995). Coarse, permeable tills have the larger diffusitivies. From the cores recovered in 1997, we now know that Black Rapids Glacier till is characterized by a broad range of grain sizes -- from large cobbles to silt – and so is in the middle to lower end of this range of diffusivity. Standard analysis shows that the characteristic time, τ, required for an abrupt change in P_{pw} to propagate a distance z down into a till layer is given by:

$$\tau \approx \frac{z^2}{4k} \qquad (4)$$

The amplitude of the pressure pulse at depth z at time τ is about 15% of that applied at the surface. For example, an abrupt pore-water pressure change at the top of the till

layer would propagate only 0.07 to 1.8 m (depending on k) in 36 minutes, at which depth it would have a relative magnitude of only 15%. For a 5 m thick layer of Black Rapids Glacier till, this diffusion time is on the order of hundreds of hours -- significantly longer than the 36 minutes required by our observations. Therefore, pore-water pressure, and thus the amount of pore-water, is not likely to change quickly in response to a rapid increase in hydraulic system pressure caused by the jökulhlaups.

Since significant changes in till density are mainly due to changes in the amount of pore-water, we believe that the density of the subglacial till did not change substantially during the seismic anomalies. In the remaining analysis, we must use a constant assumed density (porosity) because our seismic measurements do not provide a direct measurement of it. Typical values of till porosity lie between 20 and 40% (Clarke, 1987; Boulton and others, 1974; Boulton and Hindmarsh, 1987; Kamb, 1991; Alley and others, 1987; Fredlund and Rahardjo, 1993). However, as the till found beneath Ice Stream B (which defines the upper limit of this range) has an anomalously high clay content (Tulaczyk and others, in press) and consists of ocean-deposited sediments, it is probably not representative of subglacial tills of valley glaciers. We therefore assumed a more realistic porosity of 25% for Black Rapids Glacier till (ρ = 2250 kg m^{-3} from Eq. 3), noting that our interpretations are valid for any porosity within the range 20 to 40%.

Curves of constant reflection coefficient as a function of V_P and V_S for a fixed density (porosity) are shown in Figure 16. The regions enclosed in shaded rectangles in Figure 16 show our estimates of the permissible ranges of V_P and V_S for fully and partially saturated tills. Use of a different density simply shifts the curves left or right in this figure. For example, if we used 20 or 40% porosity, the $\Re_{PP}(50°)=0$ curve would be located at approximately the $R_{PP}(50°)$ = -.01 and +0.02 curves shown for ϕ=25%, respectively. As can be seen in this figure, solutions of (V_P, V_S, ρ) for both the normal ($\Re_{PP} > 0$) and anomalous ($\Re_{PP} = 0$) states exist within the seismic parameter space for till, and our somewhat arbitrary choice of ϕ = 25% does not affect this conclusion.

Thus we find that both the normal and anomalous seismic states can be accommodated by a model with a thick subglacial till layer.

Figure 16 can also be used to determine the minimum changes in seismic parameters that are necessary to change from the normal to anomalous states. If we assume that a minimum decrease in $\Re_{PP}$ of 0.01 is required to change from one state to another, then, from Figure 16, we see that only processes which decrease V_P by at least 40 m s^{-1}, increase V_S by at least 25 m s^{-1}, or both, can account for our observations. It is likely that the reflection coefficient in the normal state is greater than 0.01, as discussed earlier, and thus much larger changes in V_P and/or V_S would be required. For example, if $\Re_{PP} = 0.3$ in the normal state, then V_P would need to decrease by over 1000 m s^{-1} to cause the anomalies.

Figure 17 shows $\Re_{PP}$ as a function of incidence angle for illustrative combinations of V_P, V_S, and ρ for till for both $\Re_{PP}(50°)=0$ (anomalous state) and $\Re_{PP}(50°)=0.15$ (an example normal state). As can be seen from this figure, $\Re_{PP}$ is effectively zero in the anomalous state over a broad range (30° to 55°), and thus it is fairly insensitive the actual incidence angle.

CAUSES OF THE SEISMIC ANOMALIES

Knowing that the permissible wave speeds and density of till fall within the range required by our observations is a necessary, but not sufficient, condition for validation of a soft bed model. We need to determine whether any of the physical properties of till can affect these seismic parameters in the required manner, as well as find a mechanism that acts reversibly within 36 minutes through at least a 5 m thickness. Our analysis of the possibilities has led us to propose a new glaciologic mechanism for such changes, as no other mechanisms were found to be sufficient. We propose that the seismic anomalies are caused by a decrease in saturation, due probably to a local redistribution of the normal stress (overburden, P_o) on the till. After a summary of the observational

constraints, we describe this redistribution process. Then we discuss how a local decrease in normal stress can decrease pore-water pressure, causing gas to exolve and saturation to decrease. We test this model using reflection amplitude changes during the anomalies. Finally, we discuss why changes in the effective pressure of the till are not as likely, and end with a discussion of the effects of decreasing saturation on the shear strength of till.

Constraints on the possible mechanisms

Our observations and interpretations thus far place both spatial and temporal constraints on the possible causes of the seismic anomalies. We know that the till layer we are interested in, reflector PP_N (Fig. 11b), changed throughout at least 5 m of its thickness, and is about 200 m wide and 350 long. Therefore, any change responsible for the second and third seismic anomalies must occur over at least this area and thickness. Changes found in the later arriving reflections (e.g., PP_S, multiple P-P) indicate the bed changed over an area 700 m wide by 1300 m long. While we can not constrain the nature of those later changes, we do know that the mechanisms are related to that which affected reflector PP_N because both areas were affected with the same timing. Therefore, the responsible mechanism must affect a large area in as quickly as 36 minutes (as in the third anomaly), and yet persist for as long as two days (as in the second anomaly). Further, these changes must be seismically reversible. The normal state is characterized by a positive reflection coefficient and the anomalous state by a zero reflection coefficient, so the change from normal to anomalous state is characterized by a decreasing reflection coefficient. No changes in pore-water volume are possible under these time and thickness scales because the till is always in an 'undrained' state.

Proposed mechanism for changing seismic properties of till *in situ*

We propose that Black Rapids Glacier till may change from fully-saturated in the normal state to partially-saturated during the anomalous state. If a large decrease in the normal stress exerted by the ice on the till occurred, the pore-water pressure would decrease enough to cause gasses dissolved in the pore-water (perhaps originally entrapped in basal ice and liberated by melting) to come out of solution, thus decreasing saturation below 100%. The saturation change occurs by increasing the pore-space, not decreasing pore-water mass, and the process of gasses exolving and dissolving is controlled by the pore-water pressure – not the effective pressure. It is completely reversible, can occur on the time-scale of minutes, and has been widely recognized in soil mechanics (Terzaghi and others, 1996; Fredlund and Rahardjo, 1993).

If a conduit system becomes pressurized during a rapid input of water to the basal hydraulic system, the water pressure may exceed the local normal stress and hydraulically jack up the ice in a localized region (Iken and Bindschadler, 1986; Kamb and Engelhardt, 1987). Such transient increases in local water pressure have often been observed in boreholes, including those on Black Rapids Glacier. If the increase in water pressure is confined to the neighborhood of the conduits, then, because of the viscoelastic properties of ice, the region outside this neighborhood may experience a drop in local normal stress at the ice/till interface. The elastic strength of the ice can act temporarily like a bridge, spanning over the till and transferring the weight of the ice to fewer supports. The span over which such a stress redistribution occurs could possibly be quite small if feeder conduits or linked cavities of the hydraulic system were located within the reflector area. It is only required in our model that the normal stress over the seismic footprint be reduced on average, as small regions of higher normal stress within this area would probably be seismically undetectable at 50° incidence.

Such a process could redistribute normal stress over a potentially large area of the bed and be essentially reversible. The complex basal geometry of a valley glacier

may lead to jacking not only in the longitudinal direction (e.g., Iken, 1981) but transversely as well. The change from the anomalous to the normal seismic state could occur quickly (such as in the third anomaly) due to a sudden drop in water pressure of the hydraulic system, or slowly (such as in the second anomaly) by viscous relaxation. Considering that the Maxwell time, a measure of viscoelasticity, for ice is on the order of a few hours, it is plausible that such a load redistribution may last many hours.

Decreases in normal stress lead to a decrease in pore-water pressure in undrained tills (Fredlund and Rahardjo, 1993), as seen in Figure 18. As the pore-water pressure drops, dissolved gasses (probably air, in this case) will exolve (Fig. 18). The exolved gas fills the concomitant increase in pore-volume. As the till is undrained within our time-scale (i.e., pore-water mass is constant), the porosity must also be increasing slightly. This process is well documented in soil mechanics (e.g., Todd and Simmons, 1972; Fredlund and Rahardjo, 1993).

As will be discussed in the next section, a drop in saturation from 100 to 97% would cause major changes in the seismic reflections. This can occur if there is a 0.05 m increase in thickness of a 5 m thick till layer with an initial porosity of 25%. Following the second and third jökulhlaups, we observed increases in surface elevation near the glacier centerline of up to 0.15 ± 0.03 m (Fig. 11); this is on the same order as that observed on other glaciers (Iken and Bindshadler, 1986; Kamb and Engelhardt, 1987). While a portion of the total elevation change can be ascribed to longitudinal compressive strain in the ice, it is plausible that a third of it (i.e., 0.05 m) could be due to a true uplift at the bottom. Note, however, that such a large decrease in saturation is not required to satisfy this model -- a decrease of only several tenths of a percent from full saturation can meet the minimum seismic constraint of a change from positive to zero reflection coefficient. The uplift required to make such a small change occur is below our surveying resolution.

Tills can either dilate or compress during shear, depending on their physical properties and strain history. This would either decrease or increase pore-water

pressure, respectively, in an undrained till; the former could potentially cause a decrease in saturation. Such a change in saturation would be confined to the dilated layer, which would be much less than 5 m in our case (e.g., Clarke, 1987), and is therefore not a valid mechanism to explain the observed anomalies.

Laboratory measurements have qualitatively documented the type of seismic changes we propose beneath Black Rapids Glacier. For example, in an experiment on saturated limestone, Todd and Simmons (1972) found that V_P dropped instantaneously as confining pressure was dropped. After several hours in a water bath, V_P rose to the expected speed for a fully saturated sample at the new pressure. Todd and Simmons interpreted this as a rapid opening of pre-existing thin cracks, causing saturation to decrease (an initial undrained response), followed by slow filling of the new pore-space with water (a drained response).

Effects of a change in saturation on the reflection coefficients

Exploration seismologists searching for hydrocarbons look for large spatial anomalies caused by gas-filled pore-space. This is because saturation affects wave speeds, which in turn affects $\Re$. Since we can only speculate about the magnitude of temporal changes -- if any -- in saturation, this test of our model is limited to determining whether a decrease in saturation will decrease $\Re$, as required by the observations.

Glaciologists usually assume that subglacial tills are fully saturated, but no direct observations have confirmed this. Over long time scales, however, full saturation does seem to be a reasonable assumption, considering that there is a constant supply of water to the till and till can be considered drained. Further, full saturation is implicit for most theories of till deformation because they entail a single stress state variable for effective stress (i.e., $P_{eff} = P_o - P_{pw}$) to describe the mechanical behavior of the till. Although considerable soil mechanics research has shown that the mechanical aspects of a saturated soil, including volume change and shear strength, are governed by this effective stress, it does not sufficiently describe the behavior of unsaturated soils. In

this case, two independent stress state variables are required, as discussed later. We assume that *in situ* Black Rapids Glacier till is fully saturated under normal conditions.

Numerous laboratory studies have shown that a decrease in saturation from 100 to 97% causes a substantial decrease in V_P, while V_S remains unaffected, as shown in Figure 19a and summarized in Table 2a (see also Appendix E). As the saturation is decreased even further, both V_P and V_S increase slightly: dry values (S = 0%) are generally about 5% higher than the minimum reached near S = 97%. Unconsolidated sediments show a larger relative decrease (50 to 70%) than consolidated sediments and other rocks (40 to 60%).

Changes in V_P and V_S due to a decrease in S are plotted in vector form on Figure 20. Here we use the central value as a likely, yet arbitrary, normal state. We find that a decrease in saturation *decreases* $\Re_{PP}(50°)$, as required to satisfy our observations. In the example in Figure 20, we have used a conservative 25% decrease in V_P, but much larger changes are possible (e.g., Fig. 19a). In fact, changes due to saturation can reasonably produce a change from $\Re_{PP}(50°) = 0.3$ to zero -- our most stringent seismic constraint. Only a 0.1% decrease in S is required to meet the minimum required decrease in $\Re_{PP}$ of 0.01.

The effects of the decrease in saturation shown in Figure 20 across the entire range of incident angles are shown in Figure 17. There it can be seen that $\Re_{PP} \equiv 0$ over a broad range of incident angles (about 30° to 55°). Therefore the conclusions regarding saturation effects are not sensitive to our estimate of 50°.

Unsaturated tills have a significantly higher attenuation than saturated tills (Palmer and Traviolia, 1980; Dvorkin and others, 1995). In this way, an unsaturated till layer would act analogously to an acoustic ceiling tile, an analogy first suggested by Richards (1988) for the weak basal layer of Variegated Glacier during its 1982 surge.

Table 2. Summary of literature review of values of changes in V_P and V_S for till.

a) The expected variation for a decrease in saturation from 100% to 97% at constant effective pressure for consolidated and unconsolidated samples. Intermediate values should be expected for saturations between 97% and 100%. Percentages given are those of the fully saturated value. See Appendix B for details.

	Likely Percentage *Decrease* due to a Decrease in S from 100 to 97%
Consolidated Rock	
$\Delta V_P/V_P$	40-60%
$\Delta V_S/V_S$	5%
Unconsolidated Rock	
$\Delta V_P/V_P$	50-70%
$\Delta V_S/V_S$	5%

b) The expected decrease in wave speeds due to a decrease in effective pressure from 800 to 100 kPa for fully (100%) and partially (<97%) saturated samples.

	Expected *Decrease* due a 700 kPa decrease in P_{eff}
Fully saturated	
ΔV_P	< 100 m s^{-1}
ΔV_S	~ 200 m s^{-1}
Partially Saturated	
ΔV_P	~ 200 m s^{-1}
ΔV_S	~ 200 m s^{-1}

Shortcomings of changes in effective pressure

Most theories of basal motion suggest that decreased effective pressure (P_o - P_{pw}) within till leads to increased deformation there (Paterson, 1995). In this section, we show that if a change in effective pressure was solely responsible for the anomalies, the observed reflection coefficients indicate that it must *increase* at reflector PP_N. Further, we show that the only way that effective pressure can change in an undrained till is for the saturation to decrease in response to a decrease in local normal stress.

Reflection coefficients can determine the direction of change in effective pressure because increased effective pressure tends to make tighter grain-to-grain contacts, which increases wave speeds, while decreased effective pressure decreases wave speeds. P_{eff} affects V_P and V_S differently, depending on saturation, grain size, and microstructure (Appendix F). Using relations of $V_P(P_{eff})$ and $V_S(P_{eff})$ from the literature (e.g., Fig. 19b), we can determine the effects of P_{eff} on $\Re_{PP}$ using the curves in Figure 20. In this manner, we arrive at $\Re(P_{eff})$.

Similar to the analysis of the effects of saturation, we cannot determine the actual magnitude of the effect on $\Re$ due to a change in effective pressure because we do not know the initial speeds or the change in P_{eff}. We can, however, use the relative change in V_P and V_S for an assumed change in P_{eff} to determine whether an increase or decrease in P_{eff} is required to decrease $\Re$ during the seismic anomalies. We assumed a change of 100 to 800 kPa, which is within the range of pressures measured in boreholes on Black Rapids Glacier in 1996 (M. Truffer, pers. comm.). While borehole water levels do not directly measure P_{eff} in the till, we expect that such changes are within this range. Table 2b summarizes the results of a literature review (details in Appendix F). An increase in P_{eff} from 100 to 800 kPa would increase V_P till by less than 100 m s^{-1} for a fully saturated glacial till and by about 200 m s^{-1} for a partially (<97%) saturated one. V_S should increase by about 200 m s^{-1} at any saturation.

The effects on $\Re_{PP}$ are shown in Figure 20. Here we chose the same central 'normal-state' (V_P, V_S) values as before. The vector labelled 'Effective Pressure' indicates the magnitude and direction of change in $\Re_{PP}(50°)$ due to an *increase* in effective pressure from 100 to 800 kPa. As can be seen, the vector points towards the anomalous state ($\Re_{PP}(50°) = 0$), albeit obliquely. An increase in effective pressure during the anomalies is therefore a valid solution to the reflection coefficient constraints. But because of its obliqueness, it is not nearly as robust a solution as a change in saturation, and requires tighter constraints on the normal-state wave speeds. A decrease in effective pressure causes the vector to point away from the anomalous state. Our choice of the range for P_{eff} does not affect these results.

These results show that $\Re$ is much more sensitive to saturation than effective pressure. Thus, the vector sum of a 3% decrease in saturation and any reasonable *decrease* or *increase* in effective pressure will also decrease $\Re$.

While an increase in effective pressure is a valid solution for the reflection coefficient constraints, we have found no mechanism by which it can increase without a coincident change in saturation. Because $P_{eff} = P_o - P_{pw}$ for a fully saturated till, and noting that we have already ruled out changes in pore-water pressure due to diffusion, the local overburden must change. However, because the compressibility of water is much less than the compressibility of the soil structure, any increase in overburden in an undrained till is almost entirely transferred to the pore-water (Fredlund and Rahardjo, 1993, § 8.2.3). Thus, the effective pressure of a fully saturated, undrained till cannot be changed due to a change in normal stress (overburden) because there is a concomitant change in pore-water pressure such that the effective pressure remains constant (Fig. 18). It is only when the saturation is less than 100% that the effective pressure will change due to a change in overburden, as indicated by the bifurcation in Figure 18.

Shear strength of unsaturated till

The single-variable effective stress concept breaks down in an unsaturated till. Two independent stress-state variables are required for unsaturated soils because of their inherent suction, the magnitude of which depends on the grain size distribution, microstructure, strain history, and applied normal stress.

Fredlund and Rahardjo (1993) develop the force equilibrium equations for an unsaturated soil to account for what they consider to be four independent phases: soil, water, air, and a contractile skin created at the water/air interface (surface tension). When the water and soil are assumed to be incompressible, the stress state variables can be reduced to $(P_o - P_a)$ and $(P_a - P_{pw})$, where P_a is the air pressure. The first term is the net normal stress on the soil matrix and the second term is the matric suction, or capillarity. These terms determine the shear strength in a manner similar to that for saturated soils (Fredlund and Rahardjo, 1993, eq. (9.3)):

$$\tau_f = c' + (P_o - P_a) \tan \Phi' + (P_a - P_{pw}) \tan \Phi'' \qquad (5)$$

where τ_f is the shear stress on the failure plane at failure, c' is a cohesion term, and Φ' and Φ'' are constants giving the rate of increase in shear strength with net normal stress and matric suction, respectively. Φ' is always greater than Φ''. When an unsaturated soil is compressed, the gasses will dissolve and P_{pw} will equal P_a at full saturation, leading to the single effective stress for saturated soils.

The presence of matric suction in an unsaturated soil increases the shear strength of the soil. The magnitude is largely controlled by the microstructure, because the shape and size of the pores control surface tension. However, if the matric suction is caused by a decrease in P_o, as described above, then the net normal stress would *probably* decrease more than the increase in matric suction, thus weakening the till (Fig. 18 and Fredlund and Raharjo, 1993, § 9.3.4).

CONCLUSIONS

Using observations of changes in seismic reflections from Black Rapids Glacier presented in Nolan and Echelmeyer (submitted; Chapter 1), we have interpreted the basal morphology and physical mechanisms of these seismic changes using amplitude versus offset (AVO) techniques. We have tested two hypotheses for basal morphology: a hard bed model, in which a transient water layer forms between ice and bedrock, and a soft bed model, in which the properties of a layer of till change *in situ*. An iterative-type inversion of the Zoeppritz equations for the observed reflection coefficients shows that both models have seismically realizable solutions. However, glaciologically, we have ruled out the hard bed model because the seismic arrival-time constraints require the transient water layer to be more than 7 m thick over an area 200 m wide by 350 m long. Thinner water layers, although they cannot account for the changes by themselves, could not be ruled out because such layers may be seismically transparent at 50° offset. Therefore, our analysis of the possible physical causes of the seismic anomalies is focused on mechanisms that can affect tills.

The soft bed model leads to a till layer that is at least 5 m thick. We found that changes in either of two properties of this till layer could explain the change in the reflection coefficient during the anomalies: a decrease in saturation or an *increase* in effective pressure. Changes in saturation place no limitations on initial and final wave speeds of the till (both of which are unknown, but were constrained by a literature review) because it is such a robust solution. A decrease in saturation from 100 to 97% can cause a substantial (50%) decrease in P-wave speed. Such a change would cause a significant decrease in the reflection coefficient, the magnitude of this change can satisfy our most stringent observational constraints. Smaller decreases in saturation cause smaller decreases in P-wave speed, which still satisfy our minimum constraints. On the other hand, we found that the only mechanism by which effective pressure could change also requires a decrease in saturation. The reflection coefficient response is

much more sensitive to saturation than effective pressure and we therefore consider a decrease in saturation to be the primary cause of the seismic anomalies.

Changes in till saturation can occur if a subglacial conduit system becomes over-pressurized during the jökulhlaups, which can then hydraulically jack the glacier off the bed in some locations. In the areas of decreased normal stress, the pore-water pressure within the till will decrease, causing gas to come out of solution and decrease saturation. Both the jacking and degassing processes can occur quickly and reversibly, as required by the observations. This decrease in saturation would probably decrease the shear strength of the till there. Thus the shear strength of large areas of the bed can be affected by changes in other, hydraulically-isolated regions of the bed, resulting in a complex feedback system controlling ice dynamics.

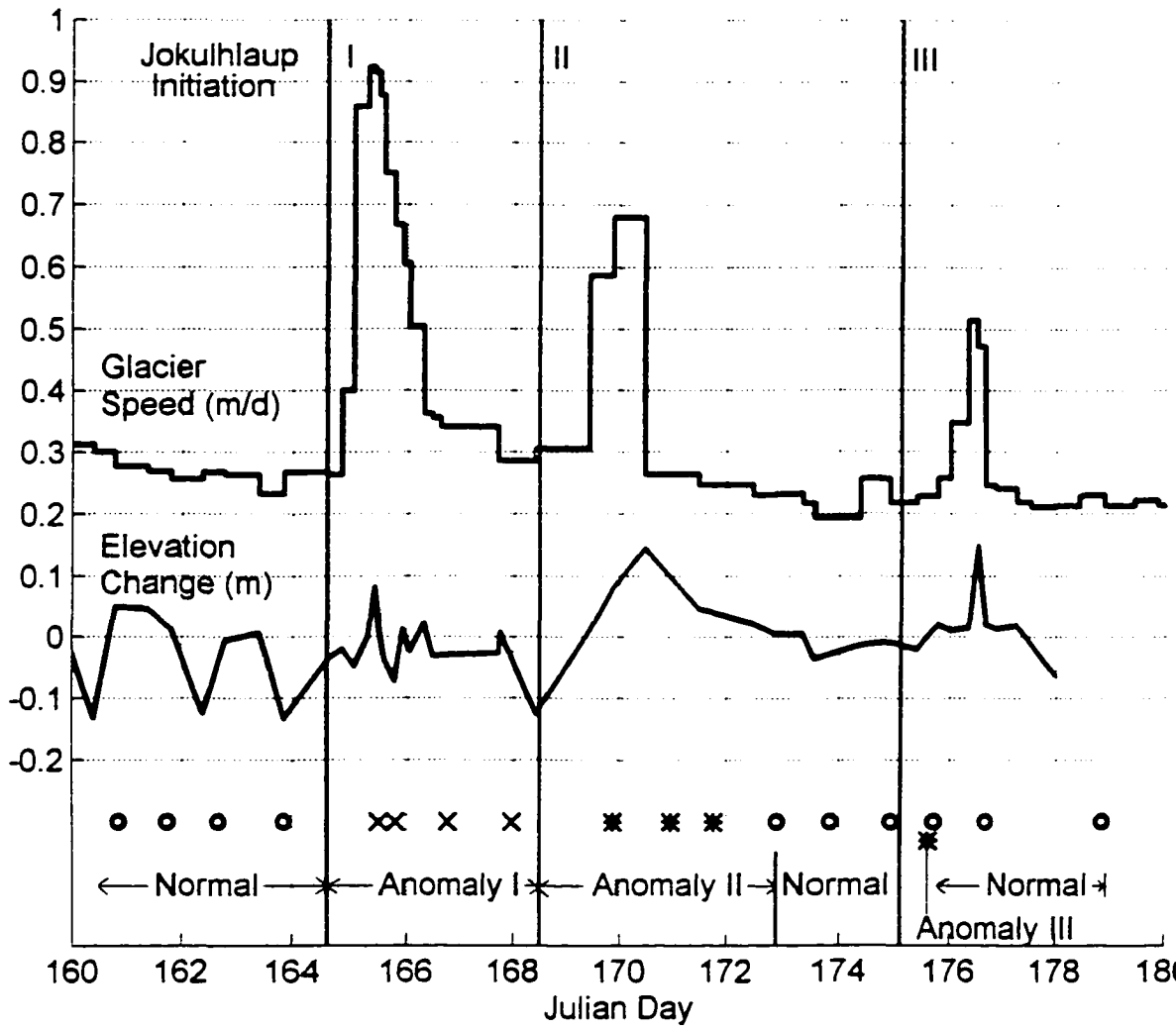

Figure 11a. Overview of observations. This portion of 16 km survey data (9 June to 29 June) brackets the lake drainages, shown as vertical lines. Elevation change is calculated from the vertical coordinate minus the mean decrease throughout the summer due to surface slope. Circles at bottom represent the 'normal' seismic measurements, while the '*' and 'x' symbols represent the two types of seismic anomalies.

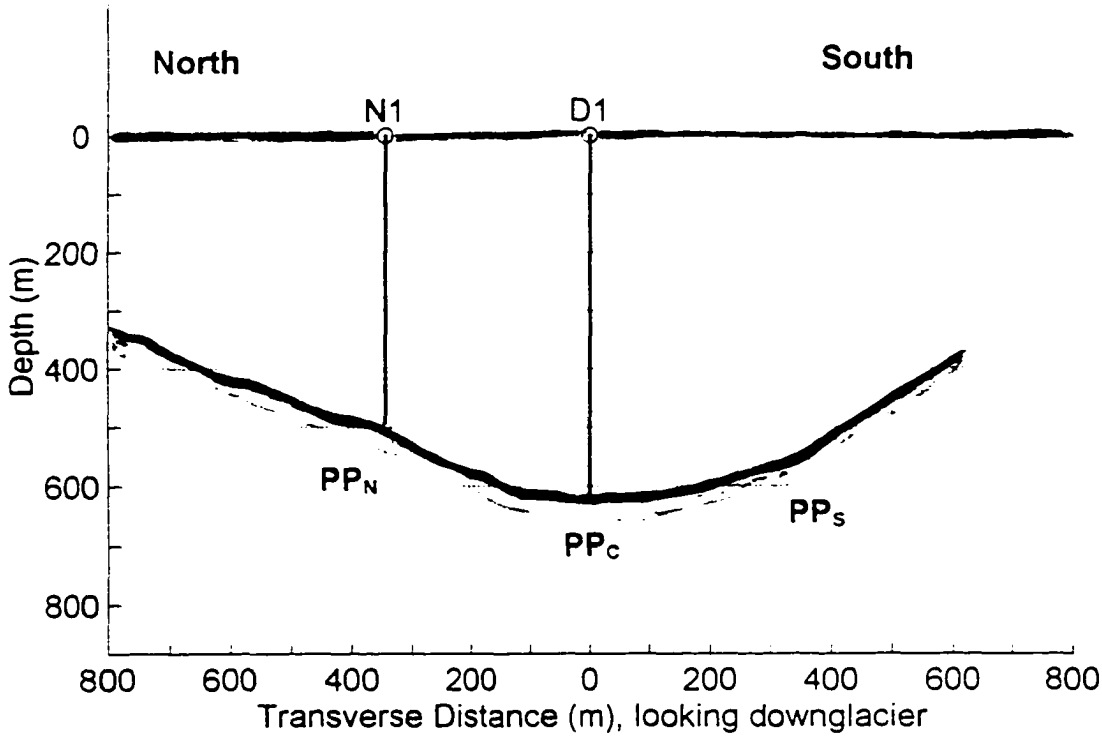

Figure 11b. Cross section of Black Rapids Glacier at 16 km. The bed was drawn from seismic, ice radar, and drilling data. Shown are the subglacial reflectors and boreholes referenced in this paper.

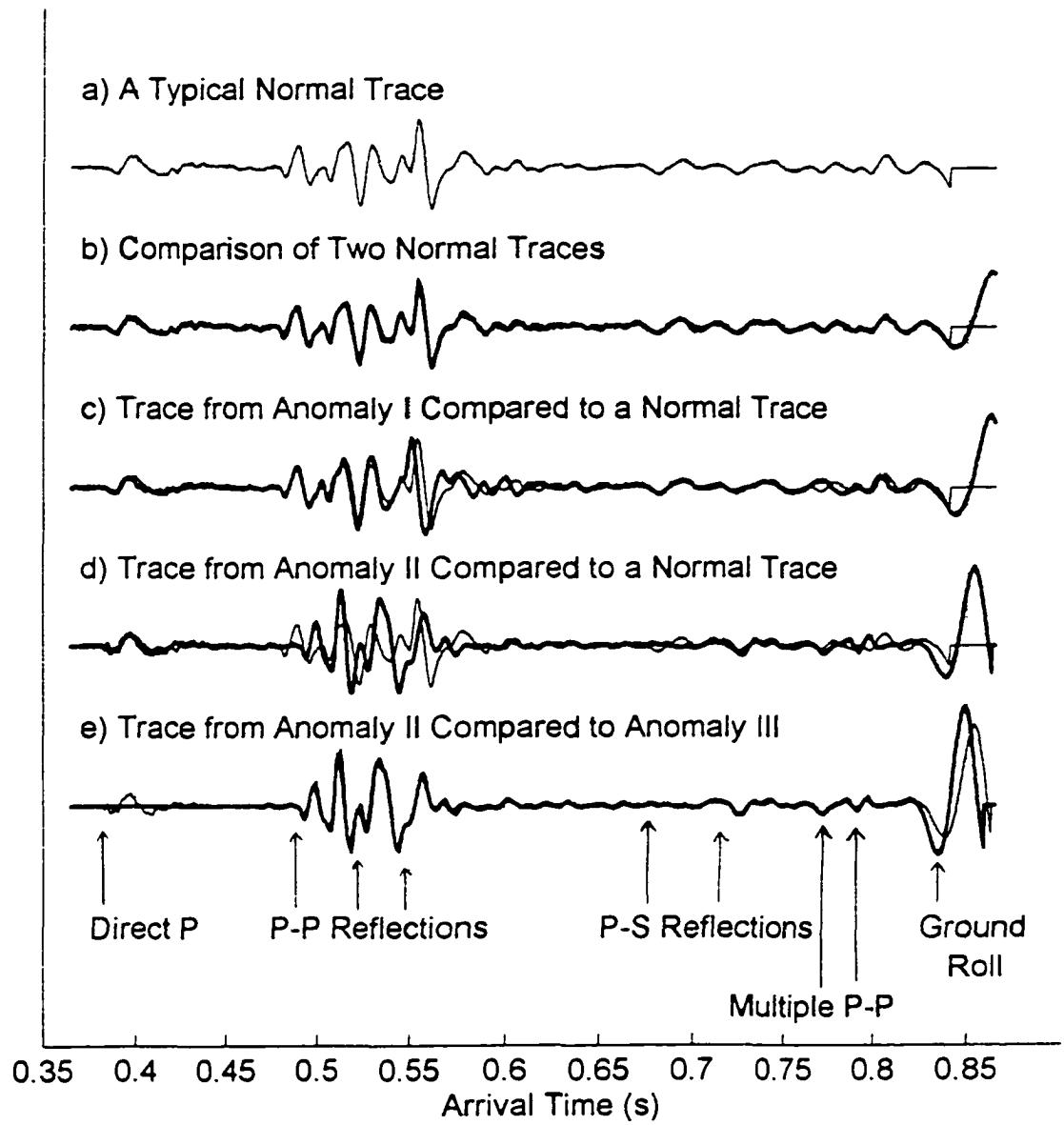

Figure 12. Comparison of sample seismic traces that reveal anomalies. The light trace shown in (a) is a normal trace that is repeated as the light trace in (b), (c), and (d). In (e), traces from the second and third anomalies are compared. Most of the interpretations in this paper are based on first P-P reflection arrival, which disappears during the second and third anomalies. Comparisons of these traces, from geophone #10, are typical of those made with the remaining 23 geophones for each daily record.

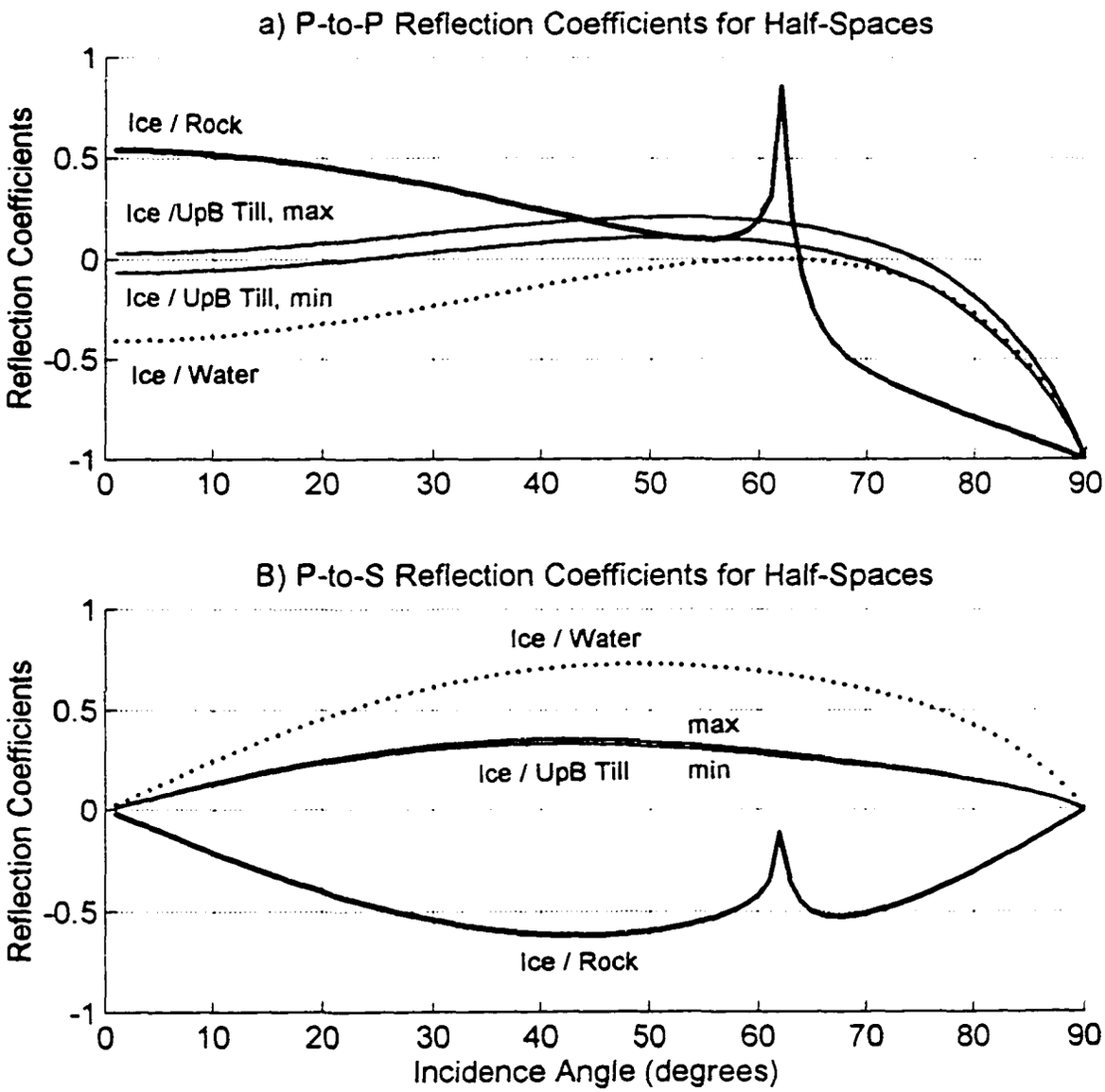

Figure 13a and 13b. Example reflection coefficients versus incidence angle for half space. Wave speeds and densities used in parts (a) through (d) are given in Table 1.

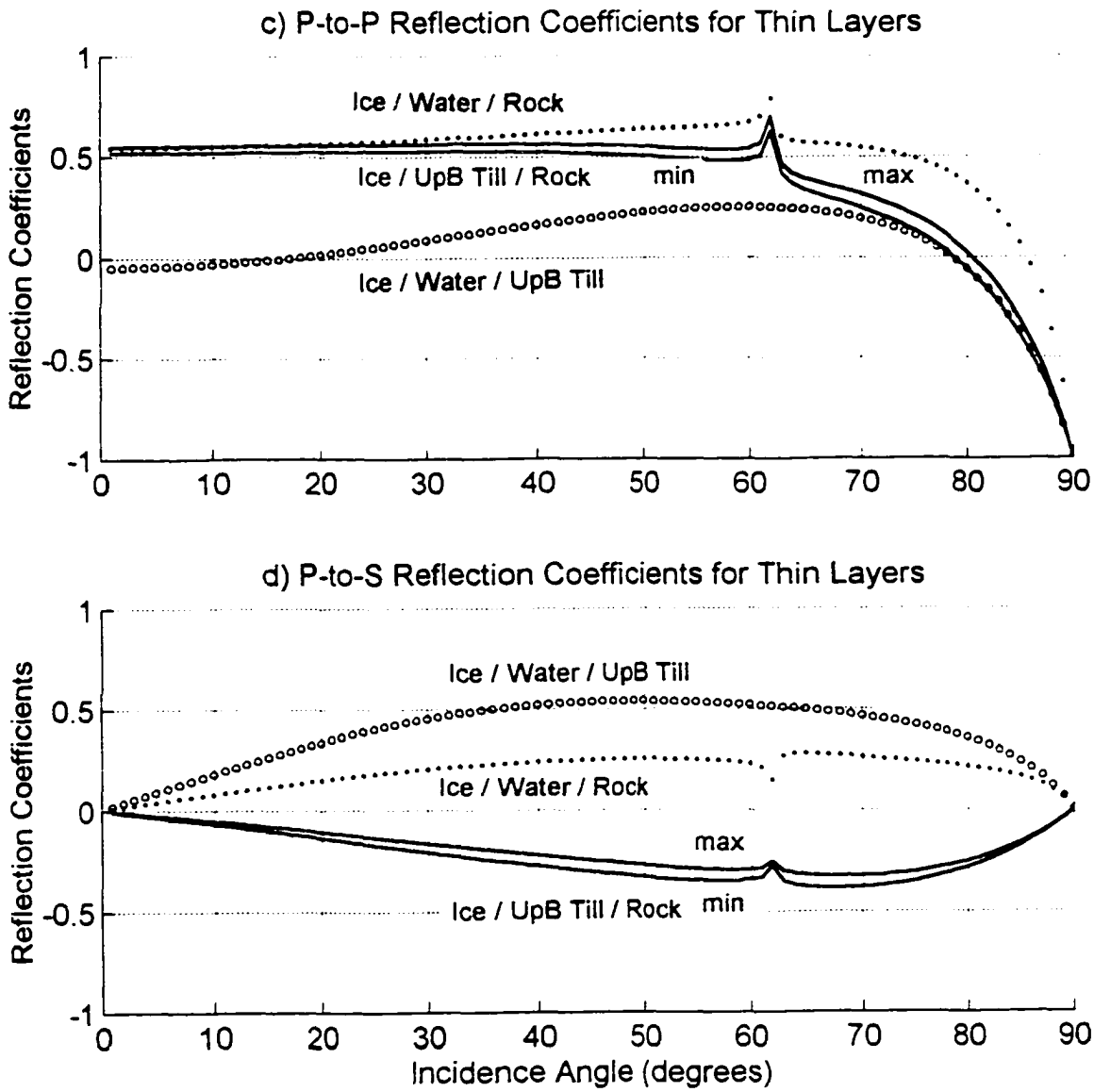

Figure 13c and 13d. Example reflection coefficients versus incidence angle for a thin layer between two half spaces. For water layers, the sum of the infinite multiple reflections within the layer is used. For solid layers, only the first multiple reflection within the layer is summed. Values used for UpB till are the mean of those given in Table 1.

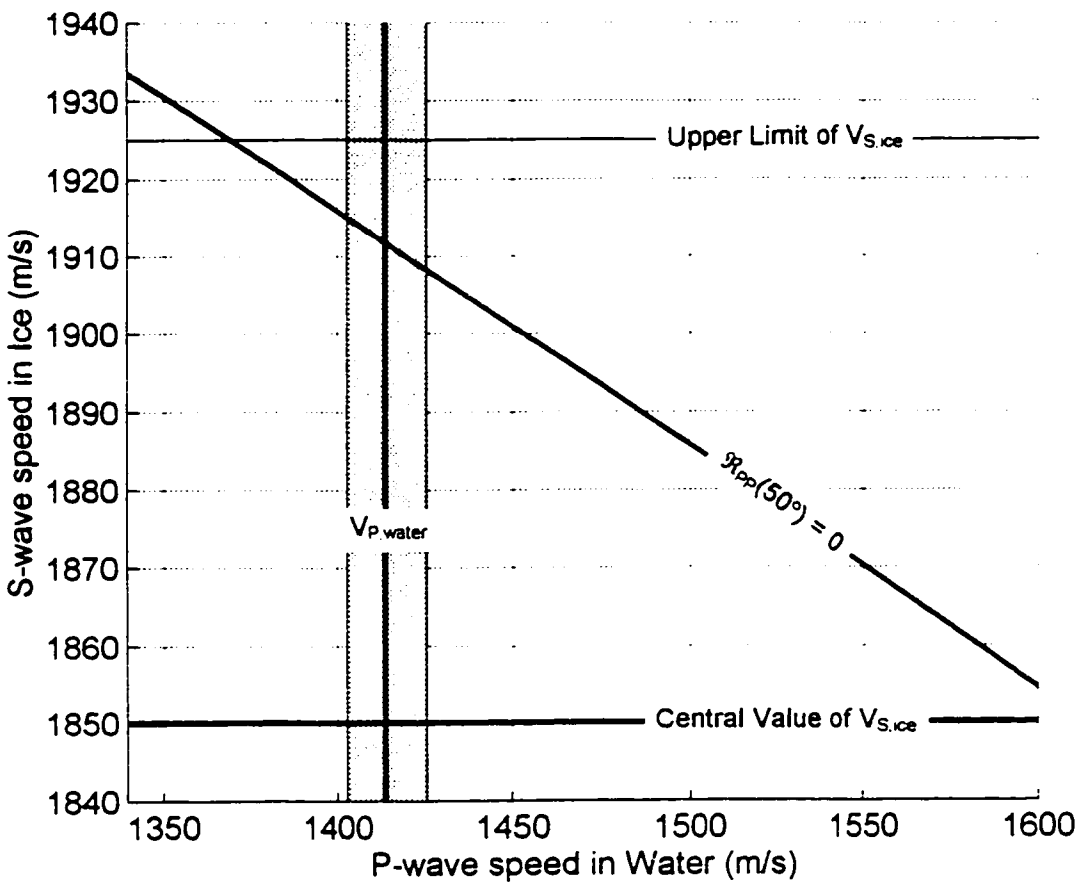

Figure 14. Seismic support for the hard bed model. The shaded region is the range of V_P for water due to the uncertainty in pressure and temperature. It intersects the loci of ($V_{P,water}$, $V_{S,ice}$) that yield $\Re_{PP}(50°)=0$. This intersection is within the uncertainty of the actual S-wave speed in temperate ice, shown as horizontal lines, indicating that water layers may be seismically transparent at an incidence angle of 50°.

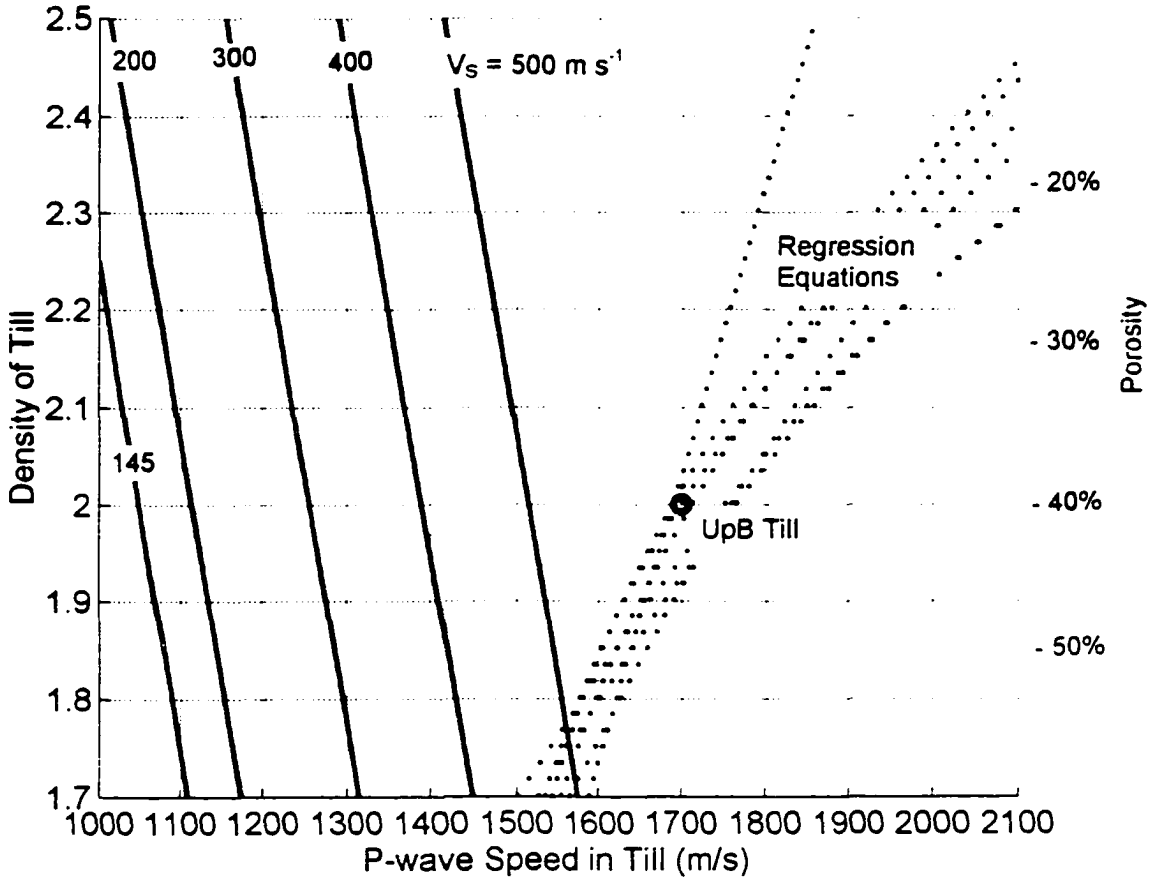

Figure 15. Loci of seismic parameters (V_P, V_S, ρ) that yield $\Re_{PP}(50°)\equiv 0$. These loci (solid curves) are the result of an iterative-type inversion of the Zoeppritz equations. Dotted lines are regression equations from various researchers (detailed in Appendix D)) that calculate V_P as a function of fully-saturated porosity (or density, using Eq. (1)).

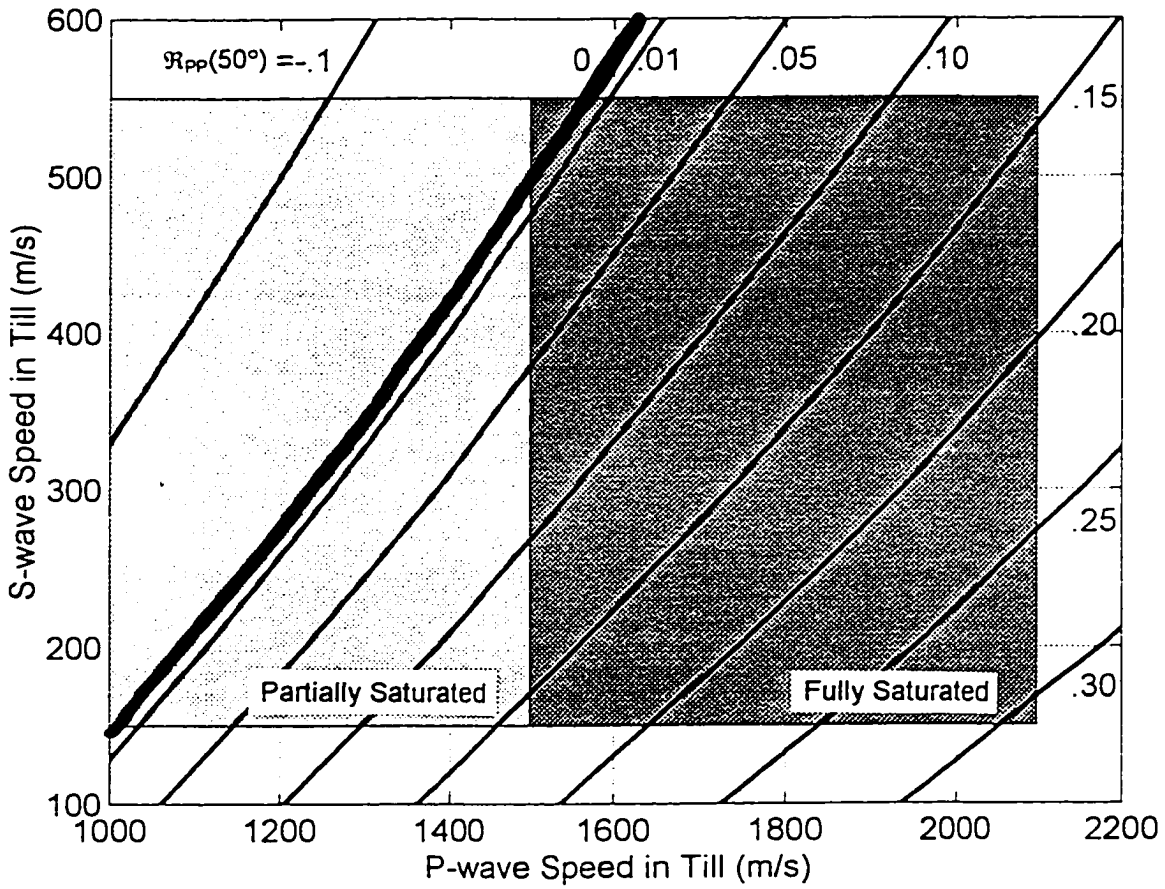

Figure 16. Seismic support for the soft bed model. Shown are the loci of seismic parameters (V_P, V_S) that yield a constant $\Re_{PP}(50°)$ (as annotated) for $\rho = 2250$ kg m^{-3}. The shaded regions are the permissible range of wave speeds of till (Appendix D). Loci for the normal state (positive $\Re_{PP}$) and the anomalous state ($\Re_{PP}$=0) lie within the permissible range, thus supporting the soft bed model

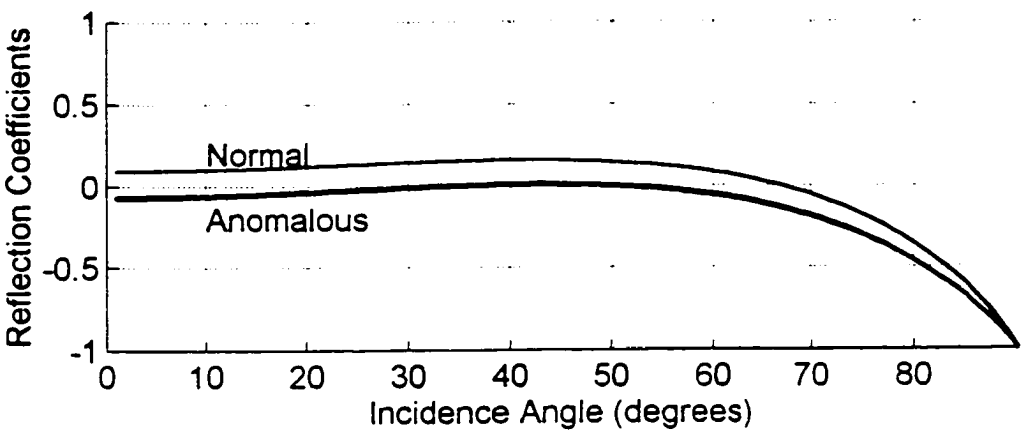

Figure 17. Example normal and anomalous state reflection coefficients. The reflection coefficients are nearly zero across a broad range of the anomalous curve (dark), indicating that our results are not sensitive to the estimated incidence angle of 50°. The normal curve (light) is calculated from V_P = 1800 m s^{-1}, V_S = 350 m s^{-1}, and ρ = 2250 kg m^{-3}. The anomalous curve differs only in that V_P = 1300 m s^{-1}, a change that can be caused by a decrease in saturation (Fig. 20).

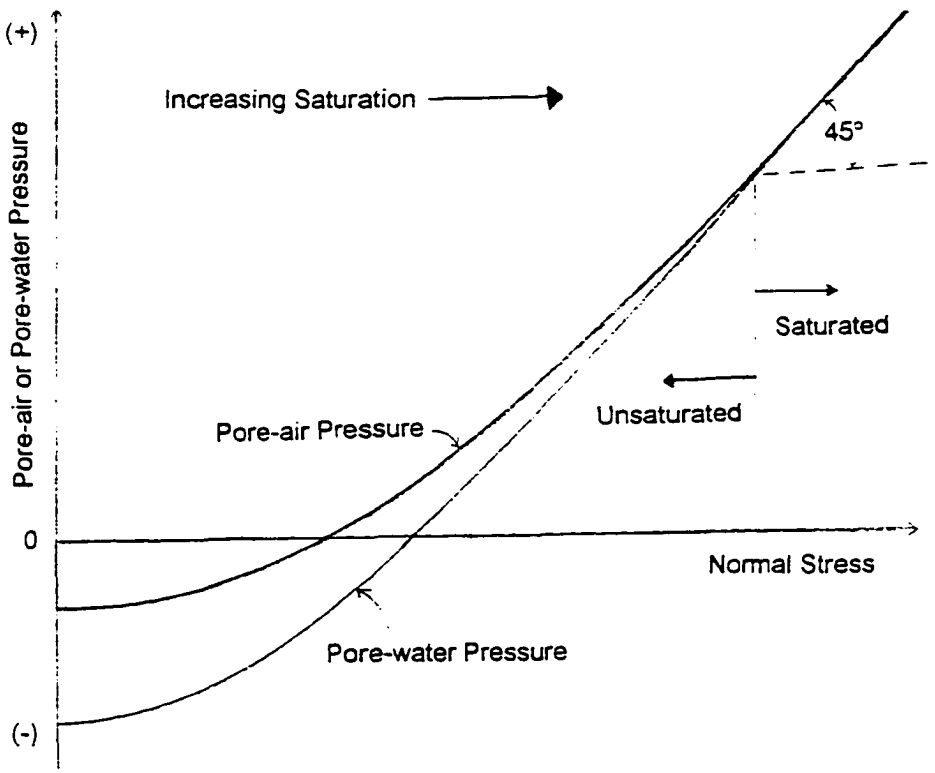

Figure 18. Pore-water and pore-air pressure undrained till as functions of normal stress. When the till is fully saturated, changes in normal stress cause a corresponding change in pore-water pressure, and the effective pressure remains constant. As the normal stress decreases, however, air exolves from the pore-water, causing saturation to decrease. Adapted from Fredlund and Rahardjo (1993, Fig. 8.8).

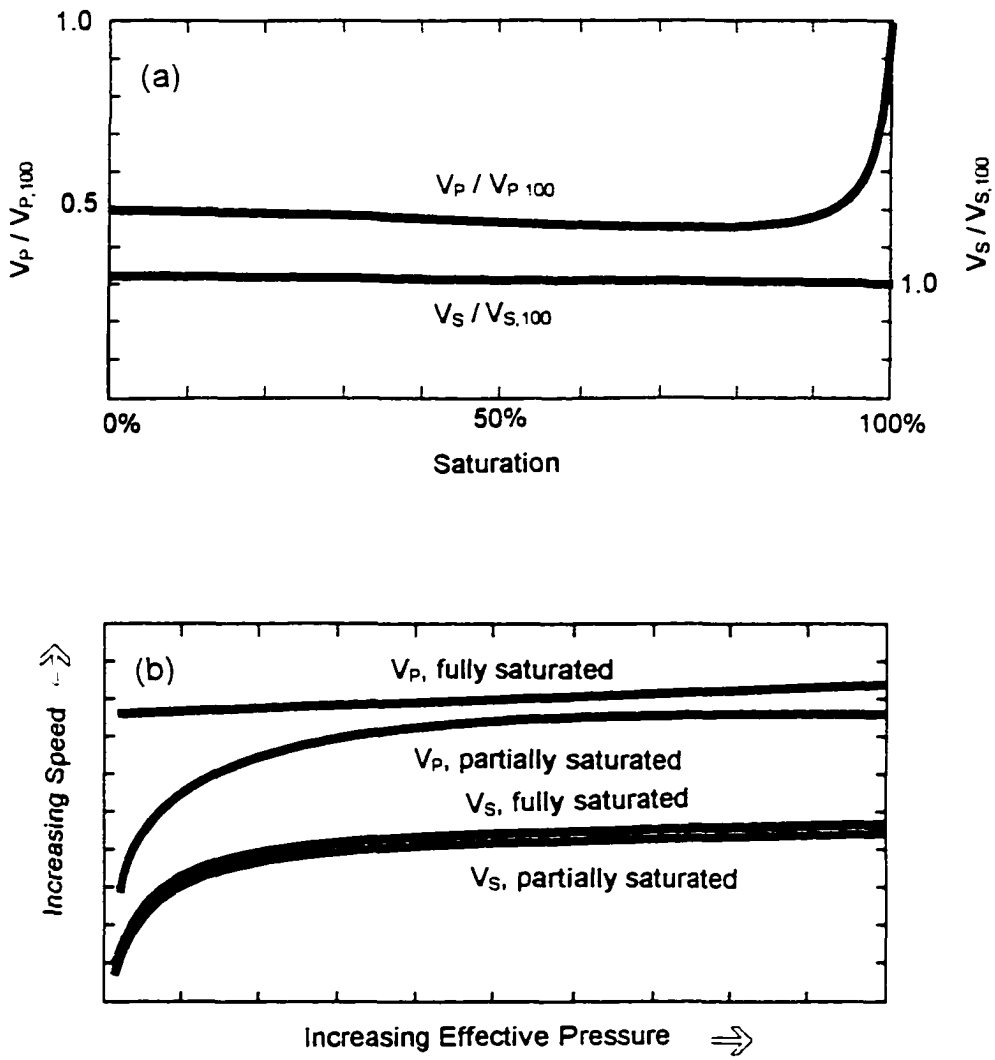

Figure 19. Illustrative effects of changes in saturation and effective pressure on seismic wave speeds. These curves are adapted from a variety of authors from measurements of rock and soil samples (see Appendices E and F). In (a), a small decrease in saturation is seen to have a large effect on V_P, but not on V_S. . In (b), fully saturated V_P is seen to be relatively insensitive to changes in effective pressure, while partially saturated V_P is about as sensitive as V_S (at any saturation).

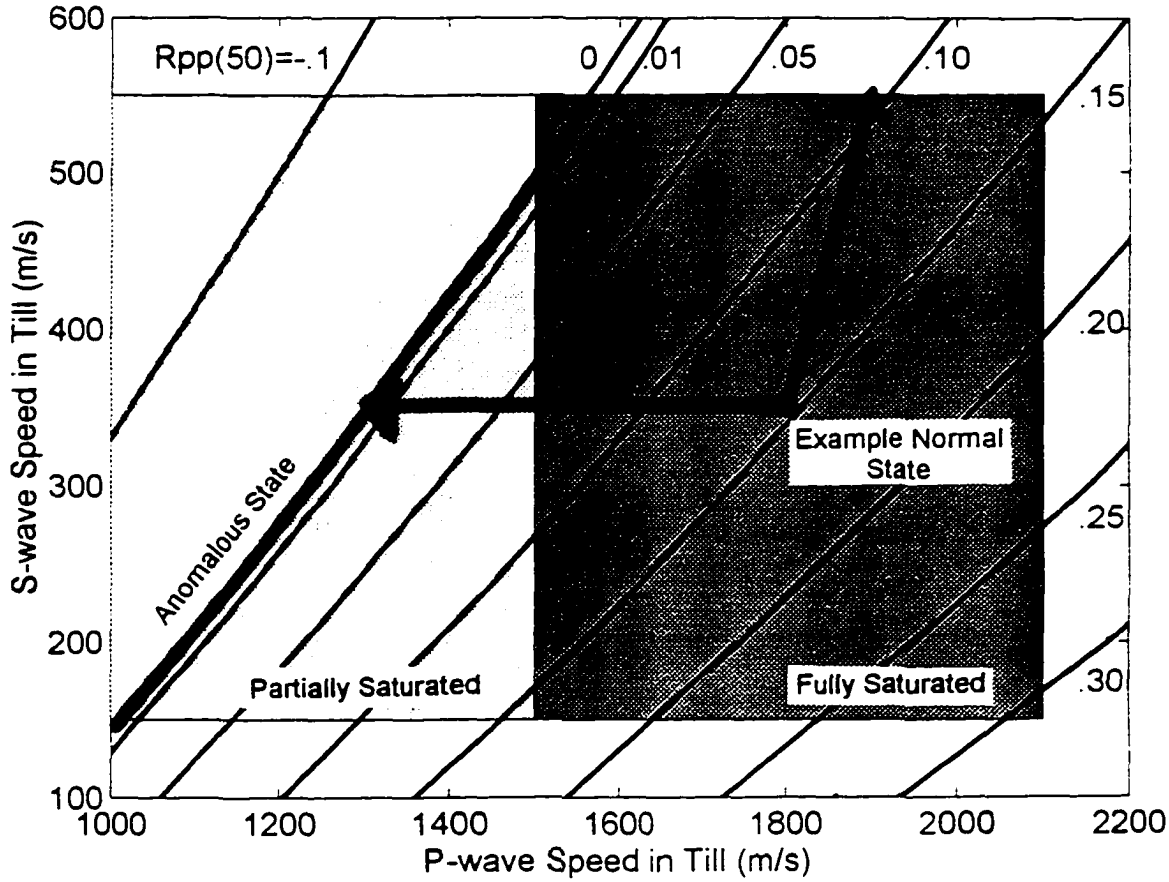

Figure 20. Changes in saturation and effective pressure that support the soft bed model. The curves are (V_P,V_S) loci of constant $\Re_{PP}(50°)$ (as annotated). The normal state is represented by a positive $\Re_{PP}(50°)$ loci and the anomalous state by $\Re_{PP}(50°)\cong 0$. The shaded regions are the permissible values V_P and V_S for partially and fully saturated tills. The vector labeled 'Saturation' represents a minimum change in $\Re_{PP}$ due to a decrease in saturation from 100 to 97%. The vector labeled 'Effective Pressure' represents the likely change in $\Re_{PP}$ due to an increase in P_{eff} from 100 to 800 kPa. Both of these vectors point towards the anomalous state given an arbitrary starting point within the normal state, and their direction will not change due to larger or smaller changes in P_{eff} or S.

APPENDICES

APPENDIX A: WAVE SPEED DETERMINATIONS

To determine seismic wave speeds in the temperate ice of Black Rapids Glacier, we could not employ the standard techniques of refraction and common depth point (CDP) analysis because these techniques require straight glaciers of uniform cross section and smooth beds relative to the ice thickness. We instead used our daily and longitudinal data sets, and comparisons with borehole and RES depth measurements. Consistent estimates of P-wave speed (V_p) were obtained by several different techniques.

Daily records

Travel times of the direct P-waves on our daily records were used to estimate V_p. This approach samples only the near surface ice in which the direct waves travel, and the speed so determined may be different than the bulk ice at depth due to differences in temperature, cracks, and water and bubble content. Velocity may be calculated by dividing the known offset by the arrival time, or by dividing the distance between two geophones by the difference in the arrival times at the geophones (the 'moveout'). Since our timing relative to the shot was inaccurate, the second approach was utilized, and only when a minimum of eight accurate first-arrivals per record could be identified. The mean V_p was 3710 ± 45 m s^{-1} and 3657 ± 58 m s^{-1} for the vertical and horizontal geophones, respectively, as measured on 30 records each.

The scatter is partly due to errors in the arrival times (± 1 ms leads to ±45 m s^{-1} error) and partly due to small differences in near surface ice conditions. However, there was no correlation between the scatter and the time of season or day.

Another way to extract wave speed is to compare the arrival time difference between the direct- and body-waves at a particular offset. We could not use this

method, however, because we do not know the ice thickness and bed slope with sufficient accuracy.

Longitudinal records

Direct P-wave data from the longitudinal data sets may also be used to determine V_p, giving 3707 ± 25 m s^{-1}. The moveout of the ground roll yields a Rayleigh wave speed (V_R) of 1687 and 1645 m s^{-1} for the vertical and horizontal geophones, respectively. V_R increased over the summer as the surface snow layer melted. The apparent anisotropy measured in the direct P-waves and ground roll was not observed in the P-waves measured through the body of the ice.

Plotting the square of the arrival times for a reflected wave versus the square of the offset gives another estimate of V_p. A straight line in this plot has a slope of V_p^{-2}. This method gives 3698 ± 5 m s^{-1}.

An estimate of the S-wave speed, V_s, can be obtained by dividing V_R by 0.92, the theoretical ratio between the two speeds. Choosing a late season Rayleigh wave speed to be more representative of pure ice gives V_s = 1850 ± 75 m s^{-1}.

Borehole and RES records

In the spring of 1996 we measured direct waves through the glacier using explosive sources and geophones placed in deep boreholes. Shots were placed 150 to 325 m below the surface. Four experiments gave V_p = 3716 ± 53 m s^{-1}. A further measure of V_p was obtained by comparing migrated seismic depths with the depths of five borehole drilled in 1996 (see Fig. 4). Using V_p = 3700 m s^{-1} gives ice depths that are within several meters of the borehole depths. Of course, the hot-water boreholes may not have reached the same interface as the seismic reflectors.

Comparisons of seismic and radar cross sections (T. Gades, pers. comm., 1994) from a transverse section about 300 m up-glacier of the boreholes did not yield useful constraints on V_p. The P-wave speed would need to be unreasonably high (>3850 m s^{-1}) to match the radar results. Using 3700 m s^{-1} an average depth discrepancy of about

45 meters is found between the two methods. There may have been some timing delay in the radar system or problems with the RES migration.

Comparison with previous research

Combining the various measurements of wave speeds, we obtain the following estimates for Black Rapids Glacier ice: $V_p = 3704 \pm 40$ m s^{-1}, $V_s = 1850 \pm 75$ m s^{-1}, and $V_R = 1690 \pm 40$ m s^{-1}. Roethlisberger (1972, Figs. 8 and 9) presents data on V_p and V_s versus temperature. Both show a large decrease in speed and a higher scatter as 0°C is approached, with values for V_p ranging from 3600 to 3730 m s^{-1}, and V_s between 1640 and 1730 m s^{-1} (with 7 data points) at 0°C. Controlled laboratory experiments indicate that the scatter is probably real, and that the speed is sensitive to liquid at the grain boundaries. The latter is dependent on the distribution of impurities and local heat transfer (Roethlisberger, 1972).

Bubble content must also be an important factor in the sudden decrease in wave speed near 0°C. Mavko and Nur (1975) present a theory for the seismic properties a solid matrix saturated with its own melt; they use the term 'squirt flow'. They find that the seismic properties of the composite material (in their case, the asthenosphere) change due to differences in compressibility and the movement of the liquid relative to the solid. The pore fluid can flow into vapor-filled void spaces (microcracks) during the passage of an elastic wave. Thus, the degree of saturation and the viscosity of the fluid will affect seismic wave speeds and attenuation in the partially melted medium. As the ice at the grain boundaries melts, the attendant decrease in volume may change the saturation of bulk ice and thus its compressional wave speed, but not its shear wave speed. This process would affect temperate ice more than cold ice, and explain both the decrease in speeds with increasing temperature as well as the high scatter near melting temperatures. Details on the role of saturation in controlling wave speeds are given in Nolan (1997) and N&E (Chapter 2).

APPENDIX B: ADJUSTING ERRORS IN TIMING

For daily data, the simplest approach to account for our timing errors is to pick the first arrival of the direct P-wave from one particular geophone and shift all the traces by the same value. This assumes that the P-wave speed is not varying, which is a reasonable first approximation. We modified this simple approach by picking first arrivals for all of the best direct P-waves, fitting a least-squares line to them, then shifting the records based on this best-fit line. The last step was done by calculating the arrival time for geophone #11 using the best fit line and shifting all the traces by a common value. This technique minimizes random errors associated with picking arrival times from a single geophone.

A similar method was used in correcting the longitudinal data. As the shot offset varied in increments of geophone spread length (300 m), the first arrival of the direct P-wave to the last geophone in a record should match that of the first geophone in the next record. Lines of best fit through these first picks were used to shift the records.

When the timing delays were so large that the direct waves was cut-off, as was the case on about 12 daily records, alternative methods were devised using similar approaches with the ground roll and the reflected P-waves, but neither of these methods were as accurate. The ground roll varies throughout the summer as the snow melts and the reflection arrival times are possibly changing daily. Errors in the longitudinal records so corrected did not suffer as much because they were collected within several hours of each other, minimizing the chances for temporal changes in wave velocity.

By overlaying two daily records, it became immediately obvious -- to within the accuracy of the sample rate -- whether the shifting was done properly or not. This was because the records were nearly identical. The largest difference found in the original

shift was 2 ms, and most were less. Thus, we assume that the relative timing errors are about 1 ms.

APPENDIX C: ZOEPPRITZ EQUATIONS AND ATTENUATION

Zoeppritz Equations

The study of seismic reflection coefficients is dominated by the analysis of contrasts in wave speeds and densities. The analytical solution for reflection coefficients for perfectly elastic materials was derived by Zoeppritz near the turn of century and are a mainstay of seismic interpretation. At normal incidence, they reduce to Equation 1 because there is no P-to-S conversion. Here we reproduce these equations, as given by Aki and Richards (1980), in a form easily coded into a computer program.

$$M = \begin{bmatrix} -\alpha_1 p & -\cos j_1 & \alpha_2 p & \cos j_2 \\ \cos i_1 & -\beta_1 p & \cos i_2 & -\beta_2 p \\ 2\rho_1\beta_1^2 p\cos i_1 & \rho_1\beta_1(1-2\beta_1^2p^2) & 2\rho_2\beta_2^2 p\cos i_2 & \rho_2\beta_2(1-2\beta_2^2p^2) \\ -\rho_1\alpha_1(1-2\beta_1^2p^2) & 2\rho_1 B_1^2 p\cos j_1 & \rho_2\alpha_2(1-2\beta_2^2p^2) & -2\rho_2\beta_2^2 p\cos j_2 \end{bmatrix}$$

$$N = \begin{bmatrix} \alpha_1 p & \cos j_1 & -\alpha_2 p & -\cos j_2 \\ \cos i_1 & -\beta_1 p & \cos i_2 & -\beta_2 p \\ 2\rho_1\beta_1^2 p\cos i_1 & \rho_1\beta_1(1-2\beta_1^2p^2) & 2\rho_2 B_2^2\cos i_2 & \rho_2\beta_2(1-2\beta_2^2p^2) \\ \rho_1\alpha_1(1-2\beta_1^2p^2) & -2\rho_1\beta_1^2 p\cos j_1 & -\rho_2\alpha_2(1-2\beta_2^2p^2) & 2\rho_2\beta_2^2 p\cos j_2 \end{bmatrix}$$

$$\Re = \begin{bmatrix} PP & SP & PP & SP \\ PS & SS & PS & SP \\ PP & SP & PP & SP \\ PS & SS & PS & SP \end{bmatrix} = M^{-1}N \qquad \text{(C-1)}$$

where α and B are P- and S-wave speed, respectively, 1 and 2 represent the upper and lower medium, respectively, i and j are incidence angles for P- and S-waves, respectively, the superscipt '\' and '/' represent down and up going waves, respectively, and p is the ray parameter (sin i / α). For example, the "$\Re_{PP}$" we use in the text is given by the upper left term of $\Re$ in Eq. C1, with a downgoing, incident P reflected upwards as a P-wave.

The Zoeppritz equations are notorious for errors in both journal and book reproduction, as well as individual coding, but are correctly reproduced in Aki and Richards (1980). We independently derived and coded these equations and compared them to our coding of their equations as a double check, and got the same results. As discussed in the text, we included Figure 13, in part, because the only previous plot of such data published in the Journal of Glaciology (Richards, 1988) is in error.

Attenuation Contrasts

Studies of seismic attenuation are typically concerned with energy losses through a medium. Bourbie (1982), however, has analytically and experimentally considered the effects of contrasts in attenuation on reflection coefficients. He found such that such contrasts can have a signficant effect on energy partitioning under certain conditions. While these conditions are not met for most rock/rock interfaces, we believe, based on his results, that they may be met in soft bed environments. Here we reproduce his main analytic results along with those findings which may be of interest to glaciologists.

The effects of attenuation contrasts appear in laboratory observations when the elastic reflection coefficient is very small ($< |0.1|$). As is evident from our Figure 13, at normal incidence ice/till interfaces will usually have elastic reflection coefficients much smaller than this ($< |0.05|$). At normal incidence, Bourbie (1982) found that the actual reflection coefficient ($\Re_{net}$) can be approximated by summing the elastic ($\Re_{el}$) and anelastic ($\Re_q$) components:

$$\Re_{net} = \frac{\rho_1\alpha_{10} - \rho_2\alpha_{20}}{\rho_1\alpha_{10} + \rho_2\alpha_{20}} + \frac{1}{2\pi}\left(\frac{1}{Q_{01}} - \frac{1}{Q_{02}}\right)\ln\left|\frac{\omega}{\omega_0}\right| + \frac{i}{4}\left|\frac{1}{Q_{01}} - \frac{1}{Q_{02}}\right| \qquad \text{(C-2)}$$

where Q_{01} and Q_{02} represent the quality factor (a measure of attenuation) in the upper and lower media, respectively, and the subscript 0 indicates that the α's and Q's are taken at a reference angular frequency w_o.

Equation C-2 does not hold for non-normal incidence angles. Below are expressions presented by Bourbie (1982) for $\Re_{net}$ as a function of incidence angle, in a form suitable for easy computer programming. They are essentially the Zoeppritz equations with complex wave speeds due to attenuation. The phase angle between the real and imaginary components of the wave speeds is given by the loss tangent γ:

$$\gamma = \left(\frac{1}{\pi}\right)\operatorname{atan}\left(\frac{1}{Q_2}\right) \qquad \text{(C-3)}$$

For large Q, as in ice, g is zero. For low Q, as possible in till, the phase angle leads to frequency dependent wave speeds:

$$\alpha_2(\omega) = \alpha_0\left(\frac{\omega}{\omega_0}\right)^{\gamma} e^{\left(1-\frac{\pi}{2}\right)\gamma} \qquad \text{(C-4)}$$

$$\beta_2(\omega) = \beta_0\left(\frac{\omega}{\omega_0}\right)^{\gamma} e^{\left(1-\frac{\pi}{2}\right)\gamma} \qquad \text{(C-5)}$$

where the zero subscript indicates measurement at the reference frequency wo. The final equations, solved only for P-wave incident from the upper media (ice), are:

$$A = \begin{bmatrix} k & h_1 & -k & h_2 \\ -d_1 & k & -d_2 & -k \\ -2kd_1\mu_1 & -(h_1^2-k^2)\mu_1 & -2kd_2\mu_2 & (h_2^2-k)\mu_2 \\ (h_1^2-k^2)\mu_1 & -2kh_1\mu_1 & -\mu_2(h_2^2-k^2) & -2kh_2\mu_2 \end{bmatrix}$$

$$B = \begin{bmatrix} -k \\ -d_1 \\ -2kd_1u_1 \\ -\mu_1(h_1^2-k^2) \end{bmatrix}$$

$$\Re = \begin{bmatrix} \Re_{PP} \\ \Re_{PS} \\ T_{PP} \\ T_{PS} \end{bmatrix} = A^{-1}B \qquad \text{(C-6)}$$

where k and d are the components of the propagation vector for the reflected or transmitted P-wave and k and h are the components for the reflected or transmitted S-waves (k is the same for all four waves from Snell's law), given by:

$$\mathrm{k} = \frac{\omega \sin \mathrm{i}_1}{\alpha_1}$$

$$\mathrm{d}_1 = \frac{\omega \cos \mathrm{i}_1}{\alpha_1} \qquad d_2 = \left(\frac{\omega^2}{\alpha_2^2} - k^2\right)^{\frac{1}{2}}$$

$$\mathrm{h}_1 = \frac{\omega \cos \mathrm{j}_1}{\beta_1} \qquad h_2 = \left(\frac{\omega^2}{\beta^2} - k^2\right)^{\frac{1}{2}}$$

$$\mu_1 = \rho\beta_1^2 \qquad \mu_2 = \rho_2\beta_2^2$$

In till with low Q, d, h, and μ (the shear modulus) will be complex because α and β are complex (Eq. C-4 and C-5).

APPENDIX D: RANGE OF WAVE SPEEDS

As a first approximation, it is sometimes assumed that porosity is an indirect measure of the till dilation that accompanies deformation, and further that wave speed measurements are a good indicator of porosity (e.g., Blankenship and others, 1987; Atre and Bentley, 1993; Smith, 1997). However, these assumptions require caution. For example, Eberhardt-Phillips and others (1989) have made a study of seismic wave speeds in fully saturated, unconsolidated ocean sediments as a function of porosity, clay content (C) and effective pressure. They found that clay content is as important as porosity in determining wave speeds. This means that spatial gradients in clay content may create effects as large as those in porosity. Several other spatially-varying properties also affect wave speeds at this level, and they must be considered before making morphological interpretations based on wave speeds alone.

The importance of grain size distribution on seismic properties has long been noted (e.g., Hamilton, 1970, 1976; Morgan, 1969; Hamdi and Taylor-Smith, 1981; Marion and others, 1992). Prasad and Meissner (1992) found that V_P of unconsolidated samples varied by as much as 250 m s^{-1} between different grain sizes and angularity. At the low effective pressures common in subglacial conditions, V_P ranged from 1750 to 2000 m s^{-1} and from 550 to 700 m s^{-1} for fully saturated and dry samples, respectively. V_S was found to vary little with grain size, and for low P_{eff} it was found to be about 300 to 350 m s^{-1} for both fully saturated and dry samples.

Clay content is especially important in determining wave speeds. Marion and others (1992) found a peak in V_P as clay content was experimentally increased in an

unconsolidated sand/clay mixture. At P_{eff}=10 MPa, they found that V_P was 2149 m s^{-1} for pure sand and 1950 m s^{-1} for clay, but when C was 40% by weight, the speed reached a maximum of 2500 m s^{-1}. This effect was amplified at higher effective pressures.

These grain size effects make comparisons between different tills difficult, if not impossible. For example, the wave speed measurements of till beneath Ice Stream B (Blankenship and others, 1987) may not apply to till beneath Black Rapids Glacier. This is because the Antarctic till has an unusually high clay content of >30%. (Tulaczyk and others, in press), whereas Black Rapids Glacier till has less than 7% (M. Truffer, pers. comm.). We also might expect till wave speeds to vary along ice streams and long glaciers if erosional clay content increases in the downstream direction, or if the type of bedrock from which the till is derived varies spatially.

The microstructure (the shape of the grains and their arrangement) also has a large influence of the acoustic properties of rocks and tills. Bourbie and Zinszner (1985) compared sandstones with nearly the same grain size and porosity. They found that wave speeds and attenuation in those sandstones with thinner, flatter pores were more sensitive to changes in effective pressure than those with round pores. The change in V_P due to a change in effective pressure from about 0.1 to 5 MPa was less than 50 m s^{-1} in a sample with round pores, while it was *ten times larger* in one with flatter pores. At 100 kPa the P-wave speed was 5270 and 4250 m s^{-1} for these two samples, respectively. These authors found a stronger correlation between microstructure and V_P than between porosity and wave speed.

This effect of microstructure is due to so-called "squirt flow" (Mavko and Nur, 1979; Dvorkin and Nur, 1993; Dvorkin and others, 1994 & 1995; Palmer and Traviolia, 1980). These studies show that, at both seismic and ultrasonic frequencies, pore fluid is temporarily squeezed out of thin, compliant pores and into stiffer, rounder pores by a passing wave. This fluid motion is the dominant mechanism of attenuation and velocity dispersion, and controls the relationship between effective pressure and

wave speeds. Materials with many thin pore spaces will have a higher attenuation and lower wave speeds -- particularly V_P, as the bulk modulus is influenced much more than the shear modulus.

For a fixed grain size distribution and microstructure, there is a good correlation between porosity and wave speed. The dotted curves in Figure 15 (labeled 'Regression Curves') show several empirical relationships between porosity and V_P, most of which were measured for unconsolidated ocean floor sediments (Hamilton, 1976; Morgan, 1969; Hamdi and Taylor-Smith, 1981; Eberhart-Phillips and others, 1989). They show the trend in relations between V_P and ϕ at a range of effective pressures, and they loosely constrain a range of physically acceptable values for fully saturated sand/silt mixtures. Note that decreasing porosity leads to higher wave speeds.

Various measurements on fully saturated, unconsolidated sediments and tills (the regression curves in Figure 15) indicate that, for $\phi = 0.25 \pm 0.05$, V_P should be in the range 1700 to 2070 m s^{-1}. It should be noted that many of these studies were done at effective pressures well in excess those expected in our study. At P_{eff} = 100 kPa, the laboratory measurements of Marion and others (1992) on saturated mixtures of sand and clay showed a range of 1550 to 1750 m s^{-1} as porosity ranged from 40% to 20%, respectively. The seismic observations of Blankenship and others (1987) on *in situ* Ice Stream B till at low effective pressure (~40 kPa; Kamb, 1991) and anomalously high porosity (> 32%) and clay content give an estimated V_P of 1550 ± 300 m s^{-1} (our error bar).

Data on the shear wave velocity are more sparse than those for P-waves. Hamilton (1976) reports average V_S for coarse sands, sand-silts, and sand-silt-clays in ocean sediment samples to be 240, 430, and 390 m s^{-1}, respectively (as corrected to 0°C following Shumway, 1958); the actual range within the sample set was 100 to 550 m s^{-1}. V_S for Ice Stream B till (Blankenship and others, 1987) was 145 ± 30 m s^{-1} (our error bar); Hamilton's (1976) summary suggests that this low value of V_S is indicative of a high porosity and clay content, as is the case there. Prasad and Meissner (1992)

report a range for V_S of 300 to 600 m s^{-1} (depending on P_{eff}) for a range of single grain-size samples.

Considering the uncertainty due to grain size, microstructure, and porosity, we estimate the permissible range of V_P for a fully saturated till beneath Black Rapids Glacier to be 1500 to 2100 m s^{-1}, with the central value of 1800 m s^{-1} being the most likely. A permissible range for V_S is 150 to 550 m s^{-1}, with the higher values at effective pressures near 800 kPa and the lower at 100 kPa. It is likely that P_{eff} at reflector PP_N is within 10% of overburden (i.e., 450 kPa), so we consider the central value of 350 m s^{-1} to be the most likely. For reasons described in the text, the permissible range for V_S for partially saturated sediments is the same.

As described in Appendix B, partially saturated sediments can have P-wave speeds below 500 m s^{-1}. From Figure 16, these low values of V_P do not corresponds with any permissible values of V_S that would yield $\Re_{PP}(50°)=0$. Therefore, we consider the lower bound of partially saturated V_P to be 1000 m s^{-1}, corresponding to the lower bound of V_S on Figure 16. As an upper bound for partially saturated V_P, we use 1500 m s^{-1} -- the lower bound of the fully saturated range – although the actual permissible range for partially saturated V_P includes most of the fully saturated range.

APPENDIX E: SEISMIC CHANGES DUE TO SATURATION

As shown in Figure 19a, as saturation (S) decreases from 100 to 97%, there is a significant drop in V_P, but little change in V_S. Changes in saturation below about 97% have only minor effects on V_P or V_S; this is the cause of a well-known interpretative difficulty with 'bright spots' in hydrocarbon exploration -- the bright spots signify the presence of gas within the pores, but not its volumetric percentage (below about 97%). An explanation for how saturation affects wave speeds (Murphy, 1982) can be found by examining the formulae for V_P and V_S:

$$V_P = \left(\frac{K + \frac{4}{3}\mu}{\rho} \right)^{1/2}$$

$$V_S = \left(\frac{\mu}{\rho} \right)^{1/2} \qquad \text{(E-1)}$$

where K and μ are the bulk and shear moduli, respectively. In a fully saturated sample, K (the inverse of compressibility) is dominated by the compressibility of water (~51 x 10^{-11} m^2 N^{-1}). As the saturation decreases to below 97%, K decreases to that of the more compressible rock matrix (< 3 x 10^{-11} m^2 N^{-1}) and V_P decreases. As S decreases further, the density continues to decrease; this slowly increases V_P to that of the fully dry sample. The amount of gas-filled pore-space does not affect μ, so there is no decrease in V_S. However, V_S has the same 5% increase due to the decreased density as V_P.

This change in wave speed can be demonstrated by a simple experiment. Place a sealed beer bottle on a table and tap it with a wooden spoon. Then shake it up, place it on the table, and tap it again. The decrease in pitch and tone duration after shaking is due to the change in compressibility arising from the presence of bubbles in the liquid -- in effect, a drop in saturation. The frequency (pitch) of the sound is equal to $V_P/2L$, where L is approximately the length of the bottle. The attenuation (which controls the duration) is proportional to V_P^{-3}. Therefore, as the wave speed decreases, both the frequency and tone duration decrease. This works with wine and hard liquors as well – it is not a function of carbonation.

Hamilton (1976) reports data on coarse Ottawa sands with porosity of about 36%. At 100 kPa, V_P dropped from 1900 to 500 m s^{-1} from 100% to 0% saturation, respectively. At 400 kPa, V_P dropped from 2000 to 700 m s^{-1}. Thus, in our range of effective pressure, V_P dropped by 64 to 74% from the fully saturated value.

Elliot and Wiley (1975) studied unconsolidated sands (ϕ=30%) at 700kHz . At 7 MPa, V_P dropped from 2200 to 1280 m s^{-1}, decrease of 42%.

Prasad and Meissner (1992) studied unconsolidated silts and sands with fixed grain sizes at 100 kHz. At about 200 kPa, V_P of a coarse silt/fine sand decreased from 1875 to 500 m s^{-1} going from 100% to 0% saturation. At the same effective pressure, V_P of a medium-coarse sand decreased from 1950 to 650 m s^{-1}. These two samples bracket their range of variation: a decrease of 67 to 73% from fully saturated to dry conditions.

Consolidated rocks show similar, but smaller changes in V_P with saturation: Winkler and Nur (1979) studied sandstone (ϕ = 23%) at frequencies of 500 to 1700 Hz. At about 100 kPa, V_P dropped from 4000 to 1600 m s^{-1} when saturation dropped below 97%, a 60% decrease.

Domenico (1976) studied Ottawa sandstone at about 10 MPa and 200 kHz. V_P dropped from 2073 to 1280 m s^{-1}, a 38% decrease.

Gregory (1976) studied sedimentary rocks (ϕ = 4 to 41%) and gabbros at 1 Mhz. He found that saturation effects were more pronounced at porosities less than 25%, but his curves of V_P vs. S were significantly different than those of most researchers. For example, at 100 kPa, V_P of a sandstone with ϕ = 4% decreased from 4665 to 4268 m s^{-1} as S changed from 100 to 80%, but the decrease continued to 3506 m s^{-1} as saturation went to zero.

There is some uncertainty in the saturation at which the abrupt transition in V_P occurs. For example, experiments by Murphy (1982) on sandstones indicate that most of the changes in V_P has occurred by S = 97%, while those of Domenico (1976) indicate that the transition occurs at about S = 90%. The discrepancy in experimental results is likely due to the difference in frequency used in the studies (Castagna, 1993). These results show that a decrease in V_P of 25% and zero in V_S, as illustrated in Figure 20, is a conservative estimate if S goes from 100 to 97% or lower.

APPENDIX F: SEISMIC CHANGES DUE TO EFFECTIVE PRESSURE

Changes in effective pressure affect V_P and V_S in the same qualitative way in unconsolidated silt, sands, and clays, as well as sedimentary and igneous rocks (Hamilton, 1976; Winkler and Nur, 1982; Eberhart-Phillips and others, 1989; Prasad and Meissner, 1992; Hamdi and Taylor-Smith, 1982; Gregory, 1976). When the pore-space is fully saturated with water, V_P is fairly insensitive to changes in P_{eff}. When partially saturated, V_P decreases with decreasing P_{eff}. The affects on V_S are comparitively insensitive to changes in saturation. As described in the text, the single valued concept of effective pressure (i.e., $P_{eff} = P_o - P_{pw}$) breaks down for partially saturated media because gas pressure is becomes important. Most researchers nevertheless continue to report wave speeds as functions of $P_{eff} = P_o - P_{pw}$ and, for better or worse, we continue their practice here.

These effects are qualitatively shown in Figure 19b. This figure was adapted from data of Hamilton (1976) and Domenico (1976) on unconsolidated sands, and Winkler and Nur (1979) on limestones. The actual relationship is strongly affected by the grain size distribution and microstructure, and for the Black Rapids till we can only estimate the change in fully and partially saturated wave speeds due to a change in effective pressure from 100 to 800 kPa.

The data of Hamdi and Taylor-Smith (1982) are particularly useful in this light (reproduced in Nolan, 1997). They show that as P_{eff} is increased from 96 to 772 kPa, V_P is increased by 50 to 100 m s^{-1}. An increase in effective pressure from 100 to 800 kPa leads to a increase of about 200 m s^{-1} in V_S. These samples were saturated ocean sediments (clay to fine sands) with relatively high porosities (ϕ = 34 to 52%); the porosity decreasing with increasing effective pressure.

Results on other unconsolidated samples are similar. Hamilton (1976) reports V_P varied less than 100 m s^{-1} in dry sands and over 200 m s^{-1} in brine saturated sands, and that V_S varied about 180 m s^{-1} at either saturation over this range of P_{eff}. Prasad

and Meissner (1992) studied samples of single grain sizes and found that fully saturated V_P increased about 150 m s^{-1} as P_{eff} increased by 1 MPa, while fully dry V_P increased about 30 m s^{-1} MPa^{-1}. V_S increased about 70 m s^{-1} MPa^{-1} for both dry and saturated samples.

Combining these results, we estimate that an increase in P_{eff} from 100 to 800 kPa will increase V_P by about 100 m s^{-1} and 200 m s^{-1} under fully or partially saturated conditions, respectively. V_S should increase about 200 m s^{-1} at any saturation.

Table F1. Data from Hamdi and Taylor Smith (1981) on the variation of V_P, V_S and ρ with effective pressure on fully saturated ocean sediments.

Sample	P_{eff}(kPa)	96.5	772	Change
Silty Clay	Vp, m s^{-1}	1603	1701	+ 98 m s^{-1}
	Vs, m s^{-1}	157	358	+ 201 m s^{-1}
	ϕ	.520	.422	- 0.098
Fine Silt	Vp, m s^{-1}	1716	1840	+ 124 m s^{-1}
	Vs, m s^{-1}	189	421	+ 232 m s^{-1}
	ϕ	.423	.342	- 0.081
Sandy Silt	Vp, m s^{-1}	1742	1814	+ 72 m s^{-1}
	Vs, m s^{-1}	152	269	+ 117 m s^{-1}
	ϕ	.417	.362	- 0.055
Fine Sand,	Vp, m s^{-1}	1813	1857	+ 44 m s^{-1}
Silt	Vs, m s^{-1}	175	315	+ 140 m s^{-1}
	ϕ	.387	.362	- 0.025

APPENDIX G: A GOOFY POEM

Ice is nice and good for you,
Snow makes glaciers grow.

Ice can deeform viscously,
Making glaciers flow.

This is how they creep along,
Always moving slow.

But why do ice streams move so fast?
What makes surges go?

When basal motion is real high,
Effective pressure's low.

So what can seismic waves tell us
That'we don't already know?

Tiny bubbles form real fast,
In the till below.

But t'learn th'effect on its strength
Will take some post-doc dough.

REFERENCES

Aki, K. and P. Richards, 1980. *Quantitative Seismology: Theory and Methods, Vol 1.* W.H Freeman and Co., 324 pgs.

Alley, R.B., D.D. Blankenship, C.R. Bentley, and S.T. Rooney, 1987. Till beneath Ice Stream B 3. Till deformation: Evidence and implications. *J. Geophys. Res.*, **92** (B9), p. 8921-8929.

Anandakrishnan, S., and R. Alley, in press. Tidal forcing of basal microearthquakes of ice stream C, West Antarctica observed hundreds of ice-thicknesses inland: observations, modeling and basal properties. *J. Geophys. Res.*

Atre, S. and C.R. Bentley, 1993. Laterally varying basal conditions beneath Ice Streams B and C, West Antartica. *J. Glaciol.*, **39** (133), 507-514.

Bentley, C.R, 1971. Seismic evidence for moraine within the basal Antarctic ice sheet, in Crary, A.P., *ed. Antarctic Snow and Ice Studies. II.* Washington, D.C., American Geophysical Union, 89-129. (Antartic Research Series, **16**).

Blankenship, D.D, C.R. Bentley, S.T. Rooney, and R.B. Alley, 1987. Till beneath Ice Stream B 1. Properties derived from seismic travel times. *J. Geophys. Res.*, **92** (B9), 8903-8911.

Boulton, G.S., D.L. Dent and E.M. Morris, 1974. Subglacial shearing and crushing, and the role of water pressures in tills from south-east Iceland. *Geogr. Ann.*, **56A**, 135-145.

Boulton and Hindmarsh, 1987. Sediment deformation beneath glaciers: rheology and geological consequences. *J. Geophys. Res.*, **92**, 9059-9082.

Bourbie, T., O. Coussy, and B. Zinszner, 1987. *Acoustics of Porous Media.* Houston, TX, Gulf Publishing Co. 557 pgs.

Bourbie, T. and A. Nur, 1984. Effects of Attenuation on Reflections: Experimental Test. *JGR*, **89** (B7), 6197-6202.

Bourbie, T. and B. Zinszner, 1985. Hydraulic and Acoustic Properties as a function of porosity in Fontainebleau sandstone. *J. Geophys. Res.*, **90** (B13), 11524-11532.

Castagna, J., 1993. AVO analysis -- Tutorial and Review, in Castagna, J. and M. Backus, *eds. Offset-dependent reflectivity -- Theory and practice of AVO analysis.* Tulsa, OK, Society of Exploration Geophysists, 3-36. (Investigations in Geophysics, **8**).

Carazzone, J. and L. Srnka, 1993. Elastic inversion of Gulf of Mexico data, in Castagna, J. and M. Backus, *eds. Offset-dependent reflectivity -- Theory and practice of AVO analysis.* Tulsa, Oklahoma, Society of Exploration Geophysists, 303-316. (Investigations in Geophysics, **8**).

Clarke, G.K.C., 1987. Subglacial till: A physical framework for its properties and processes. *J. Geophys. Res.*, **92** (B9), 9023-9036.

Clarke, T., 1991. Glacier dynamics in the Susitna River basin, Alaska, USA. *J. Glaciol.* **37** (125) 97-106.

Clarke, T. and K. Echelmeyer, 1996. Seismic-reflection evidence for a deep subglacial trough beneath Jakobshavns Isbrae, West Greenland. *J. Glaciol.* **43** (141) 219-232.

Cochran, O., 1995. The subglacial hydraulics of the surge-type Black Rapids Glacier, Alaska: a schematic model. University of Alaska Fairbanks: Masters Thesis.

de Marsily, G., 1986. Quantitative Hydrogeology. Florida, Academic Press, Inc., 440 pgs.

Demirbag, E., C. Coruh, and J. Costain, 1993. Inversion of P-wave AVO, in Castagna, J. and M. Backus, *eds. Offset-dependent reflectivity -- Theory and practice of AVO analysis.* Tulsa, OK, Society of Exploration Geophysists, 287-302. (Investigations in Geophysics, **8**).

Domenico, S., 1976. Effects of brine-gas mixture on velocity in an unconsolidated sand reservoir. *Geophysics*, **41** (5), 882-894.

Dvorkin, J., G. Mavko, and A. Nur, 1995. Squirt flow in fully saturated rocks. *Geophysics*, **60** (1), 97-107.

Dvorkin, J., R. Nolen-Hoeksema, and A. Nur, 1994. The squirt-flow mechanism: Macroscopic description. *Geophysics*, **59** (3), 428-438.

Dvorkin, J. and A. Nur, 1993. Dynamic poroelastically: A unified model with the squirt and the Biot mechanisms. *Geophysics*, **58** (4), 524-533.

Eberhart-Phillips, D., D.H. Han, and M.D. Zoback, 1989. Empirical relationships among seismic velocity, effective pressure, porosity, and clay content in sandstone. *Geophysics*, **54** (1), 82-89.

Elliott, S., and B. Wiley, 1975. Compressional velocities of partially saturated, unconsolidated sands. *Geophysics*, **40** (6), 949-954.

Fredlund, D. and H. Rahardjo, 1993. *Soil mechanics for unsaturated soils*. New York, John Wiley and Sons, Inc., 517 pgs.

Gregory, A., 1976. Fluid saturation effects on dynamic elastic properties of sedimentary rocks. *Geophysics* **41** (5), 895-921.

Hamdi, F.A.I and D. Talyor-Smith, 1981. Soil consolidation behavior assessed by seismic velocity measurements. *Geophysical Prospecting*, **29**, 715-729.

Hamilton, E.L., 1970. Sound velocity and related properties of marine sediments, North Pacific. *J. Geophys. Res.*, **75** (23), 4423-4447.

Hamilton, E.L., 1976. Shear-wave velocity versus depth in marine sediments: A review. *Geophysics* **41** (5), 985-996.

Hance, J., 1937. The recent advance of Black Rapids Glacier, Alaska. *J. Geol.*, **45**, 775-783.

Harrison, W., L. Mayo, and D. Trabant, 1975. Temperature measurements on Black Rapids Glacier, Alaska, 1973. In Weller, G. and S. A. Bowling, *eds. Climate of the Arctic*. Fairbanks, AK, Geophysical Institute, University of Alaska, Fairbanks 350-352.

Harrison, W. and K. Echelmeyer, E. Chacho, C. Raymond, and R. Benedict, 1994. The 1987-88 surge of West Fork Glacier, Susitna Basin, Alaska, USA. *J. Glaciol.* **40** (135) 241-254.

Heinrichs, T., L. Mayo, K. Echelmeyer, and W. Harrison, 1996. Quiescent-phase evolution of a surge-type glacier: Black Rapids Glacier, Alaska, USA. *J. Glaciol.* **42** (140), 110-122.

Iken, A., 1981. The effect of the subglacial water pressure on the sliding velocity of a glacier in an idealized numerical model. *J. Glaciol.*, **27** (110), 101-119.

Iken, A. and R. Bindschadler, 1986. Combined measurements of subglacial water pressure and surface velocity of Findelengletscher. Switzerland: conclusions about drainage system and sliding mechanism. *J. Glaciol,*. **32** (110), 101-119.

Ito, H., J. DeVilbiss, and A. Nur, 1979. Compressional and shear waves in saturated rock during water-steam transition. *J. Geophys. Res.*, **84** (B9), 4731-4735.

Kamb, B., 1970. Sliding motion of glaciers: Theory and observation. *Reviews of Geophysics and Space Physics*, **8** (4), 673-728.

Kamb, B., 1991. Rheological nonlinearity and flow instability in the deforming bed mechanism of ice stream motion. *J. Geophys. Res.*, **92**, 9083-9100.

Kamb, B. and H. Englehardt, 1987. Waves of accelerated motion in a glacier approaching surge: the mini-surges of Variegated Glacier, Alaska, U.S.A. *J. Glaciol.*, **33** (113), 27-46.

Kamb, B. *and 7 others*, 1985. Glacier surge mechanism: 1982-1983 Surge of Variegated Glacier, Alaska. *Science* **227** (4686) 469-479.

Kallweit, R.S., and L.C. Wood, 1982. The limits of resolution of zero phase wavelets. *Geophysics*, **47**, 1035-1046.

Koefoed, O. and N. de Voogd, 1980. The linear properties of thin layers, with an application to synthetic seismograms over coal seams. *Geophysics*, **45** (8), 1254-1268.

Marion, D., A. Nur, H. Yin, and D. Han, 1992. Compressional velocity and porosity in sand-clay mixtures. *Geophysics*, **57** (4), 554-563.

Matheney, P., 1991. Anelastic attenuation of compressional seismic waves in glacial deposits. Northern Illinois University: Master's thesis.

Mavko, G. and A. Nur, 1975. Melt squirt in the asthenosphere. *J. Geophys. Res.*, **80** (11), 1444-1448.

Morgan, N.A., 1969. Physical properties of marine sediments as related to seismic velocities. *Geophysics*, **34** (4), 529-545.

Murphy, W., 1982. Effects of partial water saturation on attenuation in Massilon sandstone and Vycor porous glass. *J. Acoust. Soc. Am.*, **71**(6), 1458-1468.

Nolan, M., 1997. Seismic detection of transient subglacial changes beneath Black Rapids Glacier, Alaska. (Ph.D. Thesis, University of Alaska, Fairbanks.)

Nolan, M., R. Motyka, K. Echelmeyer, and D. Trabant, 1995. Ice-thickness measurements of Taku Glacier, Alaska, USA, and their relevance to its recent behavior. *J. Glaciol.*, **41** (139), 541-553.

Nokleberg, W.J.*and 6 others*, 1992. Preliminary geologic map of the Mount Hayes quadrangle, eastern Alaska Range, Alaska. *U.S. Geol. Surv. Open File Rep.* 92-594.

Palmer, I.D. and M.L. Traviolia, 1980. Attenuation by squirt flow in undersaturated gas sands. *Geophysics*, **45** (12), 1780-1792.

Paterson, W.S.B, 1995. *The physics of glaciers, 3rd ed.* England, Pergamon/Elsevier Science Ltd., 480 pgs.

Power, J. and K. Echelmeyer, 1986. Passive seismic studies on Jakobshavns Glacier in relation to calving and ice stream dynamics. Abstract in *AGU Chapman Conference on Fast Glacier Flow, 1986.*

Prasad, M. and R. Meissner, 1992. Attenuation mechanisms in sands: Laboratory versus theoretical (Biot) data. *Geophysics*, **57** (5), 710-719.

Raymond, C.F. and S. Malone, 1986. Propagating strain anomalies during mini-surges of Variegated Glacier, Alaska, U.S.A. *J. Glaciol.* **32** (111), 178-191.

Raymond, C., R. Benedict, W. Harrison, K. Echelmeyer, and M. Sturm, 1996. Hydrologic discharges and motion of Fels and Black Rapids Glaciers, Alaska, USA: implications for the structure of their drainage systems. *J. Glaciol.* **41** (138), 290-304.

Reger, R., A. Sturmann, and J. Beget, 1993. Dating Holocene moraines of Black Rapids Glacier, Delta River valley, central Alaska Range. In Solic, D. and F. Tannian, *eds., Short Notes on Alaskan geology 1993. Alaska Division of Geological and Geophysical Surveys Professional Report 113.*

Ricker, N., 1953. Wavelet contraction, wavelet expansion, and the control of seismic resolution. *Geophysics* **18** (4), 769-792.

Richards, M.A., 1988. Seismic evidence for a weak basal layer during the 1982 surge of Variegated Glacier, Alaska, U.S.A. *J. Glaciol.*, **34** (116), 111-120.

Roethlisberger, H., 1972. *Seismic exploration in cold regions I. CCREL Cold regions science and engineering Monograph* II-A2a.

Rooney, S.T., D.D. Blankenship, R.B. Alley, and C.R. Bentley, 1987. Till Beneath Ice Stream B 2. Structure and contuinuity. *J. Geophys. Res.*, **92** (B9), 8913-8920.

Sheriff, R.E. and L.P. Geldart, 1995. *Exploration Seismology*. England, Cambridge University Press. 592 pgs.

Shumway, G., 1958. Sound velocity vs. temperature in water-saturated sediments. *Geophysics*, **23** (3), 494-505.

Smith, A., in press. Variations in basal conditions on Rutford Ice Stream, West Antarctica. *J. Geophys. Res.*

Spratt, R., N. Goins, and T. Fitch, 1993. Pseudo-shear -- The analysis of AVO, Castagna, J. and M. Backus, *eds.*, *Offset-dependent reflectivity -- Theory and practice of AVO analysis*. Tulsa, OK, Society of Exploration Geophysists, 37-56. (Investigations in Geophysics, **8**).

Sturm, M. and D. Cosgrove, 1990. An unusual jökulhlaup involving potholes on Black Rapids Glacier, Alaska Range, Alaska, USA *J. Glaciol.* **32** (122), 103-104.

Terzaghi, K., R. Peck, and G. Mesri, 1996. *Soil mechanics in engineering practice, 3rd ed.* New York, John Wiley and Sons, Inc. 549 pgs.

Todd, T, and G. Simmons, 1972. Effect of pore pressure on the velocity of compressional waves in low-porosity rocks. *JGR*, 77 (20), 3731-3743.

Truffer, M., W. Harrison, K. Echelmeyer, J. Gorda-DeMallie, and T. Heinrichs, 1996. Velocity variations of surge-type Black Rapids Glacier. American Geophysical Union 1996 Fall Meeting Program, 102.

Tsingas, C. and E. Kanasewich, 1991. Seismic reflection amplitude versus angle variations over a thermally enhanced oil recovery site. *Geophysics*, **56** (2), 292-301.

Tulaczyk, S., B. Kamb, R. Scherer, and H. Englehardt, in press. Sedimentary processes at the base of a West Antarctic ice stream: constraints from textural and compositional properties of subglacial debris. *J. Sediment. Res.*

Weertman, J., 1964. Theory of glacier sliding. *J. Glaciol.*, **5**, 287-303.

Widess, M. B., 1973. How thin is a thin bed? *Geophysics* **38**, 1176-1180.

Willis, I., 1995. Intra-annual variations in glacier motion: a review. *Progress in Physical Geography*, **19** (1), 61-106.

Wilson, W, 1959. Speed of sound in distilled water as a function of temperature and pressure. *J. Acoust. Soc. Am.*, **31** (8), 1067-1072.

Winkler, K. and A. Nur, 1982. Seismic attenuation: effects of pore fluids and frictional sliding. *Geophysics*, **47** (1), 1-13.

Wolf, L.W. and J. N. Davies, 1986. Glacier-generated earthquakes from Prince William Sound, AK. *Bull. Seis. Soc. Am.*, **76** (2), 367-79.

IMAGE EVALUATION TEST TARGET (QA-3)

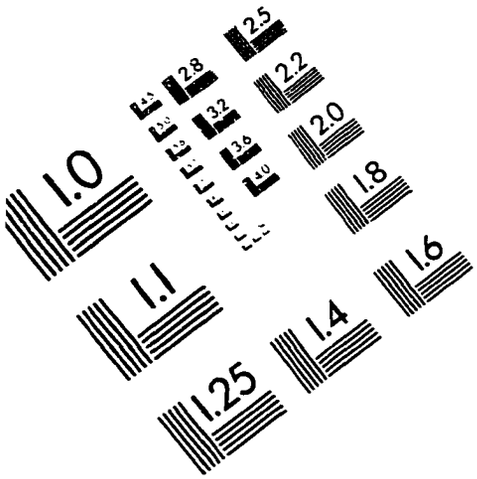

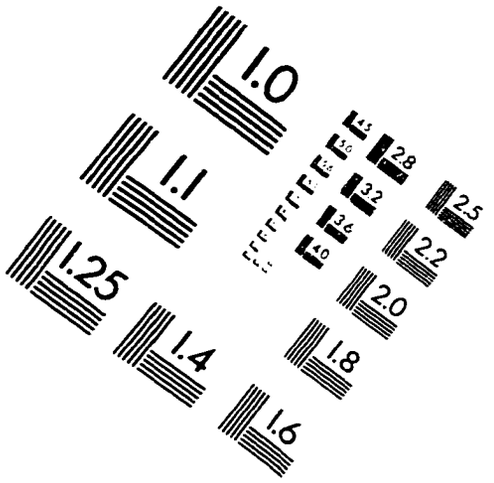

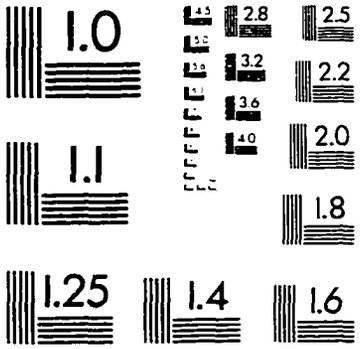

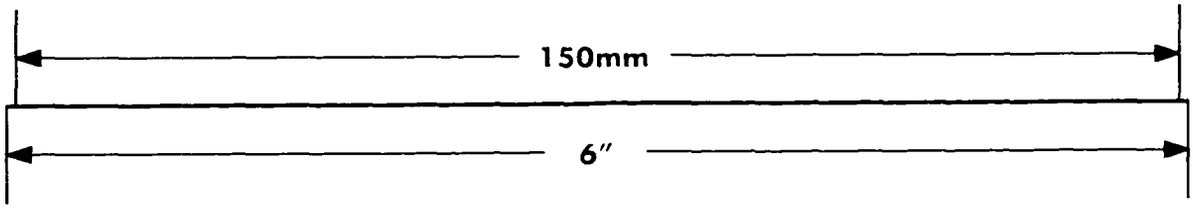

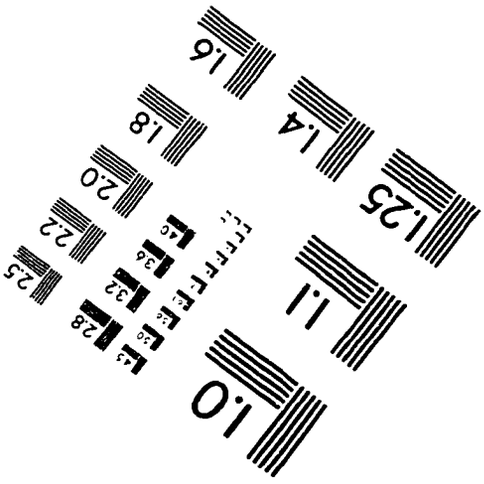

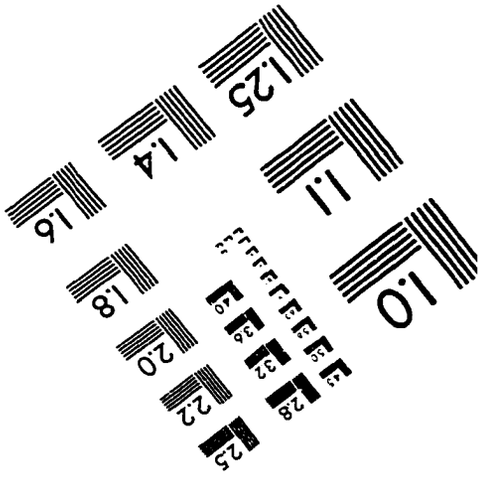

APPLIED IMAGE, Inc
1653 East Main Street
Rochester, NY 14609 USA
Phone: 716/482-0300
Fax: 716/288-5989